180(1), 2020

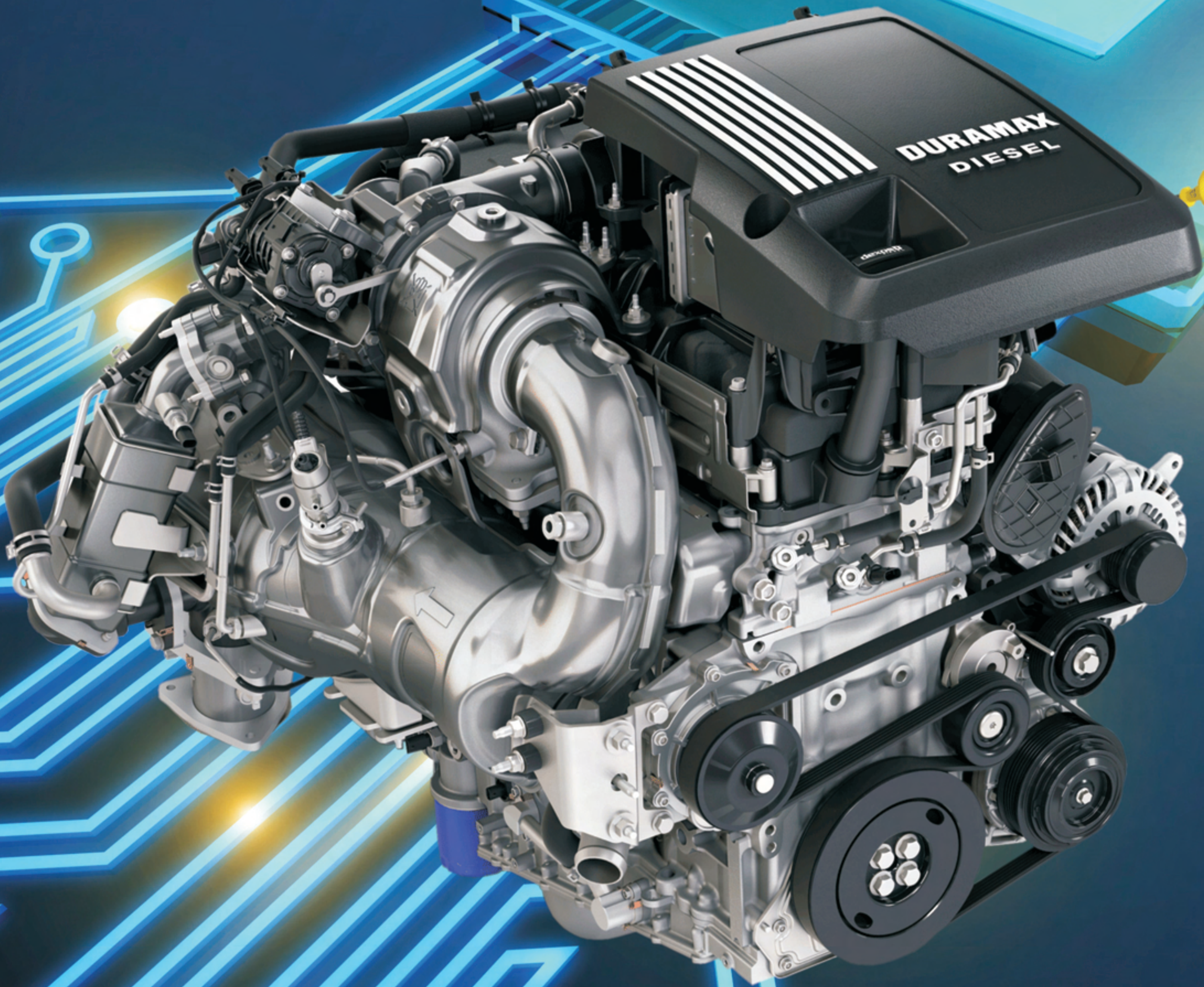

COMBUSTION ENGINES


Seria silników
D-LINE Diesel
z systemem COMMON-RAIL
vetus
D-LINE
Ewolucyjna
gama silników
VETUS serii D-Line
o mocy od 122 KM
do 210 KM

COMBUSTION ENGINES

A Scientific Magazine

2020, 180(1)

Year LIX

PL ISSN 2300-9896

Editor:

Polskie Towarzystwo Naukowe Silników Spalinowych
43-300 Bielsko-Biała, Sarni Stok 93 Street, Poland
tel.: +48 33 8130402, fax: +48 33 8125038
E-mail: sekretariat@ptnss.pl
WebSite: http://www.ptnss.pl
Papers available on-line: http://combustion-engines.eu

Contents

Editorial:
Institute of Combustion Engines and Powertrains
Poznan University of Technology
60-965 Poznan, Piotrowo 3 Street
tel.: +48 61 2244505, +48 61 2244502
E-mail: papers@ptnss.pl

Editor
Polish Scientific Society of Combustion Engines
43-300 Bielsko-Biała, Sarni Stok 93 Street, Poland
tel.: +48 33 8130402, fax: +48 33 8125038
E-mail: sekretariat@ptnss.pl
WebSite: http://www.ptnss.pl

Subscriptions
Send subscription requests to the Publisher's address.
Cost of a single issue PLZ30 + VAT.

Preparation for print
ARS NOVA Publishing House
60-782 Poznań, ul. Grunwaldzka 17/10A

Circulation: 150 copies

Printing and binding

Zakład Poligraficzny Moś i Łuczak, sp. j.,
Poznań, ul. Piwna 1

The journal is registered in the Polish technical journals content database – **BAZTECH** www.baztech.icm.edu.pl

The journal is listed in the international database
IC Journal Master List
– **Index Copernicus** www.indexcopernicus.com

Declaration of the original version
The original version of the Combustion Engines journal is the printed version.

Papers published in the
Combustion Engines
quarterly receive 20 points as stated by the Notification of the Minister of Science and Higher Education dated 31 July 2019.

Cover
I – Chevrolet-Silverado-Diesel Engine (*fot. www.wardsauto.com*);
background (cpu computer
© Photo by pingingz from Adobe Stock)
IV – Low-Speed Pre-Ignition SI Combustion Engine
(*fot. www.tunap.com*)

Article citation info:
VALVERDE-MORALES, V. Overview of the light-duty vehicles tailpipe emissions regulations in the European Union: status and upcoming type-approval and market surveillance schema. *Combustion Engines*. 2020, **180**(1), 3-7. https://doi.org/10.19206/CE-2020-101

Víctor VALVERDE-MORALES

CE-2020-101

Overview of the light-duty vehicles tailpipe emissions regulations in the European Union: status and upcoming type-approval and market surveillance schema

In order to curb pollutant emissions from light-duty vehicles in the European Union, a set of complex regulations have been approved in the recent years (2016-2018) including more stringent emissions tests, independent in-service conformity checks, and a novel type-approval framework which includes market surveillance provisions to complement the type-approval requirements. Tailpipe emissions will need to meet stringent emission limits before entering the market at type-approval and at the end of the production line, as well as during their normal life under normal conditions of use. This contribution aims at providing a comprehensive but synthetic analysis of the current regulatory context in the EU.

Key words: *WLTP, RDE, Market Surveillance, type-approval, in-service conformity*

1. Introduction

Air pollution lies amongst the most significant risks in the European Union (EU) causing circa half a million premature deaths per year as well as significant economic and environmental impacts [1, 2]. Road transport remains a key source of primary pollutants despite achieving substantial emissions reductions over the past decades [1, 3].

In order to further reduce tailpipe emissions from light-duty vehicles (LDVs) several policy instruments have been recently introduced in the EU. The Joint Research Center (JRC), the in-house research center of the European Commission has provided scientific and technical support to the development and implementation of the new laboratory-based test protocol, the WLTP as well as the on-road emissions test, the RDE.

The objective of the presentation is to provide insight on the current regulatory status in the EU regarding tailpipe emissions from LDVs in the laboratory and on the road, both at type-approval (i.e., homologation of emissions on a prototype vehicle), at the end of the production line, and during their real-life operation. In addition, an overview of the novel type-approval framework that will enter into force in 2020 is provided focusing on the role that has been assigned to JRC.

2. Worldwide harmonised Light-duty vehicles Test Procedures (WLTP)

The Commission Regulation (EU) 2017/1151 of 1st June 2017, implemented the WLTP into the EU legislation. The WLTP, in force in the EU since September 1st 2017, was first developed at the United Nations Economic Cooperation for Europe (UNECE) level [4]. The WLTP replaced the NEDC procedure as type-approval framework in the EU as the latter was outdated and did not adequately reflect real world emissions [5, 6]. Under the WLTP, the tailpipe emissions of LDVs (gases and particles), measured in laboratory conditions under standardized ambient conditions following the Type 1 test procedures (Annex XXI to regulation 2017/1151), shall meet the Euro 6 tailpipe emission limits set by the Regulation (EC) No 715/2007 and its amendments.

LDVs are driven on a chassis dynamometer on the Worldwide Light-duty Test Cycle (WLTC, Sub-Annex 1 to Annex XXI), which is longer, more transient, and reaches higher vehicle speed than its predecessor the NEDC. The WLTP describes precisely how to determine the road load coefficients of a vehicle and how to transfer them to the chassis dynamometer (Sub-Annex 4), which was one of the main loopholes of the NEDC [7]. The WLTP, which allows road load determination on a wind tunnel or a test track, clearly defines important details like how to select the tires and which tire pressure and tread depth are permissible to perform the coast down test.

Vehicle preconditioning, soaking conditions, test cell temperature and humidity ranges, as well as the operation of sampling methods are comprehensively described in the regulation to limit the exploitable test flexibilities and enhance replicability and reproducibility of emission results (Sub-Annex 6). In particular, the WLTP prescribes a precise methodology to determine the gearshift points for manual transmission vehicles (Sub-Annex 2).

Specifications of the testing equipment are also widely covered in the WLTP (Sub-Annex 5), including the calibration, sampling frequency, accuracy, and response time requirements. According to the WLTP, the measurement principles for gaseous emissions are non-dispersive infrared (NDIR) absorption for carbon dioxide and carbon monoxide, flame ionization (FID) for hydrocarbons, and chemiluminescent (CLA) or non-dispersive ultra-violet resonance absorption (NDUV) for nitrogen oxides. Pariculate matter mass is sampled on a single filter mounted within a holder in the sampled dilute exhaust gas flow and weighted in a temperature and humidity controlled weighing chamber. Fluorocarbon coated glass fibre filters or fluorocarbon membrane filters shall be used. The particle number sampling system shall consist of a volatile particle remover (VPR) upstream of a particle number counter (PNC) and suitable transfer tubing.

The WLTP also describes the testing conditions and tailpipe emission limits applying for positive ignition vehicles at idling (Type 2 test: limiting CO emissions at normal and high engine idle speeds) and at low ambient temperatures (Type 6 test: covering CO and hydrocarbons emissions at cold start at –7°C). The protocols for verifying the durability of pollution control devices (Type 5 test) lie also under the WLTP umbrella.

Received 25 September 2019; Received in revised form 12 December 2019; Accepted 15 January 2020
Available online 30 March 2020

The Conformity of Production (CoP) is an additional check on emissions compliance performed by the manufacturer on vehicles at the end of the production line. At least one verification per 5000 vehicles produced or once per year, whichever comes first, shall be performed on each CoP vehicle family (vehicles within the same family have the same fuel type, combustion type, engine displacement, transmission type, etc.). The vehicles shall conform to the Euro 6 emission limits according to a precise statistical procedure and testing protocol, which considers the emission results of a set of three up to sixteen vehicles (Fig. 1). The Type Approval Authority (TAA) shall select randomly the vehicles until a pass or fail decision is reached according to the statistical procedure. It is responsibility of the TAA to audit the CoP documentation at least once per year and to perform additional physical tests in case it is not satisfied with the auditing procedure or at least once every three years.

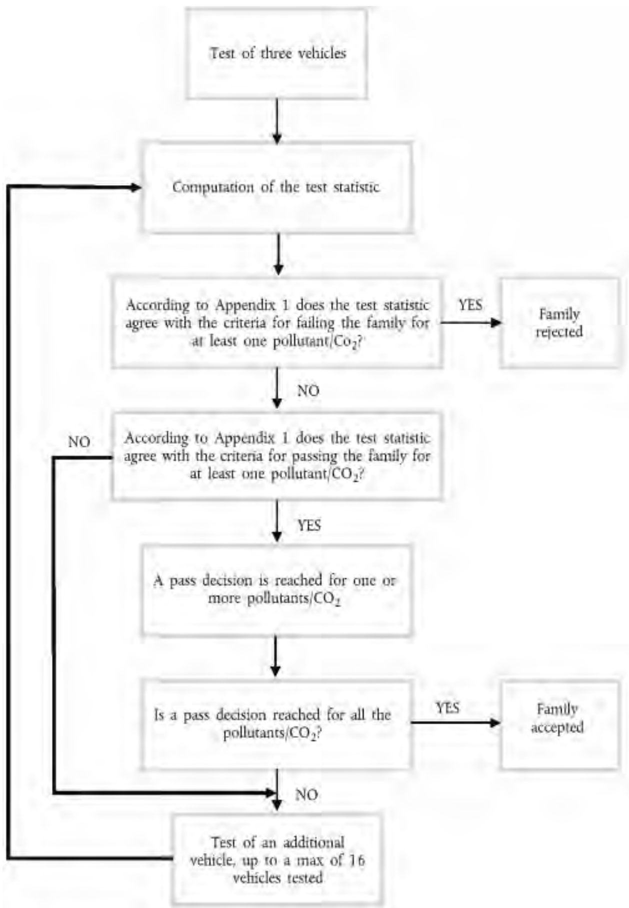

Fig. 1. Overview of the procedure to check the conformity of the vehicle for a Type 1 test [1]

3. Real Driving Emissions (RDE) regulation

Following the approach used to assess the emissions performance of heavy-duty vehicles under real life operation through Portable Emissions Measurement Systems (PEMS), the EU has developed the Real Driving Emissions (RDE) regulation for LDVs in the period 2011-2018. The RDE aims at securing low tailpipe emissions of passenger cars and light commercial vehicles under real traffic operation under normal conditions of use.

The RDE, which has been introduced in the EU legislation through four regulatory packages (RDE1: EU 2016/427, RDE2: EU 2016/646, RDE3: EU 2017/1154, and RDE4: EU 2018/1832), is applicable for all new vehicles since September 1st 2018. Vehicles tested under the RDE regulation need not-to-exceed (NTE) certain nitrogen oxides and solid particle number limits over a route that complies with a series of testing boundaries (ambient temperature between –7°C and 35°C, maximum altitude of 1 300 m.a.s.l., test duration between 90 and 120 minutes, at least 16 km driven on urban, rural and motorway conditions, etc.). The RDE boundary conditions were set in a way to cover most of the driving situations within the EU while allowing PEMS to be used within their optimal operating conditions. The fact that on-road tests complying with the RDE requirements can be performed in countless combinations of ambient and traffic conditions, driving styles, and payload largely limits the potential of cycle optimization (as occurred in the past when vehicle emissions were checked only under the NEDC test protocol). The fact that RDE NTE limits need to be met under a wide range of conditions has become a major driver of current engine and after-treatment systems development over the last years [8].

RDE1 describes the testing procedure, provides the technical requirements for PEMS and defines the ex-post emissions calculations and evaluation methods. RDE2 introduced the NTE compliance request to the urban driving on top of the entire RDE trip and set new boundary conditions for diving dynamics and cumulative positive elevation gain. The extended documentation package, which consists of a description of the base and auxiliary emissions strategies to be shared with the TAA was introduced in RDE2 as a way to prevent defeat devices. RDE3 comprised a provision to include emissions during cold start operation in the final RDE emission values, and set the technical parameters to assess emissions of plug-in hybrid electric vehicles. RDE4 introduced the In-Service Conformity (ISC) provisions to evaluate the emissions performance of vehicles during their normal life as well as modifications to the ex-post evaluation methods to ensure practicality and effective emissions testing.

The NTE limit is the Type I test limit multiplied by a conformity factor (CF) that includes a margin accounting for the additional measurement uncertainty of PEMS relative to standard laboratory equipment. NO_x CF was set by RDE2 and modified in RDE4, whereas the PN CF was introduced in RDE3. The RDE regulation includes a procedure to review the margin in light of technological improvements of PEMS. The JRC has developed a methodological framework for the revision of the NO_x margin [9] that uses the error propagation rule and takes into account the uncertainties of gas analysers, exhaust mass flowmeters, and global positioning system. The NO_x margin applicable to new type approved vehicles from January 2020 was set at 0.43 considering a worst-case scenario for zero NO_x drift.

In order to support best practices and avoid wrongdoings during on-road emissions tests in the context of the RDE regulation, the JRC has developed a guidance document [10] covering all aspects of PEMS testing from installation (Fig. 2) to calibration and execution of tests.

Fig. 2. PEMS installation [2]

4. In-Service Conformity (ISC)

From September 1st 2019, the ISC provisions will be applicable to all new vehicles to ensure that LDVs comply with their emission limits throughout their normal life (up to a mileage of 100 000 km or five years, whichever occurs first) and not only at type-approval. ISC, which was introduced by EU regulation 2018/1832 of November 5th 2018 (RDE4), defines the procedures and responsibilities to check tailpipe emissions compliance during RDE as well as WLTP Type 1 and Type 6 tests.

In order to prioritize the ISC testing, the Granting Type-Approval Authorities (GTAA) will perform risk assessments based on remote-sensing (Fig. 3), simplified measurement systems and/or other sources of tailpipe emissions. The outcome of the risk assessment shall be a list of vehicle families with potential issues regarding their emissions performance that will undergo detailed scrutiny through actual ISC testing.

Fig. 3. Remote-sensing instruments are placed in the road-side and provide an instantaneous reading of vehicle emissions passing-by [3]

ISC tests shall be performed by vehicle manufacturers, GTAAs, and may be additionally performed by third parties through accredited laboratories. The accreditations seek to guarantee that vehicle inspection (ISO 17020) and emissions compliance checks (ISO 17025 and) are fair, properly executed, and that instrumentation fully complies with the regulation requirements. Accredited laboratories will have access to transparency lists, which contain the necessary information to perform testing in type-approval like conditions (road load settings, how to enable dyno mode, gear-shifting pattern, etc.). Manufactures will need to perform ISC testing at least on 5% of their families every year (with a minimum of two families). In order to strengthen the ISC procedure, the GTAA is additionally responsible to audit the ISC testing performed by the manufacturer and accredited laboratories. The ISC procedure allows, for the first time in history, that consumer and environmental organizations, for example, officially confront the emissions compliance of vehicles through accredited laboratories.

The results of ISC tests will be pooled together into a publicly accessible electronic platform hosted by the European Commission (different user profiles will have different access to data privileges). An ad-hoc ISC statistical procedure has been developed to robustly assess the emissions compliance of a given vehicle family while minimising the testing burden, the environmental risk (compliance with ISC but incompliance with NTE limits), and the manufactures' risk (incompliance with ISC but compliance with NTE limits). For RDE and WLTP Type 1 tests, the ISC pass-or-fail decision requires a minimum of three vehicles and is reached with a maximum of ten vehicles depending on the number of individual failed tests (Fig. 4). A simplified statistical approach is used for WLTP Type 6 test where a decision may be reached after three tests.

Failed result count f	3	4	5	6	7	8	9	10
10								FAIL
9							FAIL	FAIL
8						FAIL	FAIL	FAIL
7					FAIL	FAIL	FAIL	FAIL
6				FAIL	FAIL	FAIL	FAIL	FAIL
5			FAIL	FAIL	FAIL	UND	UND	PASS
4		FAIL	FAIL	UND	UND	UND	UND	PASS
3	FAIL	FAIL	UND	UND	UND	UND	PASS	PASS
2	UND	UND	UND	UND	PASS	PASS	PASS	PASS
1	UND	PASS	PASS	PASS	PASS	PASS	PASS	PASS
0	PASS	PASS	PASS	PASS	PASS	PASS	PASS	PASS
	3	4	5	6	7	8	9	10

Cumulative sample size n

Fig. 4. Decision chart for the ISC statistical procedure applying for type-approved vehicles from January 1st 2020 (UND: undecided) [4]

On top the statistical procedure described above, an additional clause is defined for outliers, i.e., vehicles that emit pollutants way above the NTE limits. The presence of outliers in ISC tests may lead to a direct fail outcome for the whole family even if the minimum number of tests is not yet reached. The presence of two intermediate outliers (emissions > 1.3 * NTE limit) or one extreme outlier (emissions > 2.5 * NTE limit) in a sample shall lead to a fail of the sample.

Within 10 days of the end of the ISC testing, the GTAA shall start detailed investigations with the manufacturer in order to decide whether the ISC family passes or fails the ISC procedure. In case of excess emissions, the manufacturer shall provide to the GTAA a description of the 'possible cause of the failures, which parts of the family might be affected, whether other families might be affected, or why the problem which caused the failure at the original ISC tests is not related to in-service conformity, if applicable'. In the case a vehicle family does not comply with the emissions limits comprehensive remedial measures shall be put in place by the vehicle manufacturer to restore effective and durable after-treatment systems. The plan describing the remedial measures shall be provided to the GTAA within 45 working days including a demonstration of the effectiveness and durability of the proposed measures and a communication plan to vehicle owners and repair workshops. Within 15 working days, the GTAA needs to accept or decline the remedial plan. If the GTAA does not accept it, it is entitled to take all appropriate measures to restore conformity, including withdrawal of the type-approval and notify its decision to all Member States and the Commission. Member States shall take measures to ensure that the approved plan of remedial measures is applied within two years to at least 90% of affected vehicles registered in their territory.

In order to foster transparency, the ISC regulation foresees that the GTAA needs to make publicly available and free of charge, a report containing all the results of all the finalised ISC investigations of the previous year, by the 31 March of each year.

The JRC is currently working on accrediting its testing procedures for RDE and WLTP (ISO 17025) and for vehicle inspection (ISO 17020) in order to be in the position to actively participate in ISC testing.

5. New Type-Approval Framework and Market Surveillance

EU regulation 2018/858 of May 30th 2018 describes the new framework for the type-approval and CoP of motor vehicles in the EU that will replace Directive 2007/46/EC from September 1st 2020. As overall goals, the new framework pursues raising the technical quality and robustness of the type-approval procedure, facilitate its enforcement, prevent market distortions, increase transparency, minimize the administrative burden, and foster the independence of authorities in order to ensure a high level of safety and environmental performance of light and heavy-duty vehicles.

The new framework entitles Member States to act against non-compliant vehicles on their territory without the need to wait for the GTAA to take action.

In order to strengthen the collaboration among Member States, the regulation foresees the creation of an advisory Forum for Exchange of Information on Enforcement that shall include representatives of national authorities and the Commission.

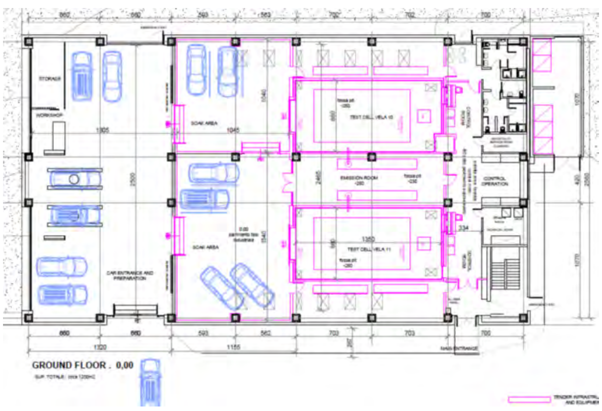

Fig. 5. New Vehicle Emissions Laboratories (VELA 10 and VELA 11) building plan [5]

The new type-approval framework introduces also an effective market surveillance system to control the conformity of vehicles already in circulation. In this sense, Member States as well as the European Commission will name Market Surveillance Authorities responsible to perform independent vehicle compliance tests on vehicles already on the market. The European Commission oversight of the whole type-approval procedure includes taking measures (e.g., ordering vehicle recalls, giving fines, and even revoking type-approval certificates) against non-compliant vehicles. The Commission shall also audit the procedures put in place by approval authorities to grant type-approvals, and execute conformity of production at least once every five years.

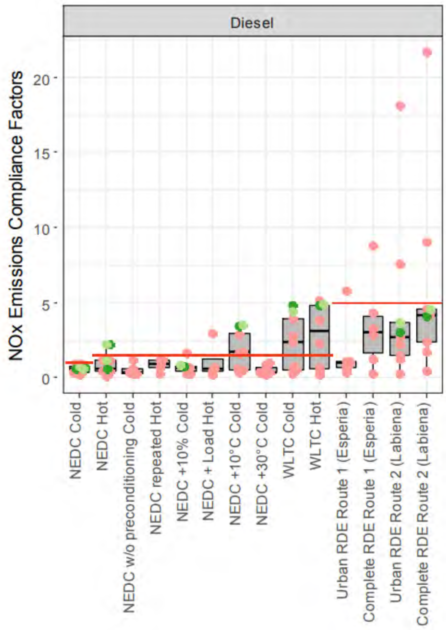

Fig. 6. NO_x emissions/NO_x standards (Compliance Factors) over laboratory and on-road tests. Horizontal red lines indicate limits or recommended thresholds for Compliance Factors. Green and red dots represent individual Euro 5b and Euro 6b vehicles, respectively [6]

The JRC will be the European Commission Service responsible for the execution of the market surveillance tests (emissions and safety) as well as inspection of the work of technical services (peer-review mechanism). New personnel, facilities (Fig. 5), and instrumentation have been allocated at JRC to start carrying out Market Surveillance activities from September 1st 2020.

Since early 2017, the JRC has been carrying out independent tailpipe emissions compliance checks on LDVs in the laboratory and on the road, following standard and alternative NEDC, WLTP and RDE procedures [11]. The alternative laboratory tests include back-to-back NEDC and WLTP tests (i.e., with warm engine), setting the test cell at 10°C and 30°C, modifying the speed trace, etc. The outcomes of such activities aim at contributing to the development of robust vehicle screening methodologies and testing protocols in the context of upcoming Market Surveillance obligations.

The work conducted at JRC also focus on developing and enhancing testing protocols and data processing tools to identify vehicles that present emission patterns which could be caused by potential use of defeat devices (Fig. 6).

Acknowledgements

This work is presented on behalf of the colleagues of the Sustainable Transport Unit (JRC) supporting the development and implementation of vehicle emissions regulations in the EU.

Nomenclature

CF conformity factor
CoP conformity of production
GTAA Granting Type-Approval Authority
ISC In-Service Conformity
JRC Joint Research Center
NEDC New European Driving Cycle
PEMS Portable Emissions Measurement System
RDE Real Driving Emissions
TAA Type Approval Authority
WLTP Worldwide harmonized Light-duty vehicles Test Procedures

Bibliography

[1] EUROPEAN ENVIRONMENT AGENCY. EEA Report No 12/2018 Air quality in Europe — 2018 report. https://doi.org/10.2800/777411
[2] CE DELFT. Health impacts and costs of diesel emissions in the EU. 2018, Publication code: 18.4R30.140.
[3] EUROPEAN ENVIRONMENT AGENCY. EEA Briefing No 15/2018. Progress of EU transport sector towards its environment and climate objectives. https://doi.org/10.2800/954310
[4] TUTUIANU, M., CIUFFO, B., HANIU, T. et al. Development of a world-wide harmonized light duty test cycle (WLTC). *Transport. Res. Part D*. 2015, **40**, 61-75. https://doi.org/10.1016/j.trd.2015.07.011
[5] FONTARAS, G., ZACHAROF, N., CIUFFO, B. Fuel consumption and CO_2 emissions from passenger cars in Europe – Laboratory versus real-world emissions. *Progr. Energy Combust. Sci.* 2017, **60**, 97-131. https:// doi.org/10.1016/j.pecs.2016.12.004
[6] WEISS, M., BONNEL, P., HUMMEL, R. et al. On-road emissions of light-duty vehicles in Europe. *Environ. Sci. Technol*. 2011, **45**, 8575-8581. https://doi.org/10.1021/es2008424
[7] PAVLOVIC, P., CIUFFO, B., FONTARAS, G. et al. Assessment of test cycle flexibilities, driving behavior, and their impacts on CO_2 results. *TRB 96th Annual Meeting*. 2017.
[8] BIELACZYC, P., WOODBURN, J., Trends in automotive emission legislation: impact on LD engine development, fuels, lubricants and test methods: a global view, with a focus on WLTP and RDE regulations. *Emiss. Control Sci. Technol.* 2019, **5**, 86-98. https://doi.org/10.1007/s40825-019-0112-3
[9] GIECHASKIEL, B., CLAIROTTE, M., VALVERDE, V. et al. Framework for the assessment of PEMS (Portable Emissions Measurement Systems) uncertainty. *Environ. Res.* 2018, **166**, 251-260. https://doi.org/10.1016/j.envres.2018.06.012
[10] VALVERDE, V., BONNEL, P. On-road testing with Portable Emissions Measurement Systems (PEMS). Guidance note for light-duty vehicles. JRC Technical Report. 2018. https://doi.org/10.2760/08294
[11] CLAIROTTE, M., VALVERDE, V., BONNEL, P. et al. Joint Research Centre 2017 light-duty vehicles emissions testing. Contribution to the EU market surveillance: testing protocols and vehicle emissions performance. 2018. https://doi.org/10.2760/83327

Víctor Valverde-Morales, Ph.D. – Sustainable Transport Unit Joint Research Center, European Commission.
e-mail: *victor.valverde-morales@ec.europa.eu*

Article citation info:
FRIEDL, H., FRAIDL, G., KAPUS, P. *Highest efficiency and ultra low emission – internal combustion engine 4.0*. Combustion Engines. 2020, **180**(1), 8-16. https://doi.org/10.19206/CE-2020-102

Hubert FRIEDL
Günter FRAIDL
Paul KAPUS

CE-2020-102

Highest efficiency and ultra low emission – internal combustion engine 4.0

In the future, the simultaneous reduction of pollutant and CO_2 emissions will require significantly enhanced powertrain functionalities that cannot only be adequately represented by the ICE (internal combustion engine) alone. Both automated transmissions and especially powertrain electrification can help to meet efficiently those extended requirements. The extended functionalities are no longer applied exclusively with the ICE itself ("Fully Flexible Internal Combustion Engine"), but distributed across the entire powertrain ("Fully Flexible Powertrain"). In addition, the powertrain will be fully networked with the vehicle environment and thus will utilize all data that are useful for emission and consumption-optimized operation of the ICE.

Combustion engine and electrification often complement each other in a synergetic way. This makes it extremely sensible for the combustion engine to evolve in future from a "single fighter" to a "team player". If one compares the requirements of such an ICE with the definition of Industry 4.0, then there are extensive correspondences. Thus, it seems quite opportune to call such a fully networked combustion engine designed to meet future needs as "Internal Combustion Engine 4.0 (ICE 4.0)". This even more so, as such a name can also be derived from the history: e.g. ICE 1.0 describes the combustion engines of the first mass-produced vehicles, ICE 2.0 the combustion engines emission-optimized since the 1960s and ICE 3.0 the highly optimized "Fully Flexible Combustion Engine", which currently offers a high torque and performance potential combined with low fuel consumption and pollutant emissions.

In addition to further improvements in fuel consumption, the "Combustion Engine 4.0" offers such a low level of pollutant emissions that can best be described as "Zero Impact Emission". This means that such future ICE´s will no longer have a negative impact on the imission situation in urban areas. With the e-fuels topic, the ICE also has the potential to become both CO_2- and pollutant-neutral in the medium and long term. This means that the ICE – also in passenger cars – will continue to be an essential and necessary cornerstone for future powertrain portfolios for the next decades.

Key words: *passenger car, gasoline, diesel, hybrid, powertrain*

1. Introduction

The combustion engine is currently undergoing the most turbulent phase in its more than 100-year of history. From the undeniable enabler of individual mobility, the ICE is partly driven into a negative image as an air polluter and no longer being a future oriented technology. Particularly in Europe, the combination of exceeding imission limits in major cities with the emissions issue of the Diesel engine, has had a lasting impact on the image of the ICE. Potential city access restrictions not only generate anxiety scenarios, but also increasingly determine the buying behavior of the customer and thus, not at least, question the future of the Diesel engine in passenger cars. In the public discussion, however, most often neither the resulting losses in people's assets and the contribution of non-automotive pollutant emitters to the imission situation are considered.

Looking at the challenges of the ICE in a technically rational way against a global background, it is probably less the issue of pollutants, but rather the sustainable reduction of CO_2 emissions, that presents the biggest challenge, Fig. 1.

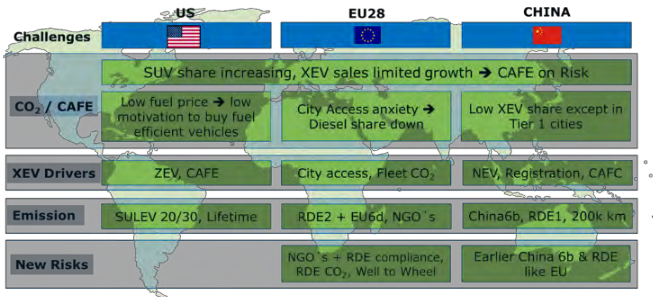

Fig. 1. Global and regional challenges for the ICE

The fulfillment of the worldwide CO_2 resp. fuel consumption fleet limits is hampered both by a strongly increasing portion of vehicles with high weight and driving resistance (SUV boom) and thus unfavorable consumption behavior compared to the passenger car as well as a still restrained purchase behavior for XEV's.

In the US, low fuel prices give the customer a low economic motivation to buy CO_2-efficient vehicles. In addition, since the US legislation is traditionally more pollutant-oriented than emissions-oriented, a more modest transition to electromobility is expected.

In Europe, on the other hand, demanding CO_2 reductions in conjunction with declining Diesel and SUV shares, requires a relatively rapid expansion of electrification just to meet the CO_2 fleet targets. In addition, the shift towards electrification is enhanced additionally by the ongoing discussions about bans for the ICE.

In China, above all, the imission situation in mega cities and the resulting registration restrictions and exemptions for new energy vehicles (NEVs) are a major motivation for electric drives.

Although the United States, especially California, have been at the forefront of low pollutant emission legislation for decades, in future both China with its extremely low thresholds in the test cycle (China 6b) and demanding durability requirements, and especially Europe with a very challenging RDE legislation will become the pacemakers.

The short- and medium-term technology trends can be estimated in a first approximation from the already apparent or expected legislation, where strong regional differences are to be expected. Long-term trends, on the other hand, are mainly due to the CO_2 reductions required to meet the cli-

Received 25 September 2019; Received in revised form 12 December 2019; Accepted 15 January 2020
Available online 30 March 2020

mate goals. However, these must be seen as balance between the CO_2 emissions of the transport sector ("Tank- to-Wheel") and the provision of primary energy ("Well-to-Tank"). Although the division into individual sectors allows the definition of separate target values, there is the risk that over the time course the overall optimum of CO_2 reduction will not always be achieved. For example, a reduction of purely vehicle-related tank-to-wheel emissions by electric vehicles only becomes effective in the total CO_2 emissions, if the well-to-tank emissions of the energy supply are reduced beforehand.

Of course, in addition to technical progress in development, a wealth of legal and political influencing factors determines the long-term development of technology. The issues of registration and access restrictions ("Diesel-Ban", "ICE-Stop") certainly play a decisive role, Fig. 2.

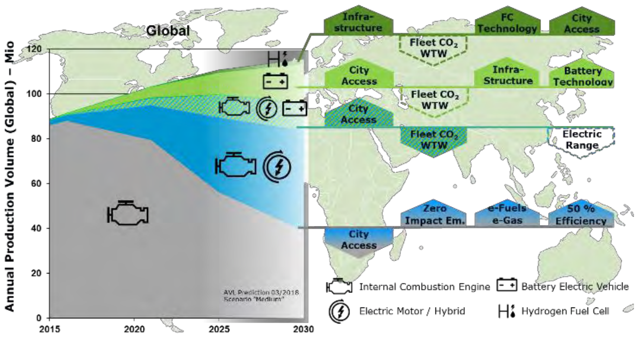

Fig. 2. Main factors influencing the long-term global technology distribution [1]

In addition to the reduction of pollutant emissions, fulfilling the fleet CO_2 limits is a key driver for electric vehicles, whose emission contribution is currently rated "zero". Thus, a transition from a tank-to-wheel to a well-to-wheel approach with today's powerplant CO_2 footprint would significantly reduce the lever of the electric vehicles in fleet CO_2 and, above all, reduce the attractiveness of plug-in hybrids (PHEV). Similarly, advances in battery technologies are also competing the need for PHEV as a long-haul solution, even though the general fast-charging issue of increasing inventory of BEVs with very high battery capacity in long-haul operations is challenging.

The success of the fuel cell is much more determined by the infrastructure than in the case of the battery-powered vehicle. Here, in a global view, both the storage and the distribution of hydrogen are still inhibitions. However, vehicle refueling itself can be solved in a practical way by the possible transfer of high energy contents within a brief time.

With the ICE, on the other hand, the topics "Zero Impact Emission" and "e-Fuels" as well as "e-Gas" also make it possible to operate the ICE practically pollutant-free and CO_2-neutral, thus bringing it to a level with renewable sources in terms of environmental impact in a then fair competition again.

2. A new generation of ICE´s

Basically, there are two options for meeting future CO_2 fleet targets and emission limits:

- **Electrification focus**: The emphasis is placed on the highest possible proportion of electrification (BEV + PHEV), if necessary, a corresponding market penetration is promoted with price support measures. In the case of conventional drives, the focus is primarily only on the adaptation to the legal boundaries, most of the CO_2 fleet reduction is represented by BEV and PHEV.
- **Balanced approach**: In addition to the "marketable" growth of BEV + PHEV, the further reduction of CO_2 emissions is the result of a significant advancement of ICE based powertrains utilizing synergies with affordable electrification measures.

However, looking at the current evolution of CO_2 fleet levels in Europe – the progression of CO_2 reduction is well above the target corridor for meeting the fleet targets for 2020 due to rising SUV and falling diesel emissions – all technical options for CO_2 reduction will have to be exploited. In conjunction with the also tightened RDE requirements, this requires a sustainable improvement or new development of ICE based powertrains.

Since the issue of real world emissions will increasingly come into the focus, it is becoming more sensible to increasingly use the traffic and environmental information available through the networking of the automobile to optimize fuel consumption and pollutant emission of the powertrain. To use such a potential, it is necessary to integrate electrical functionalities into the powertrain in addition to refined ICE attributes.

If one compares these requirements to future powertrains with the definition of Industry 4.0, in Germany, then surprising matches are found:

Definition Industry 4.0 [2] (in extracts, in the following in italics):

- "*Industrial production should be integrated with modern information and communication technology*". This also applies also to automobile and optimized powertrain management.
- "*The technical basis for this are intelligent and digitally networked systems. With their help, a largely self-organized production is to be possible: people, machines, equipment, logistics and products communicate and cooperate directly with each other in Industry 4.0*". This sentence describes in an analogous manner also autonomous driving functions and the networking of the automobile.
- "*Networking should make it possible to optimize not just a single production step but an entire value chain*". Also in the automobile, it will be possible in the future, to optimize not only the driving itself, but the entire transport process including energy-optimal route selection, maximizing the recuperation potentials and automation of assistance functions such as automatic parking.
- "*The network should also encompass all phases of the product's lifecycle – from the idea of a product to development, manufacturing, use and maintenance to recycling*." In the future, the evaluation of the automobile and the various drives will also be increasingly carried out on a "lifecycle" basis involving production, operation and recycling.

Thus, it is perfectly opportune to call an ICE designed comprehensively for future needs as "Internal Combustion

Engine 4.0 (ICE 4.0)". But also from the history can be derived such a name, Fig. 3.

"ICE 1.0" describes the combustion engines of the first mass-produced vehicles. Affordability and reliability were the defining parameters.

In California, the first emission limits for motor vehicles were already set in the 1960s, which is certainly a decisive milestone, e.g. defined as "ICE 2.0".

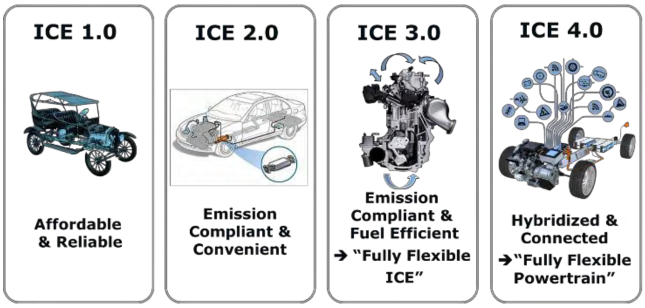

Fig. 3. Generations of ICE based passenger car power- train systems

In the following decades, the limit values for pollutant emissions and fleet consumption target values to be proven on the chassis dynamometer were steadily tightened and required significantly increased variability, the "Fully Flexible Internal Combustion Engine – here described as "ICE 3.0".

The future requirements regarding pollutant as well as CO_2 emissions, require significantly extended functionalities of the powertrain, which no longer can be mapped exclusively within the ICE ("Fully Flexible Combustion Engine") but must be distributed to the entire drive train ("Fully Flexible Powertrain"). In addition, the drivetrain will be networked with the vehicle environment, enabling all data useful for emission-optimal powertrain operation to be utilized, and will increasingly be powered by CO_2-neutral fuels from renewable sources – "ICE 4.0".

Zero Impact Emission

In addition to the currently negatively biased image of the ICE, the complex discussions regarding access restrictions for emission-critical zones are causing uncertainty among the buyer. Especially the lack of clearly defined future framework conditions becomes an existential threat to the Diesel engine in passenger cars already short term.

In the medium and long term, a general sales stop of ICE is increasingly being discussed, without considering the untapped potential of future ICE-based powertrain systems. To remain accepted, at least in the European public opinion, it is generally necessary for the ICE to lower its pollutant emissions to a level that is no longer relevant for the environment. With EU6dtemp incl. RDE, a decisive step has already been made in this direction. It can be assumed that such vehicles will certainly fall below the imission limit values in today's imission-critical zones.

"Zero Impact Emission" means that emissions are so low that they have no impact on air quality. To assess this, Fig. 4 shows the emission characteristics of a standard EU6dtemp vehicle with a supercharged DI Gasoline engine in the WLTP cycle.

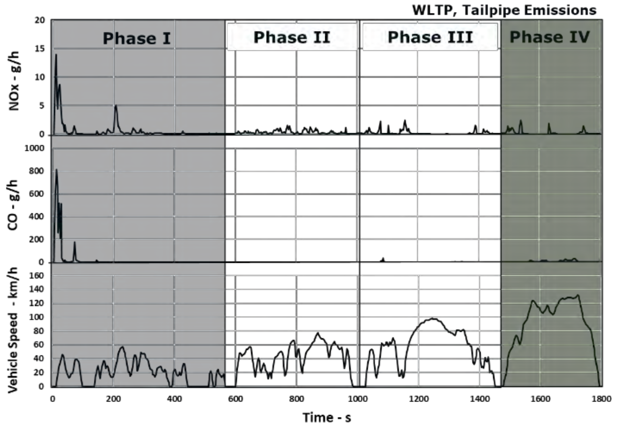

Fig. 4. Pollutant emission of an EU6dtemp vehicle with Gasoline engine in the WLTP

With the Gasoline engine, a strong concentration of pollutant emissions on the non-warmed up or highly dynamic engine operation is obvious. These relations are not only valid for this single vehicle, but are also confirmed on a broad statistical basis, Fig. 5.

If one looks at the pollutant emissions in warmed up condition, then an emission level of only 2–5 mg/km is observed, which is an order of magnitude lower then under cold conditions. If a model simulation of critical imission measurement points for Germany – e.g. the Neckartor in Stuttgart [3] – is done then it can be seen that the vehicle emissions only contribute by 0.2–0.5 $\mu g/m^3$. This is uncritical compared to the legal limit (40 $\mu g/m^3$) as well as compared to the emissions of the non-automotive sector (approx. 18 $\mu g/m^3$). So for warm engine EU6d temp vehicles could already be called „Zero Impact Emission".

Starting from the EU6d temp status, the main challenge for further emission reductions are with the improvement of pollutant emissions at ICE start and in non-warmed up operating range, as well as in the temperature management of the exhaust gas aftertreatment. In addition, various measures to limit pollutant emissions are required in the upper load range.

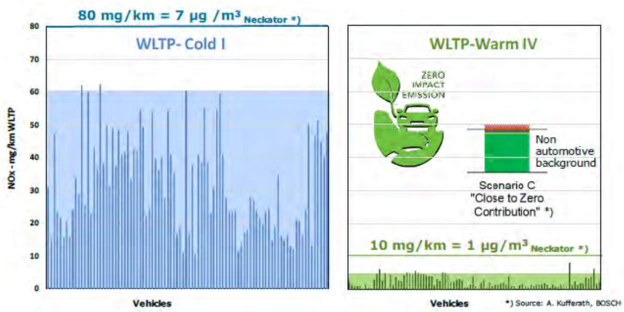

Fig. 5: Emission behavior of EU6dtemp vehicles with Gasoline engines

For both concern areas, it makes sense to utilize synergy effects with mild hybridization. If you set e. g. a suitably designed 48V system to make the cold operation primarily electrically and at the same time to condition the exhaust aftertreatment by means of catalyst heating, the cold emissions can be significantly reduced. Since this mild hybridization also dampens emission-relevant dynamic peaks even when warm (limitation of the ICE dynamics), it is possible to achieve an emission level that justifies talking about "Zero Impact Emission".

3. Electrification of the ICE

In the future, the simultaneous reduction of both pollutant and CO_2 emissions will require significantly enhanced functionalities of the powertrain, which can only be insufficiently represented by the ICE alone. Both automated transmissions and electrification can help to efficiently cover the extended functionalities. These functionalities are no longer exclusively applied within the ICE itself ("Fully Flexible Internal Combustion Engine"), but distributed across the entire powertrain ("Fully Flexible Powertrain"), Fig. 6.

Clever balancing of the complementary properties of electrification and ICE results in a synergetic potential for improvement in terms of reducing both pollutant and CO_2 emissions. Thus, in future the ICE will change "from a lone fighter to a team player".

As a result, especially with a high degree of electrification, a simplification of the ICE will be also possible. If e.g. the lowest load range of the ICE is replaced by purely electric driving or load shift by charging the battery, the layout of the ICE can focus on the area of best specific fuel consumption respectively low specific pollutant emissions (with Gasoline engine e.g. layout of the turbocharger for higher mass flow, possibly omission of variable valve lift, modified layout of variable compression, etc.).

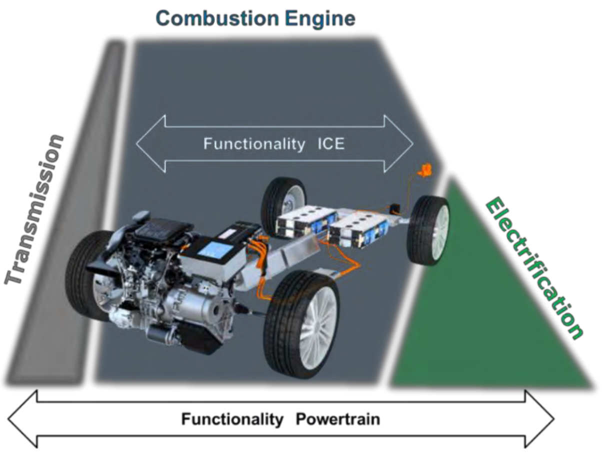

Fig. 6. From "Fully Flexible Combustion Engine" to "Fully Flexible Powertrain" [1]

Already a sufficiently graded automated transmission with a large spread helps to operate the ICE in most of the driving situations in the respectively optimum map area – usually best specific fuel consumption ("Sweet Spot Follower" – yellow area in Fig. 7). With appropriate hybridization, even at low power demand the load point can be shifted towards a high-efficiency range either by electrical recuperation and charging of the battery or, in the case of sufficient battery charge, driven purely electrically (lower green area in Fig. 7).

In the upper load range, of course, the electrical torque can be used to increase the total torque (dashed green line). Regarding emission and fuel consumption reduction, however, it is more sensible to reduce the torque and dynamic demand of the ICE by means of the additional electrical torque at least partially, especially with low engine speeds (upper green area in Fig. 7). This not only allows avoidance of operating ranges with unfavorable performance of the ICE, but also additional synergy effects e.g. a modified design of the turbocharger better matched to the higher flow range (expansion of the stoichiometric operating range). In view of the expected changes in RDE legislation [4], such a "dynamic limitation" of the ICE also gains additional importance for a robust RDE calibration. However, the electrical torque is only temporary, according to the electric energy available, which must be considered in the system design accordingly.

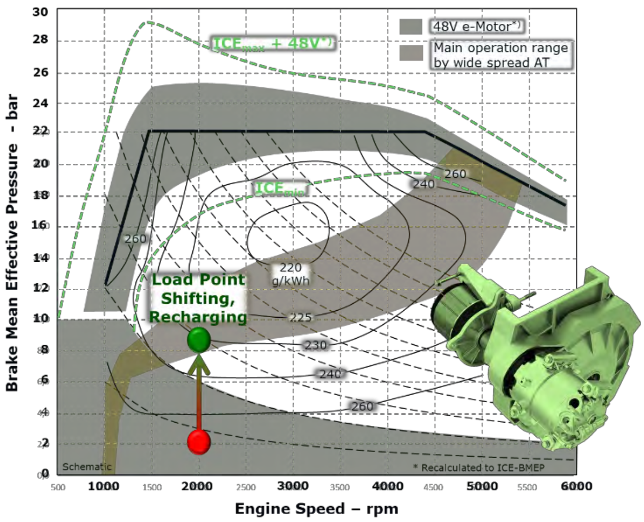

Fig. 7. Interaction of ICE, Automated Transmission and Mild Hybridization (48V)

Depending on the respective ICE, transmission and electrification strategy, different arrangements of the electric motor prove to be the respectively most favorable variant, Fig. 8. Both modular and dedicated solutions are used [5, 6].

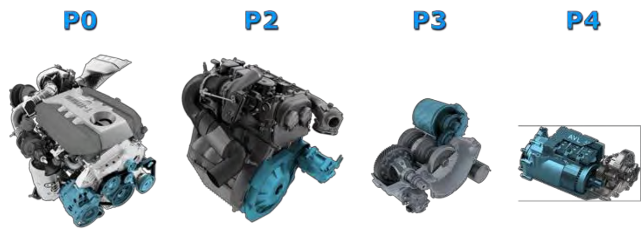

Fig. 8. Electrification of ICE-based powertrain systems

4. Development of the Gasoline Engine

4.1. Challenges

Due to its in stoichiometric operation highly efficient exhaust aftertreatment, the Gasoline engine has so far been much less in the center of public emission discussions than the Diesel engine. However, the new RDE legislation, especially the tightening of Package 3 and 4, represents a huge challenge. Thus, e.g. the dynamic limitation introduced to restrict aggressive driving allows, to a certain extent, even extreme driving maneuvers such as full load drive-off with cold engine. Consequently, reducing the dynamics of the cold drive-off becomes a crucial criterion for safely meeting future RDE requirements.

The strongest temperature and dynamic influence is obtained in the gasoline engine for the number of particles, Fig. 9.

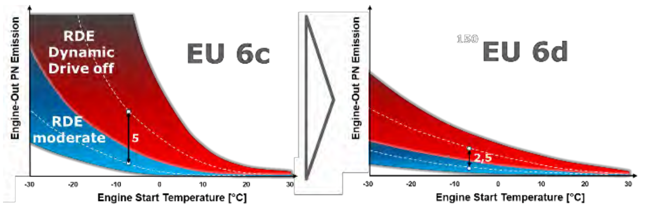

Fig. 9. Influence of start temperature and driving style on the engine-out particulate emissions in the RDE city section – TGDI engines

Since particulate filters for Gasoline engines, at least in the new or freshly regenerated state have significantly lower filtration efficiencies than Diesel particulate filters, a reduction of the particle engine out emissions is still required despite the broad introduction of the particulate filter also with Gasoline engine. By detail optimization both the temperature and the dynamic sensitivity of PN generation could be significantly improved from an EU6c status, Fig. 10 left, towards an EU6d status, Fig. 9 right.

Compared to the Diesel engine, the Gasoline engine has a much higher sensitivity to higher exhaust gas back pressure, which gains in importance through the future requirement for stoichiometric operation in the entire map. Thus, the trade-off between filtration efficiency and exhaust back pressure of the GPF becomes a defining parameter for the Gasoline engine. Fig. 10 shows an overview of different filter types with respective filter soot loadings of 0, 1 and 3 g/l.

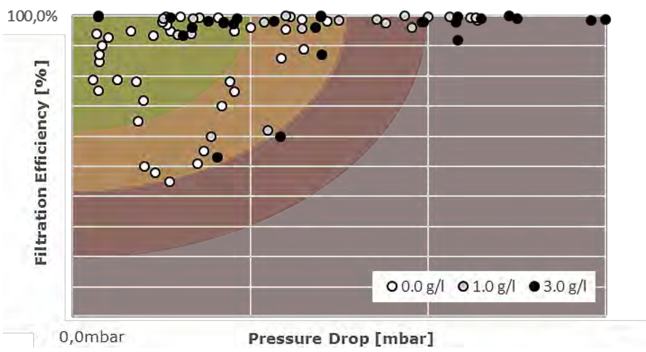

Fig. 10. Trade-off between filter efficiency and exhaust back pressure with different soot loadings

While in the past, high filtration efficiencies were almost inevitably associated with high backpressure (red and yellow areas in Fig. 10), current developments are already leading to much more favorable relations – green area in Fig. 10 – although partially with compromises on filter size. For gas-powered SI-engines this filter problem is eliminated, as from combustion side more or less no particle emission is generated thus increasing the attractiveness of Gas engines additionally.

Finally, the elimination of scavenging strategies necessary to safely comply with RDE-NO_x, requires appropriate compensation in torque and low-speed response, which in turn argues for a "cooperation" between ICE and powertrain electrification.

In general, some measures for the robust RDE fulfillment are in trade-off with the CO_2 emission, the central future development focus of the Gasoline engine. This increases the motivation to use low-cost electrification to reduce CO_2 emissions and to improve existing trade-offs, for example with a different layout of the turbomachinery. Since such mild hybridizations can also improve the robustness of emissions reduction in real world operation at the same time, such systems will form a broad basis for future ICE based powertrains.

4.2. Technology approaches Gasoline engine

The current technical mainstream of Gasoline engines – extended expansion by Miller/Atkinson cycle concepts – will continue in the foreseeable future, but will be further optimized by improved charging systems. In addition to this mainstream technology, however, a certain amount of technology diversification will remain. Variable Compression Ratio VCR, Spark Initiated HCCI, advanced ignition and Ultra High Pressure Injection UHP are additional focus points, Fig.11.

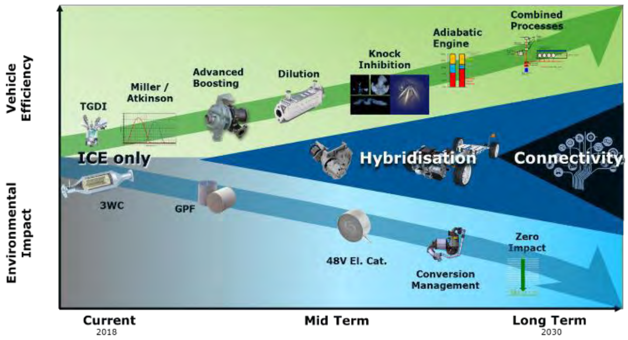

Fig. 11. Technology roadmap Gasoline engine

Once knock can be limited or eliminated isolation of the combustion chamber ("adiabatic engine") can shift energy from the low temperature to the high temperature level. In combined processes these additional energy amounts can be used. Peak efficiency levels of 45% up to 50% can be expected in the future.

Future emission requirements such as lowest particulate emissions or stoichiometric operation in the complete engine map require advanced emission concepts beyond the three way catalyst and the particle filter.

By using an electrically heated catalyst with extended preheating/post heating functionality ("conversion management") as well as by hybridization and connectivity further significant emission reduction up to "Zero Impact Emission" level is possible even for not fully warmed up engines.

Synergy effects with hybridization allow an even more fuel consumption-oriented design of the IC, especially of the charging and combustion processes. Since in future, the ICE must increasingly cover various levels of electrification, an expanded modularization will gain an increasing importance even within the ICE. While in the past, different torque and power levels of the ICE were usually covered with different geometric displacements, the topic of charging enables a power and torque spread without changing the engine geometric displacement. Miller and Atkinson cycle allow a separation of geometric and effective compression ratio. Thus, a widely spread power graduation can be displayed at the same geometric displacement within one engine family. The performance differentiation is primarily based on the extent of "Millerization", the boost pressure, the valve lift curves and the geometric compression ratio, Fig. 12.

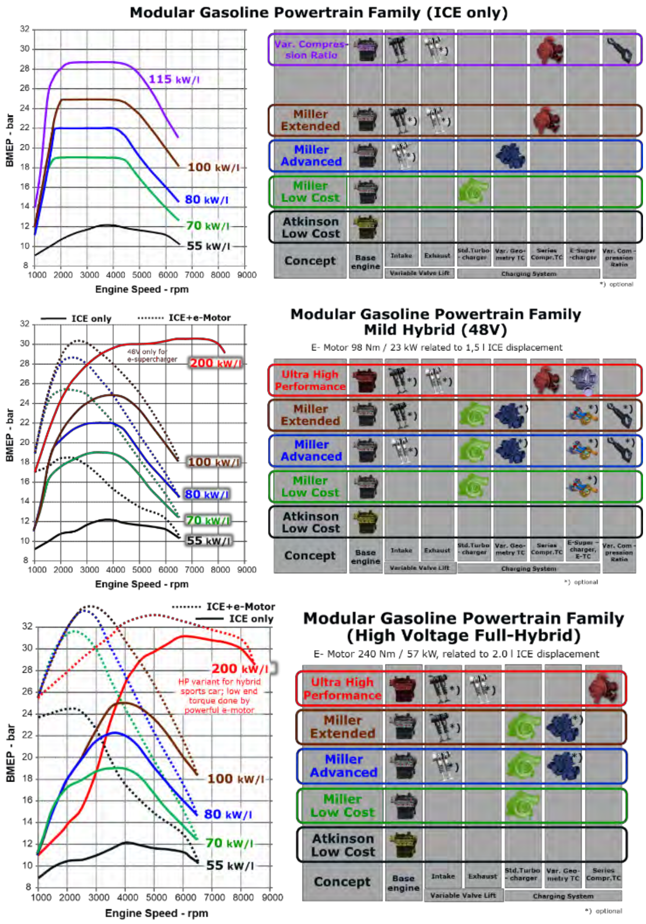

Fig. 12. Modular Gasoline engine concept with different electrification levels

While high torque at low engine speeds is a prerequisite for a fuel economy oriented powertrain layout, it usually results in some compromises with the ICE layout. Thus, an electrical torque assistance at low speeds allows a much more focused orientation of the ICE to the main operating range, Fig. 12 center. In most cases, the charging unit can also be better adapted and if necessary also simplified and the geometric compression ratio can be raised further.

Recovery of exhaust gas energy, for example by means of electrified turbochargers (e-turbo) in combination with the electrified powertrain, is a sensible addition to a further increase in efficiency.

Niche applications with extremely high specific power are made possible by using additional electrical charging. With the increased electrical power of high-voltage full hybrids, this alignment can be taken a step further, Fig.12 lower part. Since considerably higher electrical energies are converted here, an intelligent, preferably predictive energy management is required to assure reproducibility of the acceleration behavior with limited battery capacity.

In contrast to the low speed range, the direct influence of electrification in the rated power range is limited by economically justifiable battery sizes (exception: Plug In Hybrid). However, synergy effects – such as e.g. reduced exhaust back pressure can be used by modified layout of the gas exchange process respectively the turbocharger.

Nevertheless, future legal requirements such as stoichiometric operation in the entire map remain challenging and require either a compromise with CO_2 measures or additional expenses. A variety of measures is – either individually or in combination – is used to reduce the exhaust gas temperature so far that an enrichment for component protection can be avoided. Fig. 13 shows an overview of the stoichiometric power potential of the individual technologies and the cross-influence on the minimum specific fuel consumption.

Active exhaust gas cooling in the form of an integrated exhaust manifold is increasingly becoming the basic technology of turbocharged Gasoline engines, but is limited towards higher performance by the high heat input into the cooling system. Miller timing (early inlet valve closure) provides a broad basis for the implementation of high geometric compression ratio and extended expansion and is primarily used to reduce fuel consumption. Improved gas exchange (Variable Turbine Geometry, "Series Compressor Turbocharger" with intercooler) enables lower charge temperatures and better charging efficiencies. Cooled exhaust gas recirculation improves both the stoichiometric power range and the minimum fuel consumption, but at the same time increases the heat input into the cooling system. Variable geometric compression ratio, especially in conjunction with variable intake valve lift proves to be very effective both in view of stoichiometric power and fuel consumption. And finally, water injection – albeit with respective water consumption – enables stoichiometric operation up to more than 170 kW/l.

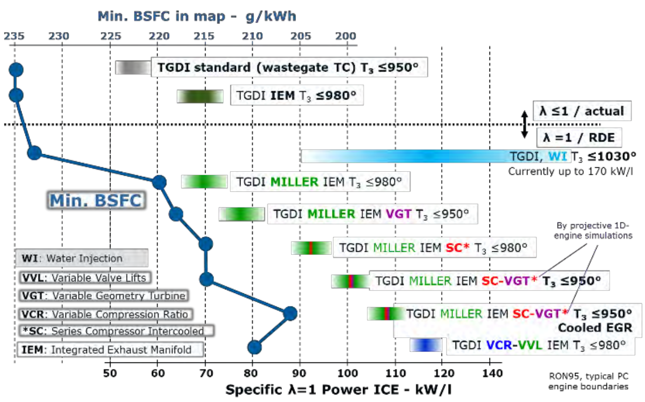

Fig. 13. Measures to increase the stoichiometric power range, RON 95

With increasing electrification, the focus of fuel consumption is shifting from the low load range (for example 2000 rpm, 2.0 bar BMEP) towards higher engine loads to the area of minimum specific fuel consumption. Thus, the ratio of maximum efficiency to maximum specific power becomes a decisive engine parameter, Fig. 14.

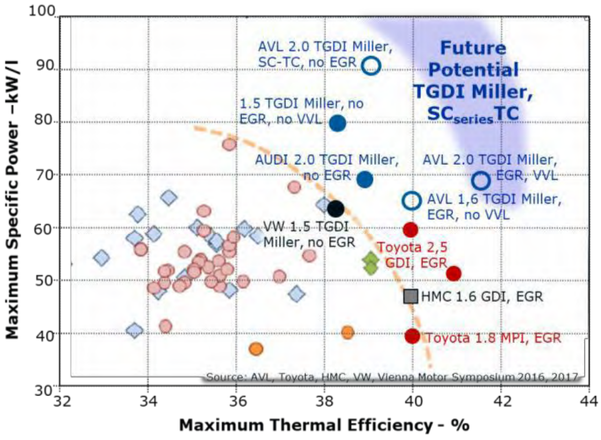

Fig. 14. Trade-off between max. efficiency and max. specific performance

Looking at the state of the art, Miller/Atkinson concepts represent the most attractive low-consumption solutions. With advanced charging systems and refined combustion processes, a significant shift of this trade-off is expected in the future, especially towards higher specific performance. However, the requirements of stoichiometric full load operation will result in increased differentiation in these specific performance levels. Although the concept engines (hollow circles in Fig. 14) are already designed for stoichiometric operation, stoichiometric full load is only applied to a few series engines yet.

While overall efficiencies of up to 45% appear feasible in the medium term for current developments, in the research stage total efficiencies of more than 50% are conceivable in the long term with complex processes. This significantly extends the trade-off between maximum efficiency and specific performance compared to the current state of the art, Fig. 15.

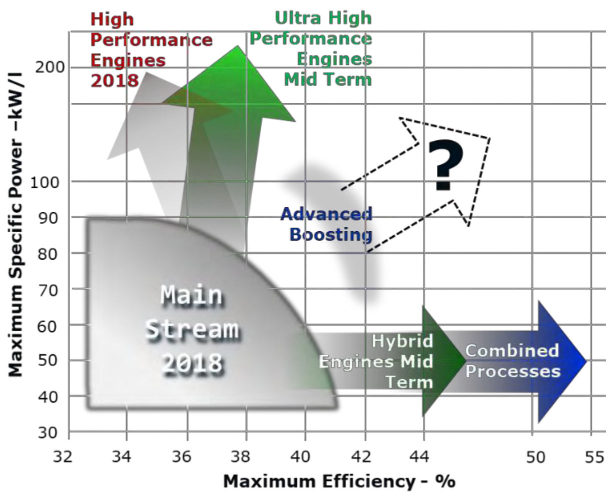

Fig. 15. Trade-off between maximum efficiency and specific power of Gasoline engines

The benchmark here are Formula 1 engines, which – not restricted by the limitations of series solutions and emission compliance – already achieve such efficiencies. If, on the other hand, one considers the boundary conditions of series engines, an increase in the compression ratio is a central topic for improving efficiency. A technically comparatively simple solution is a monovalent CNG engine that converts CNG's high anti-knock properties into additional efficiency improvements in addition to its chemical CO_2 advantage. This is a technically ideal solution that in future will also offer the possibility of using CO_2-neutral gas produced from renewable energies distributed in basically existing networks that are easy to expand. Unfortunately, this approach so far had poor customer and political resonance and thus in the past a restrained market acceptance. Hopefully CNG finally will achieve the importance it deserves.

Another much discussed approach are lean concepts. Since there are additional question marks for any form of lean operation due to the current NO_x emission discussions, avoiding knocking combustion as an enabler for higher compression may be a more promising route. However, many of the conventional knocking methods are based on charge cooling and thus from the process point of view, they are a thermodynamic loss which also increases the required cooling capacity. A practically "knock-free" Gasoline engine would enable a significant paradigm shift: an increasingly adiabatic engine which transfers the wall heat losses into exhaust gas enthalpy and allows the respective utilization of this exhaust gas energy in a subsequent expansion process, Fig. 16 upper part.

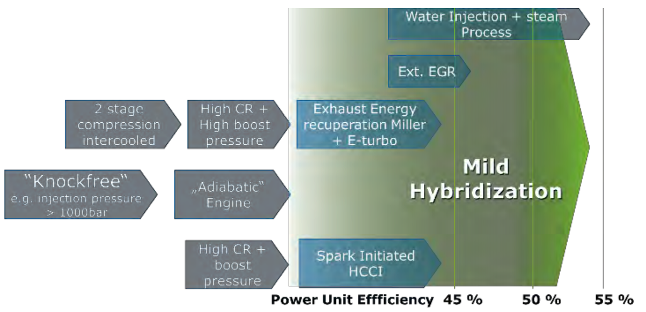

Fig. 16. Technology approaches for further increased efficiency of the Gasoline engine

Such a knock-reduced Gasoline engine would be also an ideal basis for homogeneous auto-ignition, Fig. 16 lower part. As early as 2004, AVL had demonstrated that spark ignition-triggered "auto-ignition" (AVL JCAI-Jet Controlled Auto Ignition) dramatically improves the robustness and stability of conventional HCCI technologies. However, since NOx emissions require lean exhaust aftertreatment, such a system has not been prioritized furthermore but has been switched to more emission-stable stoichiometric approaches. Another possibility for improving the knocking behavior, and also the charge dilution tolerance, is, for example, a pre-chamber spark plug, Fig. 17.

By appropriate alignment of the ignition jets, the combustion can be specifically accelerated in the direction of knock-critical areas and thus the knocking behavior can be improved. An advancement of 50% mass fraction burnt point of up to 8°CA was achieved.

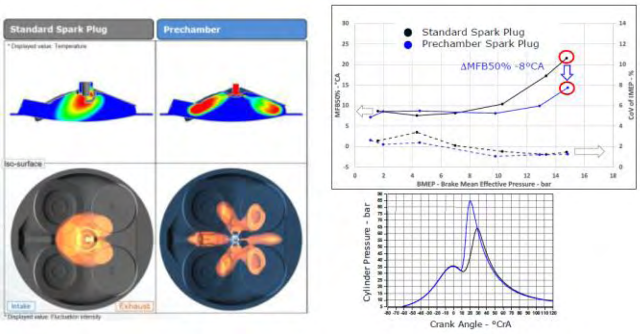

Fig. 17. Pre-chamber ignition

The most efficient measure to prevent pre-ignition and knocking, however, is the introduction of the fuel only at the end of the compression immediately before ignition, Fig. 18. The local residence time of the fuel in knock-critical areas is too low to trigger pre-ignition or knock => practically "knock-free" Gasoline engine.

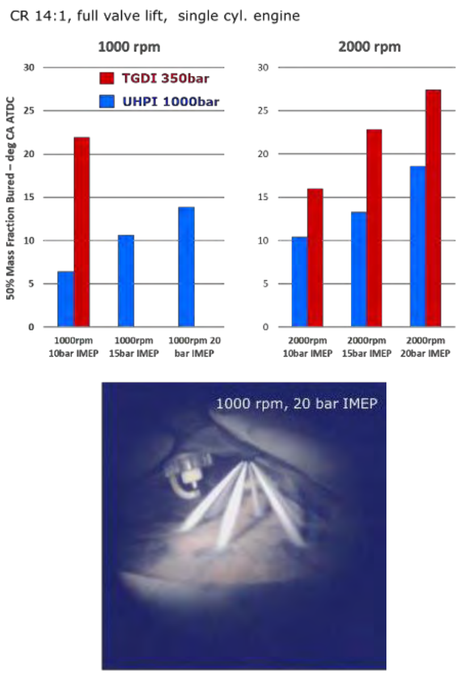

Fig. 18. "Knock-Free Engine"; Ultra High Injection Pressure

However, the very late introduction and the necessary preparation and distribution of the fuel requires extremely high injection pressures. With injection pressures > 800 bar and an adequate system design, a sufficient mixture formation quality and homogenization can be achieved even at very late injection.

Fig. 19 shows the effect of such a knock-reduced combustion process in the engine map. With increasing the geometrical compression ratio with a standard Miller combustion system, e.g. from 12 to 14, shifts the area of best BSFC ("sweet spot") towards lower engine loads, however, compromises the high load behavior quite significantly especially at low speeds, Fig.19 center.

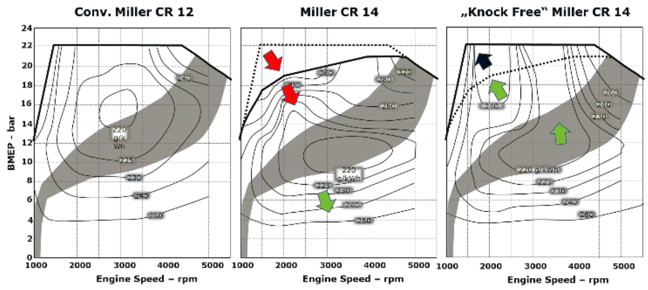

Fig. 19. Impact of a knock reduced combustion process in the engine map, no EGR

With an "ICE only" powertrain, the reduced full load torque would require a shorter drive ratio for comparable performance and thus equalize the fuel consumption benefits in the lower map range again. With a Hybrid, low-speed assistance can be provided by an electrified powertrain. Nevertheless, disadvantages would remain in the higher load range.

A knock-reduced combustion method can fully exploit the advantages of an increased compression in the lower load range, but avoids the disadvantages in the higher load range and at full load, Fig.19 right hand. Thus, such knock-reduced combustion processes represent the next step in Miller concepts.

Conclusions

Regarding the improvement of real world emissions, the transition to RDE proves to be much more effective than lowering the certification values on the chassis dynamometer – by fulfilling the current RDE legislation, in real driving conditions, the RDE-induced widespread introduction of the particulate filter on the Gasoline engine and the significantly tightened specifications for cold and high load emissions result in essential pollutant reductions. It can be assumed that such vehicles will certainly fall below the imission limits even in today's imission-critical zones.

Since the extended boundary conditions of RDE legislation are no longer limited to statistically relevant driving conditions only, but can cover virtually all possible modes of operation, the short-term fulfillment of these requirements is an incredible challenge for the automotive industry.

The uncertainty of the future markets' reaction calls for the development of modular structures of both with ICE´s, transmissions and electrification components.

In the long term, new potentials of the ICE can be seen with regard to both pollutant and CO_2 emissions. In particular, synergy effects with electrification and the networking of powertrain control with all vehicle-relevant traffic and environmental information – "Internal Combustion Engine 4.0" – enables both further fuel consumption improvements and an emission behavior that can be described as "Zero Impact Emission". This means that future combustion engines will not have a negative impact on the pollutant imission situation. With the e-fuels theme, the combustion engine also has the potential in the medium and long term to become both CO_2-neutral and pollutant-neutral.

Nomenclature

BEV	battery electric vehicle
CNG	compressed natural gas
DI	direct injection
ICE	internal combustion engine
RDE	real driving emission
SI	spark ignition

Bibliography

[1] LIST, H.O. Antriebssysteme im Wandel. 39. Internationales Wiener Motorensymposium 2018.

[2] Bundesministerium für Wirtschaft und Energie; Bundesministerium für Bildung und Forschung; Plattform Industrie 4.0: Was ist Industrie 4.0?, https://www.plattform-i40.de/I40/Navigation/DE/Industrie40/WasIndustrie40/was-ist-industrie-40.html, 2018.

[3] KUFFERATH, A., KRÜGER, M., NABER, D. et al. Der Diesel Powertrain auf dem Weg zu einem vernachlässigbaren Beitrag bei den NO_2-Immissionen in den Städten. *39. Internationales Wiener Motorensymposium* 2018.

[4] COMMISSION REGULATION (EU) …/… of XXX amending Directive 2007/46/EC, Commission Regulation (EC) No. 692/2008 and Commission Regulation (EU) 2017/1151 for the purpose of improving the emission type approval tests and procedures for light passenger and commercial vehicles, including those for in-service conformity and real-driving emissions and introducing devices for monitoring the consumption of fuel and electric energy (Ares (2018)1297632).

[5] SCHÖFFMANN, W., SORGER, H., WEISSBÄCK, M., Effiziente und kostenoptimierte Antriebseinheit für 48V-Systeme“. *MTZ.* 2017, **5**.

[6] PELS, T., DAVYDOV, V., ELLINGER, R. et al. 48V – where to place the e-machine?. *11th International MTZ Conference on Future Powertrains*, 2017.

Hubert Friedl, DEng. – AVL List GmbH.
e-mail: *hubert.friedl@avl.com*

Paul Kapus, DEng. – AVL List GmbH.
e-mail: *paul.kapus@avl.com*

Günter Fraidl, DEng. – AVL List GmbH.
e-mail: *gunter.fraidl@avl.com*

Article citation info:
ELGHAWI, U., MAYOUF, A., TSOLAKISC, A. Hydrocarbon species in SI and HCCI engine using winter grade commercial gasoline. *Combustion Engines*. 2020, **180**(1), 17-24. https://doi.org/10.19206/CE-2020-103

Usama ELGHAWI
Ahmed MAYOUF
Athanasios TSOLAKIS

CE-2020-103

Hydrocarbon species in SI and HCCI engine using winter grade commercial gasoline

The study provides a qualitative and quantitative analysis of the C5-C11 hydrocarbon species generated in Spark Ignition – Homogeneous Charge Compression Ignition (SI/HCCI) gasoline direct injection (GDI) engine at range of operating conditions. The presented results and data were obtained from the combustion of winter grade commercial gasoline containing 2% w/w ethanol (C_2H_5OH) for the engine operated in steady-state, fully warmed-up condition. The hydrocarbon analysis in exhaust gases was executed on a Gas Chromatography-Mass Spectrometer (GC-MS) apparatus directly connected to the engine exhaust via heated line.

The highest concentration of the total hydrocarbon emissions was obtained under low load HCCI engine operation at stoichiometric fuel-air ratio. The major hydrocarbon compounds detected in the collected samples were benzene, toluene, p-xylene, and naphthalene. Benzene originates from the incomplete combustion of toluene and other alkylbenzenes which are of considerable environmental interest.

During the SI engine operation, increase of the engine speed and load resulted in the increase of benzene and the total olefinic species with simultaneous decrease in isopentane and isooctane. The same trends are seen with the engine operating under HCCI mode, but since the combustion temperature is always lower than SI mode under the same engine conditions, the oxidation of fuel paraffin in the former case was less. As a result, the total olefins and benzene levels in HCCI mode were lower than the corresponding amount observed in SI mode. Aromatic compounds (e.g., toluene), except for benzene, were produced at lower levels in the exhaust when the engine speed and load for both modes were increased.

Key words: *homogeneous charge compression ignition (HCCI), Gas chromatography-mass spectrometer (GC–MS), hydrocarbon speciation, regulated and unregulated emissions*

1. Introduction

Individual hydrocarbon species from the combustion of fuel such as oxygenated and polycyclic aromatic hydrocarbons (formaldehyde, acetaldehyde, benzene, 1,3 butadiene and polycyclic organic material) have been reported as health risk components.

Benzene enrichment from aromatic fuels is of considerable environmental interest. A risk assessment by Johnson et al. [1] indicates that an exposure of 1–5 ppm in ambient air for 40 years is associated with an increased risk of acute myeloid leukaemia. Based on the epidemiological evidence, benzene is considered as a human carcinogen (group 1) by the International Agency for Research on Cancer (IARC). Benzene and 1,3-butadiene are classified by the US Environmental Protection Agency (EPA) as group B2 probable human carcinogen of medium carcinogenic hazards [2]. Although for Toluene the pronounced toxic effects of high and long-term exposure are well-known [3, 4], the health effects of short-term exposure remain uncertain. Toluene, ethylbenzene and xylenes negatively affects the central nervous system, disturbed coordination, causes drowsiness, headache [5, 6] and mental disorders ATSDR [7].

Although, in modern vehicles corrective solutions in eliminating pollutants are available, such as the use of catalytic converters, a preventive technology is always preferable, which requires a good understanding of the in-cylinder air-fuel mixing and combustion processes. Detailed hydrocarbon emissions analysis, including speciation and quantification, is a powerful tool that can be used to understand the significance of the fuel composition and additives, engine operating conditions and emission control hardware, on the hydrocarbon component formation and help in the optimization of the combustion process.

Gasoline-fuelled engines will continue to be one of the main choices for passenger cars, therefore improving fuel efficiency and reducing the emission of toxic non-regulated yet compounds are of great importance [8]. Gasoline Homogeneous Charge Compression Ignition (HCCI) Engines have the potential to reduce significantly nitrogen oxides (NO_x) emission and improve fuel consumption, under certain speed-load operating conditions in comparison to Spark Ignition (SI) operating mode [9].

Studies on the analysis of the hydrocarbon species in the exhaust gas of the SI engines started as early as the middle of 1950s by Walker and O'Hara [10]. Much work has been completed using the (GC–MS) technique by researchers in automotive industry

One of the early studies on the hydrocarbons species in the HCCI engine exhaust from the combustion of pure hydrocarbon components was carried out by [11]. Three different saturated hydrocarbons (n-pentane, n-hexane, and n-heptane); were studied; and their ignitability was also investigated. In the case of n-hexane fuel, at low-temperature combustion, olefins such as 1-hexene and 2-hexene and aldehydes were the products of oxidation, and olefins such as 1-butene, propylene, and ethylene were the product of decomposition (Scheme I). In the case of n-heptane fuel, the percentage olefins formed is less than the corresponding percentage formed from n-hexane combustion; 2-ethyl-3-methyl-oxetane and other cyclic ethers were also detected. The results obtained from the n-pentane oxidation process were similar to the results obtained from n-hexane, but the accumulation of olefins and aldehydes during the low-temperature oxidation period was greater than that seen in n-hexane case.

Received 25 September 2019; Received in revised form 12 December 2019; Accepted 15 January 2020
Available online 30 March 2020

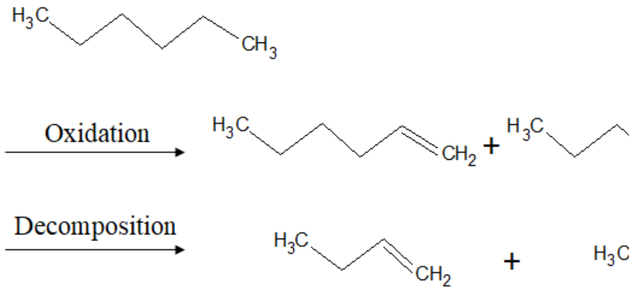

Scheme I. Oxidation and reduction of n-hexane

Kaiser et al. [12] showed that; the major primary products formed in the case of iso-pentane fuel, using HCCI engine single cylinder, were; 17% 2-methyl-1-butene, 10% 3-methyl-1-butene, 9% 2-methyl-2-butene, 8% isobutene, 4% 2-butene, and 3% 3-methyl-tetrahydrofuran, in addition to high yield formaldehyde (29%). In the case of iso-octane, the major primary products were: 39% isobutene and 29% formaldehyde.

The results of hydrocarbon speciation from HCCI engine revealed that the unburned fuel was the main product seen in the exhaust followed by methane [13]. Oxidized and decomposed products were also detected; the highest concentration of olefins resulted from the combustion was ethylene and the highest concentration of aldehydes was formaldehyde. Naphthenes and other aromatics were also detected in the exhaust gases but with very small concentrations.

Dec et al. [14], drew detailed exhaust speciation measurements from an HCCI engine fueled with isooctane over a range of air/fuel ratio. Similar to n-heptane, the unburned isooctane was by far the largest contributor to the emissions at all fueling rates, followed by formation of 2-methyl-1-propene (isobutene), which is a known breakdown product of isooctane. Different HC species were detected and identified as breakdown products of isooctane (e.g. methane, ethylene, and propylene).

Shibata et al. [15] examined the effects of the fuel components structure on auto-ignition characteristics and HCCI engine performance. Thirteen different hydrocarbons, four different paraffins, three different naphthenes, and six different aromatics, were chosen for this investigation. The results showed the relation between the hydrocarbon structure and research octane number. It was clearly shown that the ignitability differences of the hydrocarbon were mainly caused by the straight chain length of alkanes and side chains, the ring size of naphthenes, and the Benzene ring in aromatics.

Hunicz and Medina [16] provide comprehensive quantitative data on hydrocarbon species concentrations in exhaust gases from a (SI/HCCI) engine fuelled with gasoline. A Fourier transform infrared gas analyser was used for detailed speciation of hydrocarbons upstream and downstream of TWC. A fractions of selected species in HCs emissions for variable operating conditions was detected (CH_4, C_2H_2, C_2H_4, C_2H_6, C_3H_6, C_4H_6, n-C_5H_{12}, isoC_5H_{12} and $C_6H_5CH_3$). However, emission of all species are higher for HCCI combustion mode under late injection strategy than for SI combustion.

Yang et. al. [17] concluded that unburned hydrocarbon emissions in HCCI engine are strongly dependent on the parent fuel's autoignition chemistry, with less dependence on the peak bulk temperature, in contrast to the CO emissions.

In our previous work Elghawi et al. [18, 19], we reported on the relationship between the commercial gasoline fuel components containing 2% w/w ethanol and the combustion products in the engine exhaust of carbonyl emissions as well as vapour-phase and particulate-bound PAHs profile generated by the same engine and using the same winter grade commercial gasoline.

The objective of this study is to identify and quantify the exhaust hydrocarbon species ranged from C_5 to C_{11}, formed in the combustion of the winter grade commercial gasoline during SI and HCCI combustion mode.

2. Experimental

2.1. The Engine

The experimental engine was a 3 L gasoline direct-injection (wall guided) V6 engine; the engine specifications are listed in Table 1. The engine was coupled to a Froude EC 38 eddy current dynamometer. The valve-train was modified to permit operation in HCCI mode by the provision of a cam profile switching mechanism. This cam profile switching (CPS) system was used to switch between SI and HCCI modes. This system allowed on-line switching of valve lift from 9 mm (SI operation) to 3 mm (HCCI) operation. The HCCI operation was achieved by internal EGR, using negative valve overlap that trap exhaust gases in order to retain enough energy for auto-ignition. The penalty of HCCI operation by the trapping of EGR is typically the limitation of its operating envelope (Fig. 1). At the low boundary, it is limited by misfire due to limited tolerance for EGR. Whereas, at the high boundary the limitation is typically due to knock tendencies. The variable valve timing system of the engine made it possible to change the valve timing for the inlet and exhaust valves within a 60 crank angle (CA) degree range. The HCCI starting procedure involves a warm-up period when the engine is operated in SI mode until the oil and coolant temperatures reach 90^{o}C. In HCCI mode the engine was operated with a wide-open throttle significantly reducing pumping losses. A DSPACE-based system coupled to a computer using MATLAB/SIMULINK software was used to control the engine parameters during operation and data acquisition. The fuel flow rate to the engine was measured with the use of an AVL gravimetric meter. The fuel injection pulse width was adjusted by the engine management system to maintain the required engine operation condition and A/F ratio.

Table 1. Engine specification summary

Description	Specification
Engine type:	Jaguar research V6, 24-V, GDI
Bore:	89 mm
Stroke:	79.5 mm
Fuel:	Gasoline, RON 95
Compression ratio:	11.3
Intake valve timing:	Variable
Exhaust valve timing:	Variable
Intake temperature:	Variable

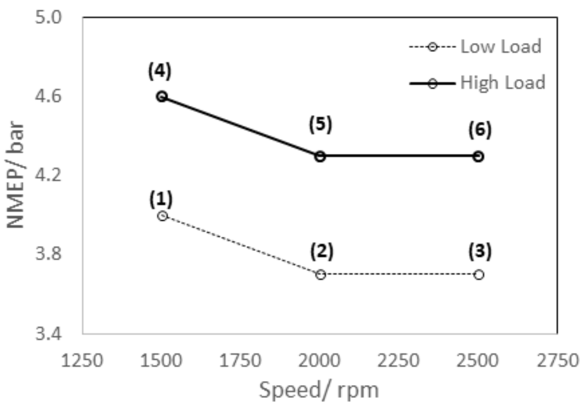

Fig. 1. Selected points on speed/load map from this study

2.2. Gasoline Fuel used

The fuel used in this study was standard unleaded gasoline, its research octane number (RON) is 95. The properties of winter grade commercial gasoline containing 2% w/w ethanol (C_2H_5OH) are listed in Table 2.

Table 2. Properties and composition of gasoline used as received from the distributed company

Winter grade gasoline	% w/w	RON
Oxygen	0.74	
Alkanes	57	
Aromatic (total)	36	
Toluene	12	120
p- and o-Xylene	11	145, 120
Trimethylbenzene	10	> 100
Other aromatics	3	
Alkenes	5.7	
Additives	<1.0	

The composition and concentration of winter grade commercial gasoline used in this study were analyzed by GC-MS, Hewlett-Packard HP 5890 series II connected to MS, TRIO-1. The gas-chromatographic parameters used for speciation of the commercial gasoline used in this study presented in Table 3, and the result of the analysis is shown in Fig. 2.

Table 3. Gas-chromatographic parameters used for speciation of commercial gasoline

Parameters	HP 5890 series II
Column:	J&W Scientific DB-1: 50 m; 0.32 mm ID; 0.25 μm film
Detector:	MS, TRIO-1 Ion Source 200 ^{0}C; 40: 450 amu
Oven ramp:	• 80 ^{0}C initial; 3 minutes hold • 4 ^{0}C /minute to 250 ^{0}C • 5-minute final hold (Flush) • Total run is 50 minutes
Flow Rate:	6 ml/minute; He

Identifying the hydrocarbon components in the fuel is the key step in speciation HCs in the engine exhaust. By using retention time of some known compounds and the NIST library together, the peaks in the chromatogram of the analyte were identified and assigned to their proper compound. The fuel used consists primarily light aliphatic hydrocarbons (butane, pentane, methyl-pentane, hexane, methyl-hexane, heptane and octane), aromatic compounds (toluene, p&o-xylenes and trimethyl-benzenes), and small amount of olefinic hydrocarbons (pentenes, hexenes, heptenes, octenes and nonenes).

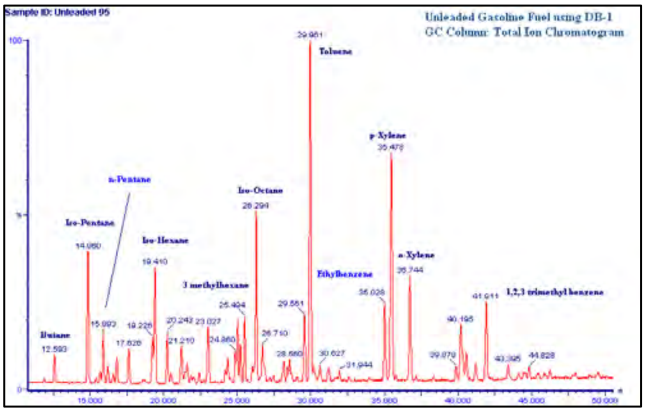

Fig. 2. GC-MS characterisation of the components in used commercial gasoline fuel

2.3. Analysis of Regulated Gases

A Horiba MEXA 7100 DEGR equipped with a heated intake line was used to measure regulated emissions, including total hydrocarbon, carbon monoxide, carbon dioxide, NO_x and oxygen in the exhaust. The heated line and pre-filter are maintained at 190ºC. The analyzer equipped with flame ionization detector (FID) was used to measure total hydrocarbon in ppm methane (CH_4) equivalent. The measurement of HC represents wet HC concentration. Carbon monoxide (CO) and carbon dioxide (CO_2) were analyzed by non-dispersive infrared (NDIR) detector and NO_x by a chemiluminescence detector (ClD). The λ (air/fuel ratio relative to stoichiometric), temperature and pressure of the exhaust gases at the engine exhaust manifold were also measured. The system was calibrated using suitable bottled span and zero calibration gases by using British Oxygen Company (BOS) standards with different concentrations.

The calculations of specific emissions are based on the Directive 1999/96/EC of the European Parliament and of the Council of the European Union [20]. This document describes the procedures and rules which should be applied when gaseous emissions from internal combustion engines are considered.

2.4. Speciation of Hydrocarbon C_5–C_{11}

Hydrocarbon speciation was performed online by a GC-MS, Fisons GC 8000 series connected to MS, Fisons MD 800. The gas samples were introduced via the heated line at 200^{0}C into a six port Valco valve outfitted with a 1ml sample loop. A 30-meter long x 0.53 mm i.d. capillary column with a 3μm film thickness DB-1 was used, which allowed the polar and non-polar compounds to be detected simultaneously. The column head pressure was maintained at 35 psi. The helium carrier gas flow rate was pressure controlled with a flow rate of 6 ml/min. The component standards were generally stable in concentration when the gas was released from the cylinder at this flow rate. The temperature program settings (Table 4) permits to flush out the heavier hydrocarbon to cope with different engine operational mode. Standard mixtures of paraffin's, olefins and HCs with known concentrations were used as a reference sample. The retention time of each species were calibrated daily before each set of experiment by analyzing a standard sample of gases that contain 15 components purchased from British Oxygen Company (BOS). The concentration of the components of standard sample were generally stable when the gas was released from the cylinder at 6 ml/min flow rate. The runtime was 22 minutes and the retention time of detected species is given in Table 5. The chromatograms obtained for the emission products from both operation modes of the engine at the same speed and load points at NMEP 4.0 bar and 2000 rpm engine speed and running at lambda = 1 are shown in Fig. 3, and the hydrocarbon species (C_5–C_{11}) are presented in Table 4.

Table 4. Gas-chromatographic parameters used for detection of C_5–C_{11} compounds

Parameters	GC 8000 series
Column:	DB-1, 30 m; 0.53mm ID; 3µm film
Detector:	MS, Fisons MD 800 Ion Source 200°C; 35: 200 amu
Oven ramp:	• 40°C initial; 2 minutes hold • 10°C /minute to 200°C; 5 minutes hold • 5-minute final hold (Flush)
Flow Rate:	6 ml/minute; He

Table 5. Retention time of standard sample components

Peak No	Compound	Retention Time (minute)
1	Iso-Butane	3.231
2,3	1,3-Butadiene + n-Butane	3.401
4	Iso-pentane	4.161
5	1-Pentene	4.321
6	n-Pentane	4.471
7	n-Hexane	6.012
8	Benzene	7.233
9	n-Heptane	8.173
10	Iso-octane	8.785
11	Toluene	9.534
12	EthylBenzene	11.54
13	p-xylene	11.72
14	Naphthalene	18.19
15	Methyl-naphthalene	20.66

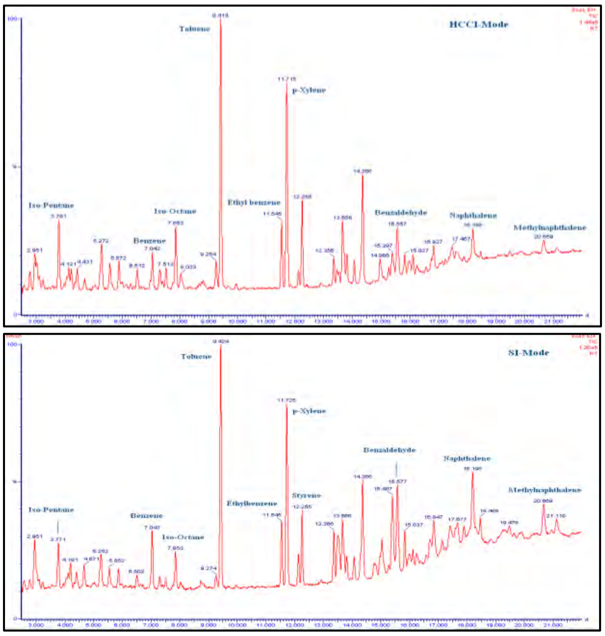

Fig. 3. The chromatograms obtained for the emission products from HCCI (upper) and SI mode (lower) of the engine at the same speed and load points, and running at lambda = 1

The area of each peak represents the concentration of that specific organic compound. Mass spectrometer (DM-800) was used as a detector; the VG Mass-Lab software was used to acquire and integrate the basic gas chromatographic data. These important compounds are the only compounds that was possible to detect using J&W scientific DB-1 column.

2.5. Engine Operation Conditions

One great challenge of implementing HCCI combustion is the limited operating range in which HCCI combustion is feasible compared to conventional SI operation. Six-speed/load engine test points (Fig. 1) were selected for the emissions speciation as shown in Table 6 and 7, where NMEP is Net Indicated Mean Effective Pressure.

Table 6. Operation Conditions and Parameters of the V6 Engine in SI and HCCI modes (all for λ = 1.0)

Common conditions			SI mode						HCCI mode					
Point	Speed rpm	NMEP (bar)	Total HC ppm eq. to CH_4	CO %	CO_2 %	NO_x ppm	O_2 %	Exh. Temp °C	Total HC ppm eq. to CH_4	CO %	CO_2 %	NO_x ppm	O_2 %	Exh. Temp °C
(1)	1500	4.0	1920	0.63	13.84	420	1.06	572	3400	0.52	14.01	42	1.19	382
(2)	2000	3.7	1760	0.88	13.74	830	1.05	601	3040	0.55	13.92	75	1.19	384
(3)	2500	3.7	1730	0.75	13.80	1080	1.02	641	2830	0.68	13.92	114	1.10	398
(4)	1500	4.6	2260	0.69	13.84	630	1.09	591	2660	0.62	14.17	166	0.95	402
(5)	2000	4.3	1960	0.76	13.81	1040	1.07	624	2190	0.63	14.21	104	0.80	404
(6)	2500	4.3	1430	0.70	14.36	1140	0.86	662	1640	0.47	14.39	163	0.74	432

Table 7. Operation Conditions and Parameters of the V6 Engine in SI and HCCI modes (all for λ = 1.0). Normalized emission values and fuel consumption

Common conditions			SI mode				HCCI mode			
Point	Speed rpm	NMEP (bar)	HC g/kWh	CO g/kWh	NO_x g/kWh	Fuel Consumption g/hr	HC g/kWh	CO g/kWh	NO_x g/kWh	Fuel Consumption g/hr
(1)	1500	4.0	7.30	34.8	4.2	3500	12.70	23.6	0.20	3000
(2)	2000	3.7	7.00	41.4	7.8	3900	10.10	25.4	0.09	3300
(3)	2500	3.7	6.10	36.6	9.8	4400	9.10	27.2	0.10	3700
(4)	1500	4.6	7.50	35.2	7.6	4400	8.90	26.7	1.40	3800
(5)	2000	4.3	7.30	36.4	10.0	5100	7.40	27.0	0.80	4600
(6)	2500	4.3	5.40	35.4	11.1	5500	6.00	21.2	1.30	4900

Table 8. Measured species in the exhaust at different conditions in SI and HCCI modes (ppm)

SI mode						
Testing point	Point (1)	Point (2)	Point (3)	Point (4)	Point (5)	Point (6)
Speed/ rpm	1500	2000	2500	1500	2000	2500
NMEP (bar)	4.0	3.7	3.7	4.6	4.3	4.3
Benzene	128	141	151	148	155	165
Toluene	382	331	319	400	358	262
C_6H_6 % in C_1–C_{11}	6.7 %	8.0 %	8.7 %	6.5 %	7.6 %	11.5 %
C_7H_8 % in C_1–C_{11}	19.9%	18.8%	18.4 %	17.7 %	18.2 %	18.3 %
Total HC (C_1–C_{11})	1920	1760	1730	2260	1960	1430
HCCI mode						
Benzene	38	76	81	79	91	113
Toluene	608	512	447	434	334	219
C_6H_6 % in C_1–C_{11}	1.1 %	2.5 %	2.8 %	2.9 %	4.1 %	6.9 %
C_7H_8 % in C_1–C_{11}	17.8 %	16.8 %	15.8 %	16.3%	15.3 %	13.4 %
Total HC (C_1–C_{11})	3400	3040	2830	2660	2190	1640

3. Results and discussion

3.1. Speciation and Quantification of Heavier Hydrocarbon (C_5–C_{11})

The benzene mole fractions increased by increasing the operation load (Table 8). Benzene results from the incomplete combustion of toluene and other alkyl-benzenes, as observed by Kaiser et. al. [21]. The formation of benzene during combustion of the fuel used in this study that contains < 1.0 % benzene explains its observed enrichment in the exhaust relative to other aromatic fuel components available in this commercial gasoline fuel. Emission of benzene increase by increasing the engine speed and load and constitutes an appreciable fraction of the total emission (Table 8). In our work; the observed benzene concentration; is ranging from 38 ppm in case of HCCI mode point (1) to 165 ppm in case of the engine operation on SI mode point (6). This difference in the concentration is due to the increased post-flame oxidation in SI mode, which explains why in SI mode benzene formation is favoured over toluene. This behavior was also observed by Villinger et al. [22].

Table 9. Hydrocarbon species (C_5–C_{11}) at NMEP 4.0 (bar) and 2000 rpm engine speed, of the V6 Engine in SI and HCCI modes and for λ = 1.0

Hydrocarbon species	HCCI mode (PPM)	SI mode (PPM)
Iso-pentane C_5H_{11}	102	38
Benzene C_6H_6	82	148
1-pentene C_5H_{10}	23	27
n-pentane C_5H_{12}	61	46
n-hexane C_6H_{14}	57	33
Iso-octane C_8H_{18}	18	83
Toluene C_7H_8	423	344
Ethylbenzene C_8H_{10}	89	123
p-xylene C_8H_{10}	421	305
Naphthalene $C_{10}H_8$	309	251
Methyl naphthalene $C_{11}H_{10}$	211	97
Total C_5–C_{11}	1796	1495
Total C_1–C_{11}	2615	1860
Percentage of C_5–C_{11}/C_1–C_{11}	68.7%	80.3%

The engine operation at HCCI mode follows the same trend as in the SI mode (Table 6 and 8), but since the combustion temperature is always lower for HCCI (Table 6), the oxidation of fuel paraffin is less. As a result, the amount of total olefins, methane and benzene are lower than in SI mode, for instance the total HC at point (1) in HCCI mode was 3400 ppm and in SI mode was 1920 ppm (Table 8). Tailpipe studies observed that the exhaust benzene emissions are dependent on the benzene and the total aromatics content of the fuel [23, 24]. Although benzene currently is not regulated, it has raised health concern especially if generated in appreciable quantities [25, 26].

For toluene as well as for the other aromatics (e.g. xylenes) except benzene, there is a decrease in the exhaust concentration when both engine speed and load conditions are increased, a trend seen in both combustion modes. In the SI mode the concentration of toluene is always lower under the same operation conditions. Both toluene and xylene, are contributing in the formation of benzene due to their aromatic based structure. Schuetzle et al. [27] showed that a substantial increase in benzene concentration was observed when toluene or xylene is added to the gasoline fuel.

3.2. Formation of Hydrocarbon and regulated emissions in SI and HCCI modes

In gasoline engines (SI/HCCI) under stoichiometric conditions, the balance of the HC emissions from paraffinic or alkanes, (more than half of the composition of the fuel in this study) consists primarily of olefins formed by β-scission of C-C bonds of the higher molecular weight fuels; followed by H-atom abstraction. It was concluded by Kaiser et al. [21, 28, 29] that for alkanes, β-scission and H-atom loss reactions play important roles in determining the combustion products emitted from the exhaust once an alkyl radical is formed. To a lesser extent, disproportionation reactions forming methyl radicals may generate C_2H_4 from highly branched alkanes such as iso-octane [21]. Due to the different molecular structures of parent paraffines, the H-abstraction results in a variety of alkyl radicals. The alkyl radicals are consumed in three parallel paths: (i) abstraction of another H-atom from an alkyl radical by another alkyl radical to form an olefin, (ii) abstraction of another H-atom from an alkyl radical by oxygen to form an olefin and a hydroperoxy radical, and (iii) oxygen addition to the radical to form an alkyl peroxy radical (scheme II).

$$\mathrm{R-CH_2-CH_2-CH_2-R'} \longrightarrow \mathrm{R-CH_2^{\circ}+CH_2^{\circ}-CH_2-R'} \quad (\beta-\text{scission})$$

$$\mathrm{R-CH_2^{\circ}+CH_2^{\circ}-CH_2-R'} \longrightarrow \mathrm{R-CH_3+CH_2=CH-R}$$

Received 25 September 2019; Received in revised form 12 December 2019; Accepted 15 January 2020
Available online 30 March 2020

$$O_2 + CH_2^{\circ} - CH_2 - R' \longrightarrow H - O_2^{\circ} + CH_2 = CH - R$$

$$O_2 + CH_2^{\circ} - CH_2 - R' \longrightarrow O_2^{\circ} - CH_2 = CH - R$$

Scheme II. β-scission and hydrogen abstraction reaction of alkane

At high temperatures, paraffinic species are converted into olefins through H-atom abstraction reaction, as in the case of SI operation mode, in which there is a build-up of methyl radicals that recombine into ethane. However, in HCCI operation mode, no such reaction occurs, and therefore ethane was not detected in HCCI emissions [30].

Abstraction of H-atoms also occurs from alkenes at high temperature of particular importance, the abstraction of allylic H-atoms (H-atoms bonded to a carbon atom next to a double bond). There are three types of H-atom abstraction from alkenes that depend on the type of abstractable H-atoms (Scheme III), these types are: (1) Abstraction of primary allylic H-atom if it is bonded to a carbon atom that bonded to two other H atoms. (2) Abstraction of secondary allylic H-atom if it is bonded to a carbon atom bonded to one other H atom; and (3) Abstraction of tertiary allylic H-atom if it is bonded to a carbon atom bonded to no other H atom. Abstraction of an allylic H-atom leads to the formation of a resonance-stabilized radical as it is shown in scheme III.

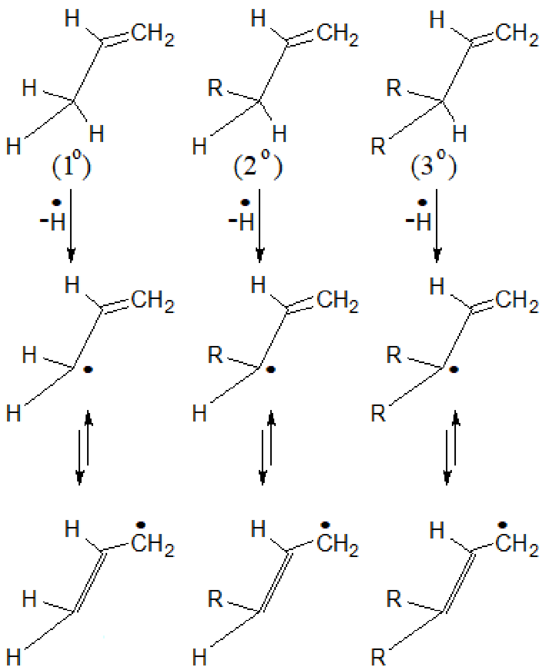

Scheme III. Abstraction of an allylic H-atom

Aromatics constitute approximately one third of the composition of the commercial gasoline used in this study. These aromatics contribute to the high-octane rating and high energy density. Due to the high stability of the aromatic rings, the H-atom abstraction is difficult and slow. As a result, the induction period for aromatics oxidation is longer than for saturated HCs [31]. An engine experiment by Kaiser et al. [28] involving a mixture of ethylbenzene and the three xylene isomers (ortho-, meta- and para-), however, gave mainly aromatic emissions, which were predominantly benzene, toluene and styrene. Gregory and Jackson [32], investigated the mechanisms for the formation of exhaust hydrocarbon in SI engine, fueled with deuterium-labelled the three xylene isomers. The aromatic HCs produced by burning each of the three xylene isomers were benzene, toluene, ethylbenzene, styrene and ethyl toluene. The aliphatic observed included 1,3-butadiene, ethane and ethylene [30]. The common low molecular weight HC compounds emitted in both modes are methane, ethylene, propylene, n-butane, 1-pentene and iso-pentane, while the heavier molecular weight HC compounds are benzene and toluene are emitted. Iso-octane, ethyl-benzene and xylenes were detected but not measured.

However, at a lower temperature, the reaction between methyl and oxygen favours the formation of methyl peroxide and aldehydes. Generally, alkanes react with oxygen to form peroxy radicals. These radicals are stable at low temperature, and unstable at high temperature. So, in the case of HCCI mode, because the temperature is lower compared to SI mode, the radicals formed survive longer, and thus the chance for the radicals to rearrange and form an aldehyde and hydroxyl radicals are higher. To make a fuller comparison between SI mode and HCCI mode, and to check the level of formaldehyde formed in the HCCI mode; it would be useful to conduct investigation using Liquefied Petroleum Gas (LPG) fuel, in which there are only two alkane components and no aromatics that complicate the picture (this is quite feasible as LPG is readily available).

The raw emissions of NO_x and HC are shown in Table 6, the opposite behaviour is exhibited with respect to the residual gas content comparing SI to HCCI modes. The emission of NO_x is significantly reduced for lower loads when there is increased residual gas fraction and thus a diluted mixture, reaching extremely low concentrations. HC emissions, on the contrary, rise significantly in this region, which is very probably due to incomplete combustion. Data obtained on the contribution of C_5–C_{11} (an indicator of the amount of unburned fuel) to the total exhaust hydrocarbon with variation in engine speed and load values for both SI and HCCI modes. The C_5–C_{11} ratio is frequently used to describe the extent to which fuels burn in an engine. In this investigation, it was found that in HCCI mode the proportion of species attributed to C_5–C_{11} in total HC is higher than in the SI mode.

The low combustion temperatures achieved at HCCI mode operating points, almost completely avoids NO_x formation compare to SI mode reduction but leading to combustion attenuation due to heat transfer in the near-wall region. While NO_x results measured in this study fall rather dramatically as expected, somewhat surprisingly, however, raw emissions of CO in HCCI mode are seen to be slightly lower for all operating points when compared to SI mode. The reduction in CO emission is likely caused by the recycling of burned gases and subsequent conversion into CO_2 in the next cycle [33]. One other result concerns the potential for exhaust gas to be used in fuel reforming to produce hydrogen that would be helpful in the extension of the lower load range for HCCI operation. The exhaust gas temperature remains between 382 and 432°C throughout the HCCI operating region. This relatively high exhaust temperature is partly due to high load and to a relatively low compression ratio. A quite substantial residual gas fraction of hot gases is required and supplied by the NVO operation. Although not in all cases of HCCI operation exhaust temperatures be expected to be so high, in the cases presented here this temperature level is fully sufficient for exhaust gas after-treatment using a three-way catalyst or oxidation catalyst. This may be insufficient for a straightforward fuel reforming process and may have to be boosted by some initial partial oxidation in the reformer as in fuel reforming for diesel engines.

As a result of this study and our previous work by Elghawi et al. [18, 19], a full spectrum of hydrocarbon (C_5 to C_{11}), Carbonyls, vapour-phase and particulate-bound PAHs profile generated in the combustion of gasoline during SI and HCCI combustion mode can be obtained.

4. Conclusions

The hydrocarbon emission is heavily dependent on fuel composition, engine operation and combustion mode (i.e. HCCI or SI). Engine-out emissions analysis showed that the hydrocarbon content of HCCI exhaust (Low Temperature Combustion Engine) contained more of the heavier species (e.g. toluene, p-xylene, Naphthalene and Methyl naphthalene) than that observed in conventional SI operation mode. Overall, HCCI operation resulted in improve fuel consumption and highly reduction in NO_x compared to conventional combustion (Spark-Ignited operation). The results also show that the monocyclic aromatic hydrocarbon such as toluene are present at higher concentrations in the exhaust under HCCI operation than in the SI case. On the other hand, benzene concentrations are higher in the SI exhaust.

Acknowledgements

One of the authors (Elghawi) would like to acknowledge the Libyan Government for the provision of the scholarships and Professor Wyszynski and his group for accepting him in their laboratory in the department of Mechanical Engineering at the University of Birmingham, the UK. Jaguar is acknowledged for supporting the work with the research engine.

Bibliography

[1] JOHNSON, E.S., LANGARD, S., LIN, Y. A critique of Benzene exposure in general population. *Science of the Total Environment*. 2007, **374**,183.

[2] US Environmental Protection Agency. Estimating cancer risk from outdoor concentrations of hazardous air pollutants in 1990. EPA, Environmental Research Section. 2000, **82**, 194-206.

[3] KOSTRZEWSKI, P., PIOLROWSKI, J. Toluene determination in capillary blood as a biological indicator of exposure to low level of toluene. *Polish Journal of Occupational Medicine*. *Medicine Environmental Health*. 1991, **4**, 249-259.

[4] HAZRATI, S., ROSTAMI, R., FAZLZADEH, M. et al. Benzene, toluene, ethylbenzene and xylene concentrations in atmospheric ambient air of gasoline and CNG refueling stations. *Air Quality, Atmosphere & Health*. 2016, 9, 403-409.

[5] ANDERSEN, I., LUNDQVIST, G.R, MOLHAVE, L. et al. Human response to controlled levels of toluene in six-hour exposures. *Scandinavian Journal of Work, Environment & Health*. 1983, 9, 405-418.

[6] MAHAVAR et al. Toluene Poisoning Presenting as Bilateral Basal Ganglia Haemorrhage. *Journal of The Association of Physicians of India*. 2018, 66, 2018.

[7] ATSDR, Agency for Toxic Substances and Disease Registry. Toxicological Profile for Toluene (Update). U.S. Public Health Service, U.S. Department of Health and Human Services.2000, 357 P, Atlanta.

[8] WALLINGTON, T.J., KAISER, W.E., FARRELL V. Automotive fuels and internal combustion engines: a chemical perspective. *Chemical Society Reviews*. 2006, **35**, 335.

[9] EPPING, K., ACEVES, S., BECHTOLD, R. et al. The potential of HCCI combustion for high efficiency and low emissions, *SAE Technical Paper*. 2002-01-1923, 2002.

[10] WALKER, J., O'HARA, C. Analysis of automobile exhaust gases by mass spectrometry. *Analytical Chemistry*. 1955, 27(5), 825-828.

[11] TSURUSHIMA, T., SHIMAZAKI, N., ASAUMI, Y. Gas sampling analysis of combustion processes in an HCCI Engine. *International Journal of Engine Research*. 2000, **1**(4), 337.

[12] KAISER, E.W., MARICQ, M.M., XU, N. et al. Detailed HC species and particulate emissions from an HCCI engine as a function of air-fuel ratio. *SAE Technical Paper*. 2005-01-3749, 2005.

[13] LI, H., NEIL, S., CHIPPIOR, W. An Experimental investigation on the emission characteristics of HCCI engine operation using n-heptane. *SAE Technical Paper*. 2007-01-1854, 2007.

[14] DEC, J.E., DAVISSON, M.L., LEIF, R.N. et al. Detailed HCCI exhaust speciation and the sources of HC and OHC emissions, *SAE Technical Paper*. 2008-01-0053, 2008.

[15] SHIBATA, G., KAWAGUCHI, R., YOSHIDA, S. et al. Molecular structure of hydrocarbon and auto-ignition characteristics of HCCI engines. *SAE International Journal of Fuels and Lubricants*. 2014, **7**, 3.

[16] HUNICZ, J., MEDINA, A. Experimental study on detailed emissions speciation of an HCCI engine equipped with a three-way catalytic converter. *Energy*. 2016, **117**, 388-397.

[17] YANG, R., HARIHARAN, D., ZILG, S. et al. Efficiency and emissions characteristics of an HCCI engine fuelled by primary reference fuels. *SAE Technical Paper*. 2018-01-1255, 2018. https://doi.org/10.4271/2018-01-1255.

[18] ELGHAWI, U.M., MAYOUF, A., TSOLAKIS, A. et al. Vapour-phase and particulate-bound PAHs profile generated by an (SI/HCCI) engine from a winter grade commercial gasoline fuel. *Fuel*. 2010, **89**, 2019.

[19] ELGHAWI, U.M., MAYOUF, A. Carbonyl emissions generated by an (SI/HCCI) engine from a winter grade commercial gasoline fuel. *Fuel*. 2014, **116**, 109.

[20] OJEC Official Journal of the European Communities, L44, (16-02-2000).

[21] KAISER, E.W., SIEGL, W.O., HENIG, Y.I. et al. Effect of fuel structure on emission from a spark-ignited engine. *Environmental Science & Technology*. 1991, **25**(12), 2005-2012.

[22] VILLINGER, J., FEDERER, W., PRAUN, S. Comparative study of butadiene and B, T, X tailpipe emissions for gasoline of different octane levels. *SAE Technical Paper*. 2001-01-1643, 2001.

[23] HECK, R.M., FARRAUTO, R.J. Automobile exhaust catalysts. *Applied Catalysis A: General*. 2011, **221**, 443.
[24] GANDHI, H.S., GRAHAM, G.W., MCCABE, R.W. Automotive exhaust catalysis. *Journal of Catalysis*. 2003, **216**, 433.
[25] KASPAR, J., FORNASIERO, P., HICKEY, N. Automotive catalytic converters: current status and some perspectives. *Catalysis Today*. 2003, **77**, 419.
[26] GARIN, F. Environmental catalysis. *Catalysis Today*. 2004, **89**, 255.
[27] SCHUETZLE, D., SIEGL, W.O., JENSEN, T.E. et al. The relationship between gasoline composition and vehicle hydrocarbon emissions: A review of current studies and future research needs. *Environmental Health Perspectives*. 1994, **102** (Suppl 4), 3.
[28] KAISER, E.W., SIEGL, W.O., COTTON, D.F. et al. Effect of fuel structure on emission from a spark-ignited engine. 2. naphthene and aromatic fuels. *Environmental Science & Technology*. 1992, **26**(8), 1581.
[29] KAISER, E.W., SIEGL, W.O., COTTON, D.F. et al. Effect of fuel structure on emission from a spark-ignited engine. 3. olefinic fuels. *Environmental Science & Technology*. 1993, **27**(7), 1440.
[30] ELGHAWI, U., MISZTAL, J., TSOLAKIS, A. et al. GC–MS speciation and quantification of 1,3-butadiene and other C1–C6 hydrocarbon in SI/HCCI V6 engine exhaust. *SAE Technical Paper*. 2008-01-0012, 2008.
[31] GLASSMAN, I. Combustion. Academic Press. San Diego 1996.
[32] GREGORY, D., JACKSON, R.A. Mechanisms for the formation of exhaust hydrocarbon in a single cylinder SI engine, fueled with deuterium-labelled ortho-, meta- and para-xylene. *Combustion and Flame*. 1999, **118**, 459.
[33] ZHAO, H. HCCI and CAI engines for the automotive industry. *CRC Press*. Cambridge 2007.

Usama Elghawi – Department of Mechanical Engineering, Libyan Academy of Graduate Studies.
e-mail: *u.elghawi@aee.gov.ly*

Ahmed Mayouf – International Study group, Kingston University, United Kingdom.

Athanasios Tsolakis – Department of Mechanical Engineering, University of Birmingham, United Kingdom.
e-mail: *a.tsolakis@bham.ac.uk*

Article citation info:
JASKIERNIK, M., BUCZEK, K., WALKOWIAK, J. Simulation of the oil supply through the connecting rod to the piston cooling channels in medium speed engines. *Combustion Engines*. 2020, **180**(1), 25-30. https://doi.org/10.19206/CE-2020-104

Maciej JASKIERNIK
Konrad BUCZEK
Jędrzej WALKOWIAK

CE-2020-104

Simulation of the oil supply through the connecting rod to the piston cooling channels in medium speed engines

The importance of the oil flow simulation in connecting rod oil channels during the engine development process is recently increasing. This can be observed either in medium speed engines, where, as one of the traditional solutions, the oil for piston cooling is supplied through the connecting rod, or in automotive engine VCR (variable compression ratio) connecting rods, where engine oil is used to change the compression ratio of the engine. In both cases, precise numerical results are necessary to shorten the prototyping period and to reduce the overall development cost.

The multi-physics character of the simulation problem basically consists of the interaction between the dynamics of the crank train components and the oil flow. For the oil supply to the piston cooling channels through the connecting rod in medium speed engines, being the objective of this paper, a major influencing factor is the oil pressure behavior in the piston cooling gallery providing periodical interaction with its supply. At the same time, the connecting rod elastic deformation during engine operation can be regarded as negligible and the planar motion of the connecting rod can be reproduced by combination of translational and rotational acceleration fields in the CFD solver.

The paper includes the description of the applied simulation approach, the results and a comparison with the state-of-the art calculation without consideration of the above-mentioned influencing factors.

Key words: *oil flow simulation, piston cooling, connecting rod dynamics, medium speed engines*

1. Introduction

The thermal load of the pistons in medium speed engines is on a high level which requires proper cooling. Such cooling is typically realized by engine oil, which is provided to the piston cooling gallery transferring the heat from the piston internal surfaces. The oil flow rate utilized for piston cooling is therefore the major parameter to control piston temperature and the durability of the piston itself.

Simulating the oil supply to the piston through oil passages in the connecting rod and the piston pin represents a multi-physics problem. It basically consists of aspects of fluid mechanics which describe the flow through oil passages and the piston cooling gallery as well as of the dynamics of planar or reciprocating motions of the connecting rod and the piston and their influence on the oil flow.

Because of these various influence parameters, precise determination of the oil supply through the connecting rod for piston cooling during engine design is a very complex task. Hence, simplified engineering calculations or simulations are typically applied. Correctness of such estimations is subsequently verified by engine testing on the prototypes.

A precise simulative approach to solving such a problem includes e.g. coupling of 1D oil flow and multibody system (MBS) simulation of the connecting rod. This was recently done for the simulation of FEV's VCR connecting rod [1]. Such a simulation approach is necessary for a VCR connecting rod, where deformation of the connecting rod body influences the volume of the internal oil chambers and thus the effective connecting rod length as well as the switching process between the two compression ratios. It is however a sophisticated and time consuming approach.

For the simulation of the oil supply through the connecting rod to the piston cooling gallery in a medium speed engine with a conventional rigid connecting rod, a more time effective and straightforward methodology is required. The optimum simulation approach according to the authors is a CFD simulation, which reproduces the effects of connecting rod movement by a combination of translational and rotational acceleration fields. This can be performed with enough precision, since the deformation of the connecting rod structure has only marginal influence on the oil supply to the piston via the connecting rod oil drillings. In parallel, the variable discharge pressure from the oil passages to the piston cooling gallery should be considered by coupled CFD simulation of the oil sloshing in the piston cooling gallery.

Such simulation has been recently performed during development of a new medium speed engine in the FEV Group, which is the basis of this paper.

2. Modelling of connecting rod dynamics for CFD simulation of oil flow in the crank mechanism

The kinematics and dynamics of a crank mechanism is historically a well-known topic. The beginnings of such considerations reach even back to the era of reciprocating steam machines, being the predecessor of today's internal combustion piston engines.

Regardless of the very simple principle of transferring the reciprocating movement of the piston into rotational movement of the crankshaft, the planar movement of the connecting rod is difficult to be precisely described by mathematical functions, which can be effectively applied either in order to understand the crank mechanism kinematics or for engineering calculations. Therefore, in the classic approach, the connecting rod is reduced to a two-point mass equivalent system, in which one realizes a translational motion (along with piston) and the second one, being attached to the crankpin, the rotational motion – Fig.1.

Received 25 September 2019; Received in revised form 12 December 2019; Accepted 15 January 2020
Available online 30 March 2020

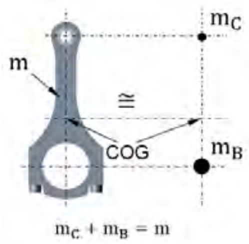

Fig. 1. Reduction of connecting rod to two-mass system [2, 3]

For the oscillating mass of connecting rod, the acceleration measured along cylinder axis (with a positive value for the vector oriented from cylinder head to crankshaft) can be expressed by following equation:

$$a_C = \omega^2 r(\cos(\varphi) + \lambda\cos(2\varphi)) \tag{1}$$

where: a_C – acceleration of connecting rod oscillating mass, ω – crankshaft angular velocity, r – crank throw radius, φ – crankshaft angle, λ – crank radius to connecting rod length ratio.

The centripetal acceleration a_B of the rotating part can be expressed easily by equation (2):

$$a_B = \omega^2 r \tag{2}$$

The above-mentioned equations (1) and (2) are simplifications, not only due to reduction of connecting rod to two-point mass system, but also due to the fact, that the motion of oscillating masses described by equation (1) takes into account only the first two elements of an infinite Tailor sequence.

Such simplified considerations can be found in nearly all textbooks related to basics of internal combustion engines (e.g. [2, 3], etc.). They are precise enough to understand or to calculate most of the effects of crank mechanism motion. These are e.g. time dependent changes of the cylinder volume during combustion and gas exchange simulations, piston and connecting rod mechanical loads, crankshaft balancing considerations, hydrodynamic bearing loads, torsional vibration excitations or bending loads of the crankshaft.

However, this simplified approach for determination of connecting rod movement is not sufficient for considerations where local mass forces acting along the connecting rod shank are of significance. Such effects are important for precise simulation of e.g. connecting rod buckling or the oil flow in the oil channels supplying engine oil from the big to small eye of the connecting rod.

For such considerations, the basics of rigid body mechanics for planar motion can be applied. Defining coordinate systems and basic locations acc. to Fig. 2, the acceleration of any point A can be described by equation 3 [4]:

$$\overrightarrow{a_A} = \overrightarrow{a_B} + \overrightarrow{a_{A|B}}^{(\tau)} + \overrightarrow{a_{A|B}}^{(n)} \tag{3}$$

where: $\overrightarrow{a_A}$ – acceleration of any point A of connecting rod, $\overrightarrow{a_B}$ – acceleration of point B subjected to rotational motion, $\overrightarrow{a_{A|B}}^{(\tau)}$ – tangential acceleration of any point A of connecting rod in relation to point B, $\overrightarrow{a_{A|B}}^{(n)}$ – normal (centripetal) acceleration of any point A of connecting rod in relation to point B.

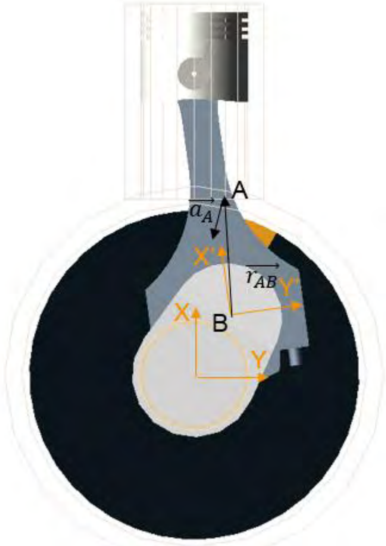

Fig. 2. Coordinate systems and basic locations in crank mechanisms

Equation (3) can be expressed by use of angular velocity $\overrightarrow{\omega_\beta}$ and angular acceleration $\overrightarrow{\varepsilon_\beta}$ of the connecting rod by the following relation:

$$\overrightarrow{a_A} = \overrightarrow{a_B} + \overrightarrow{\varepsilon_\beta} \times \overrightarrow{r_{AB}} + \overrightarrow{\omega_\beta} \times \left(\overrightarrow{\omega_\beta} \times \overrightarrow{r_{AB}}\right) \tag{4}$$

where $\overrightarrow{r_{AB}}$ is the vector of the position of point A in relation to point B.

Application of accelerations according to equation (4) expressed in the coordinate system X'Y'Z' allows to simulate the effect of connecting rod dynamics in the CFD solver. For such a case, the mesh of the connecting rod oil channels is stationary, and the flow volume is subjected to accelerations according to above-mentioned general equation.

In order to express the normal (centripetal) acceleration of point B in coordinate system X'Y'Z', the effect of connecting rod tilting needs to be considered. The result of such considerations is:

$$\overrightarrow{a_B} = r\omega^2 \begin{bmatrix} \begin{pmatrix} \lambda\sin^2(\varphi) - \\ \cos(\varphi)\sqrt{1-\lambda^2\sin^2(\varphi)} \end{pmatrix} \\ \begin{pmatrix} (-1)\lambda\sin(\varphi)\cos(\varphi) - \\ \sin(\varphi)\sqrt{1-\lambda^2\sin^2(\varphi)} \end{pmatrix} \\ 0 \end{bmatrix} \tag{5}$$

Taking into account that connecting rod angular velocity and acceleration are accordingly the first and the second time derivative of the connecting rod tilting angle, after simple considerations and mathematical transformations, they can be expressed in coordinate system X'Y'Z' as follows:

$$\overrightarrow{\omega_\beta} = \begin{bmatrix} 0 \\ 0 \\ \frac{(-1)\lambda\omega\cos(\varphi)}{\sqrt{1-\lambda^2\sin^2(\varphi)}} \end{bmatrix} \tag{6}$$

$$\overrightarrow{\varepsilon_\beta} = \begin{bmatrix} 0 \\ 0 \\ \frac{\lambda\omega^2\sin(\varphi) - \frac{\lambda^3\omega^2\sin(\varphi)\cos^2(\varphi)}{1-\lambda^2\sin^2(\varphi)}}{\sqrt{1-\lambda^2\sin^2(\varphi)}} \end{bmatrix} \tag{7}$$

The above-mentioned approach was developed for the purpose of the CFD simulation presented in this paper. Since similar considerations were not found in the relevant literature, the simple multibody analysis was done with FEV's Virtual Dynamics simulation software in order to cross-check the theoretical considerations.

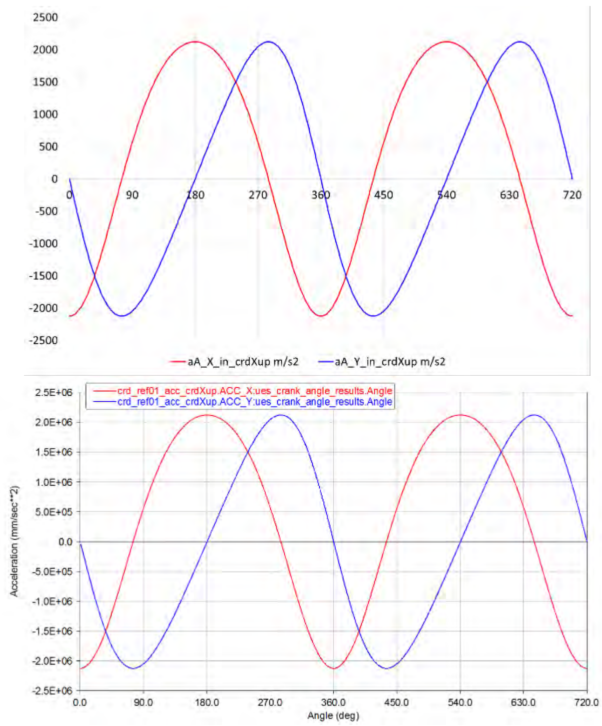

Fig. 3. Acceleration of the connecting rod's big eye center expressed in the connecting rod coordinate system calculated analytically by use of equations 4–7 (top) and simulated by use of MBS (bottom)

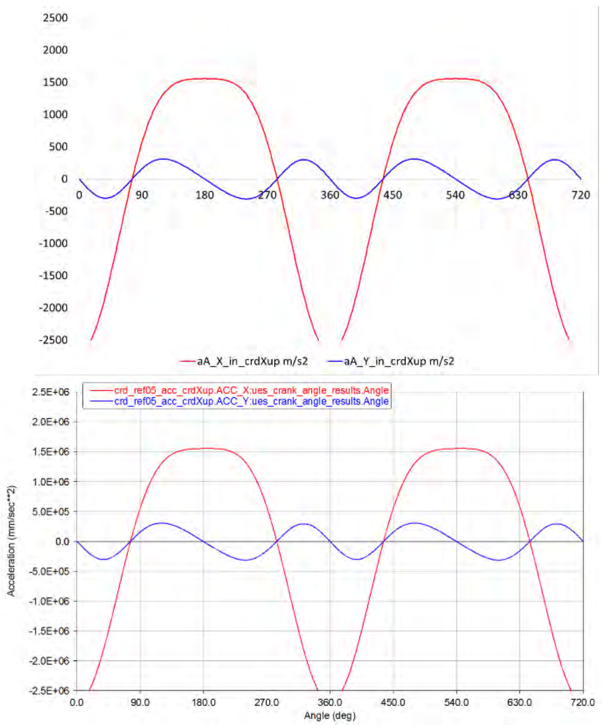

Fig. 4. Acceleration of the connecting rod's small eye center expressed in the connecting rod coordinate system calculated analytically by use of equations 4–7 (top) and simulated by use of MBS (bottom)

The acceleration was checked at the connecting rod's big eye center (Fig. 3), at the small eye center (Fig. 4) as well as at an arbitrarily selected point A (Fig. 5), and expressed in coordinate system X'Y'Z'. The position vector of point A relative to connecting rod length *L* was defined as:

$$\overrightarrow{r_{AB}} = \begin{bmatrix} 0.25\ L \\ -0.05\ L \\ 0 \end{bmatrix} \tag{8}$$

In all three cases, the acceleration calculated analytically corresponds precisely with the results derived by the MBS simulation proving the correctness of the approach expressed by equations 4–7.

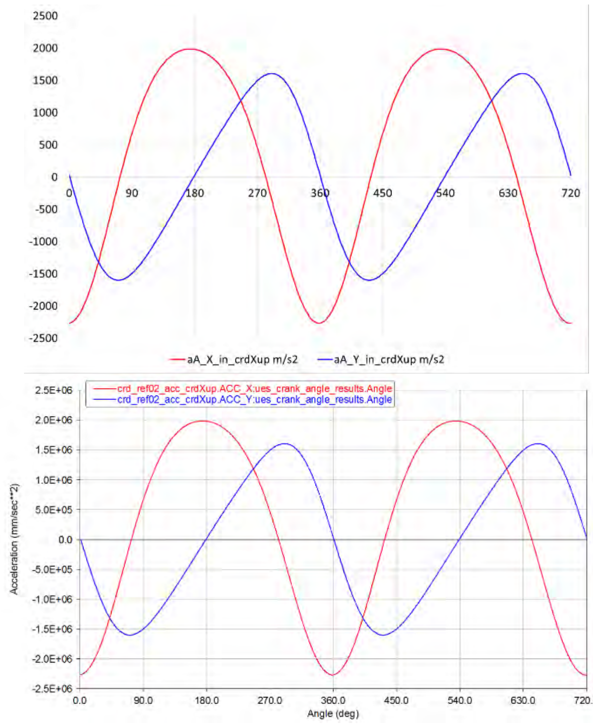

Fig. 5. Acceleration of connecting rod's point A (see text) expressed in the connecting rod coordinate system calculated analytically by use of equations 4–7 (top) and simulated by use of MBS (bottom)

3. CFD modelling of the oil flow in the crank mechanism

The precise determination of the oil flow through the connecting rod to the piston for cooling purposes and for optimization of the oil flow path by means of CFD simulation requires a properly determined modelling methodology. One of the key points of such a simulation approach is to use the exact geometry of the oil passages without any simplification which would influence the flow. The exemplary geometry used for the simulation, which results are presented in this paper, is shown in Fig. 6. It consists of the connecting rod oil drilling, a piston pin bearing groove as well as of piston pin and piston oil drillings.

The flow is described by transient Navier-Stokes and continuity conservation equations:

$$\rho \frac{Du}{Dt} = -\nabla p + \nabla * \tau + \rho \mathbf{g} \tag{9}$$

$$\frac{\partial \rho}{\partial t} + \nabla * (\rho \mathbf{u}) = 0 \tag{10}$$

where: $\frac{\mathrm{D}}{\mathrm{Dt}}$ – material derivative, ρ – density, $\mathbf{u}$ – velocity, $\nabla *$ – divergence, p – pressure, t – time, τ – stress tensor, $\mathbf{g}$ – body acceleration.

Fig. 6. Geometry used in the oil flow simulation

In the Navier-Stokes equation, the body acceleration factor was used to model the effect of connecting rod acceleration according to equations 4–7. The flow turbulence kinetic energy was calculated with a k-ε turbulence model. The flow has been assumed to be isothermal. The time dependent part of the equations has been calculated with an implicit method. For the equations discretization, the 2nd order upwind scheme was used. The SIMPLE algorithm was used for linking the Navier-Stokes and the continuity equation. The sets of discretized equations were solved using the Gauss-Siedel method.

In order to obtain reliable results, a fine quality mesh has been prepared. The numerical mesh consists of polyhedral elements. Prism layer has been included to properly model the boundary layer and, as a result, to predict pressure drop with high accuracy. Wall y+ values has been kept around 1. In the long oil drillings, the volume mesh has been obtained from a surface elements extrusion operation. With that, a more unfirmed mesh was generated.

For the inlet boundary condition, the stagnation pressure was used. The value of stagnation pressure was derived from a state-of-the-art 1-dimensional model of the engine lubrication system. The discharge was assumed to be a pressure boundary condition. The time dependent value of pressure at the model discharge was calculated in a separate CFD model for the piston cooling gallery, where the air-oil mixture is subjected to the acceleration resulting from the piston movement.

In order to conjugate both simulations, a couple of iterations has been performed. The mass flow is provided as an input from the CFD oil flow model to the oil sloshing model of the piston cooling gallery. In return, the information about average pressure at the end of the piston oil channel has been transported back to the oil prediction analysis. The coupling system is presented in the Fig. 7 below.

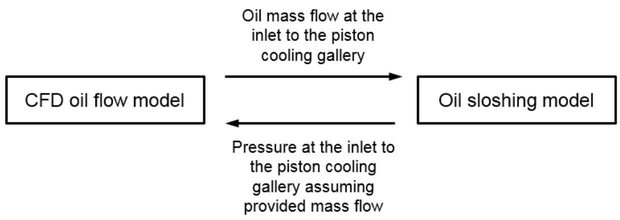

Fig. 7. Oil flow and oil sloshing models coupling

3.1. Simulation of oil sloshing in the piston cooling gallery

Oil sloshing simulation was performed separately using the Volume of Fluid (VOF) method, since the piston cooling gallery is only partially filled with oil. It describes the flow with transient Navier-Stokes equations including interaction between phases.

In this case, two fluids have been involved, one of them is engine oil, defined as a constant density liquid and the second is air, defined as ideal gas.

The inlet boundary condition applied in the model was the mass flow of oil flowing from the connecting rod bearing. It was exported from the simulation described in chapter 3. The assumed discharge boundary was constant pressure, where oil from the gallery spills into the crankcase. Pressure deviation in the crankcase has been neglected. Influence of heat transfer through walls was neglected as well, considering the isothermal case. Analysis was run long enough to reach repeatable flow conditions in every rotation of the crankshaft.

Using this simulation, the transient pressure distribution on the oil inlet has been obtained. In order to detect air sucked from the oil gallery, the monitor was set in the drilling which supplies the oil to the gallery. As expected, air was mixing with oil and part of it was entering the inlet channel, but it was removed, when the flow reversed and oil flow into gallery was reestablished.

4. Results

The presented methodology has been applied to the simulation of the oil supply through the connecting rod to the piston cooling gallery in one of the medium speed engines developed by the FEV Group. For the CFD simulation, the commercial software Star-CCM+ has been used. The analysis has been performed for rated conditions, considering the geometry of oil passages shown in Fig. 6.

For the reference, a simulation without consideration of the crank mechanisms dynamics and the variable oil discharge pressure caused by oil sloshing in the piston cooling gallery has been performed. This reference simulation represents the state-of-the art approach, where it is assumed that effects of acceleration and deceleration occurring in the crank mechanism are compensating each other. By taking into account 5 bar of absolute total pressure at the connecting rod bearing and 1 bar (absolute static pressure) at the discharge on the piston cooling gallery, the calculated oil mass flow for the chosen example was on the level of 1.260 kg/s.

In order to determine the effects of crank mechanism dynamics and oil sloshing in the piston cooling gallery, additional two simulations have been performed, considering subsequently the above-mentioned aspects.

4.1. Simulation considering crank mechanism dynamics and constant discharge pressure at the piston cooling gallery

For this simulation, the dynamics of the connecting rod was considered according to equations 4–7, but the oil sloshing model was not taken into account. In the beginning of the simulation, the piston was in the top dead center position, and the simulation was run until the cycle-to-cycle results variation has decreased to a minimum. The resultant transient mass flow is shown in the Fig. 8.

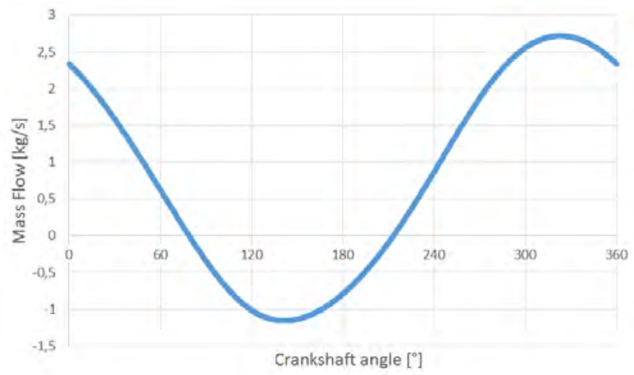

Fig. 8. Oil mass flow calculated with CFD model including the effect of connecting rod acceleration

The average mass flow is 0.765 kg/s which is only 61% of the value calculated in the reference simulation. The explanation of such differences is the nonlinear behavior of the pressure losses. During the acceleration of the flow by the connecting rod movement these losses are significantly bigger than during deceleration, and they don't compensate each other over the complete engine cycle. Additionally, a significant backflow effect has been observed, which amount is however a matter of concern.

The oil backflow typically results in a pressure rise in the connecting rod bearing, which was not considered in the performed simulation. This pressure rise should result in a decrease of the amount of oil flowing back to the bearing. The precise determination of the backflow is possible by additional oil flow simulation inside the particular bearing which is planned to be performed in the near future.

Assuming that backflow doesn't exists at all, the simulated oil flow would be about 1.050 kg/s being 84% of the oil flow calculated in the reference simulation.

4.2. Simulation considering crank mechanism dynamics and the variable discharge pressure due to oil sloshing

Using the mass flow presented in the previous chapter, the oil sloshing simulation has been performed. The base result is the transient value of the pressure at the boundary of the piston cooling gallery, which is effected by the oil-air mixture behavior. Other results refer to e.g. the piston crown cooling efficiency and the cooling gallery filling ratio. The oil flow CFD model has been updated with new discharge pressure boundary condition and run until the cycle-to-cycle results variation has decreased to minimum. Then, the simulations coupling has been introduced according to the scheme shown in Fig. 7. When both, pressure and mass flow values were repeatable, the solution has been considered to be converged. The pressure behavior during one cycle of crankshaft rotation is presented in Fig 9. Figure 10 shows the mass flow result of the converged simulation.

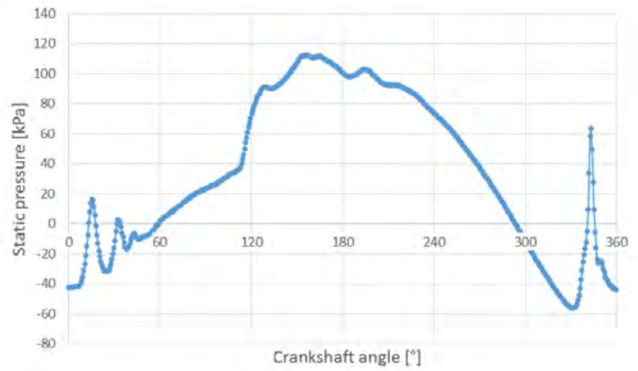

Fig. 9. Pressure behavior at the inlet to the piston cooling gallery

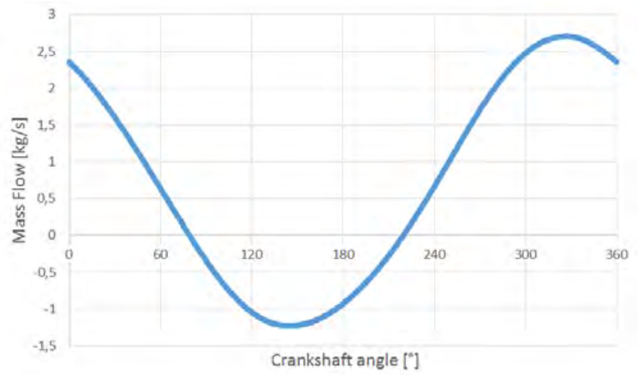

Fig. 10. Oil mass flow calculated with CFD model including the effect of connecting rod acceleration and the transient discharge pressure boundary conditions

The average value of mass flow is 0.697 kg/s, which means 9% of reduction in relation to the case, where the discharge pressure was considered to be constant.

5. Summary

The methodology for the simulation of the oil supply through the connecting rod to the piston cooling gallery in medium speed engines, being under development in the FEV Group, has been presented in this paper. Application of the advanced simulation enables to more precisely predict the piston cooling performance already in the early stages of an engine development process. A major point of the approach is consideration of the influence of connecting rod dynamics on the oil flow with a properly defined translational and rotation acceleration field integrated in the CFD simulation. Moreover, the simulation of the oil sloshing occurring in the piston cooling gallery and its influence on the discharge pressure from the oil supply passages has been introduced into the model.

The presented results show that due to the effect of connecting rod dynamics, the average value of oil mass flow is between 61 and 84% of the flow data determined without consideration of crank mechanism accelerations. The reduction by at least 16% is caused by a nonlinear behavior of pressure losses, which during the acceleration of the oil flow, caused by the connecting rod movement, are significantly higher than during deceleration. Due to this, a compensation of these effects doesn't occur over one complete engine cycle. Further reduction (up to additional 23%) is caused by the oil backflow into the connecting rod bearing, which, in the performed simulation, is believed to be overestimated. In order to define the backflow more precisely, the oil flow behavior inside the crankpin bearing needs to be investigated. This is planned to be included in the simulation process in the near future.

Consideration of the variable discharge pressure in the oil supply passages of the crank mechanism showed a further 9% reduction of the resultant oil flow, which cannot be predicted by simplified calculation techniques.

The development of the simulation of the oil-air mixture in the piston cooling gallery additionally enables to predict more precisely such parameters as cooling gallery filling ratio, oil-air mixture backflow and piston cooling efficiency. All above-mentioned simulation approaches are essential to further improve the prediction of the piston temperature distribution and distortion.

Acknowledgements

Authors would like to thank M.Sc. Eng. Ladislav Kalina, MSc. Eng. Piotr Sułkowski (FEV Polska Sp. z o.o.), Dr.-Ing. Sven Lauer, Dr.-Ing. Carl Ritterskamp and Dipl.-Ing. Ralf Rauschen (FEV Europe GmbH) for their support and contribution in the development of the simulation approach presented in this paper.

Nomenclature

VCR Variable Compression Ratio
MBS Multibody Simulation
CFD Computational Fluid Dynamics
VOF Volume of Fluid (method)

Bibliography

[1] PENDOWSKI, D. Numerical methods to investigate the dynamic behavior of a VCR conrod. *FEV Simulation and Calibration Day*. Stuttgart 2018.

[2] JĘDRZEJOWSKI, J. Mechanika układów korbowych silników samochodowych, *WKiŁ*. Warszawa 1986.

[3] MAASS, H., KLIER, H. Die Verbrennungskraftmaschine, Band 2: Kräfte, Momente und deren Ausgleich in der Verbrennungskraftmaschine. *Springer*. 1981.

[4] LEYKO, J. Mechanika ogólna. Tom 1, tom 2. *PWN*. Warszawa 2002.

Maciej Jaskiernik, MEng. – Simulation Engineer at FEV Polska Sp. z o.o.
e-mail: *jaskiernik@fev.com*

Jędrzej Walkowiak, MEng. – Simulation Engineer at FEV Polska Sp. z o.o.
e-mail: *walkowiak@fev.com*

Konrad Buczek, MEng. – Deputy team leader of CAE department at FEV Polska Sp. z o.o.
e-mail: *buczek@fev.com*

Article citation info:
GRZELAK, P., ŻÓŁTOWSKI, A. Environmental assessment of the exploitation of diesel engines powered by biofuels. *Combustion Engines*. 2020, **180**(1), 31-35. https://doi.org/10.19206/CE-2020-105

Paulina GRZELAK
Andrzej ŻÓŁTOWSKI

CE-2020-105

Environmental assessment of the exploitation of diesel engines powered by biofuels

Many factors, such as climate change and the associated risk of increasing the average temperature on the globe, energy security and the finishing of fossil fuel deposits have caused other renewable energy sources to be sought. Transport, as a branch of industry largely responsible for air pollution and greenhouse gas emissions in large cities, requires the necessary changes in the way vehicles are powered. Until now, the fuels available at petrol stations use admixtures of first generation biofuels, such as bioethanol, as a 5% additive to motor gasolines and biodiesel (FAME) as a 7% additive to diesel oil.

The article presents the idea of biorefinery installations, specifies the spectrum of substrates of the second and advanced generations, which may be a biorefinery input, including waste oils that can be used to produce hydrogenated HVO vegetable oils and other high-value products. The paper presents he existing biorefinery plant in Venice resulting from the transformation of a conventional oil refinery in which HVO fuel is produced. The article also presents the parameters of this new biofuel and compared them with the parameters of other fuels used to power self-ignition engines, such as FAME and diesel, along with discussing the prospects for HVO fuel development in Europe.

Key words: *biorefineries, biofuels, green diesel, bioeconomy, hydrotreated vegetable oil*

1. Introduction

Progressive climate change caused, among others greenhouse gas emissions (for example carbon dioxide) and drastically decreasing fossil fuel resources have forced our civilization to look for other, renewable energy carriers. One of the renewable energy sources is liquid biofuels, suitable for supplying internal combustion engines to replace conventional fuels like gasoline and diesel.

The currently existing first-generation biofuels for powering self-ignition internal combustion engines that are commonly used in Poland and in the world are, for example, biodiesel, which are fatty acid methyl esters (FAME) – including methyl esters of rapeseed oil (RME) – of oilseeds obtained as a result of cold pressing processes, extraction and transesterification. These biofuels are produced from raw materials used in the food industry.

The concept of the next generation biofuels was created, among others based on unsatisfactory results of first-generation biofuels in terms of emissions and environmental impact, both in the combustion process in internal combustion engines and in the WtW cycle ("Well to Wheel"). This cycle is related to the entire biofuel production process, taking into account every stage of it, including the type of used raw material. Competing with the food market for raw material is also a disadvantage. Second generation liquid biofuels, among others for feeding self-ignition engines, they can be produced in installations called biorefineries, in which the feed is a widely understood waste biomass.

2. Biofuels from biorefineries

As a result of the review of the implementations and research works conducted in EU countries aimed at intensifying the processes of using RES, it turned out that these works are dispersed and do not bring the expected effect, both in the environmental aspect and in terms of energy conversion savings. For this reason, a vision of an industry based on raw materials of biological origin was created, to which waste substances from primary and secondary processes of using and processing biomass were also qualified as defined in Directive 2009/28/WE [1]. Implementation of this vision should lead to the transition towards the so-called "post-oil society" by clearly separating economic growth from resource depletion and environmental impact.

After the consultations carried out in the member states, the need to separate a new industrial branch defined as industry based on biological raw materials ("Bio-Based Industries"), which should strive to optimize land use and food safety through sustainable, efficient (effective) raw materials and to a large extent limiting the amount of waste generated, industrial processing of renewable raw materials into a wide range of products of biological origin, such as:

- advanced transport fuels,
- chemicals,
- materials,
- food and feed ingredients,
- energy [2].

As a result, "bio-industry", the main component of the EU economy called the "bioeconomy", will play a significant role in stimulating sustainable growth and enhancing Europe's competitiveness through the re-industrialization and revitalization of rural areas, ensuring that tens of thousands of jobs in research, development and production over the next decade [3].

One of the ways to mitigate the negative effects of local ecosystems influence is the conversion of biomass and organic waste to various products like chemicals, biomaterials and energy, to fully use the value of biomass, creating the so-called added value and minimizing the amount of generated or naturally produced waste substances. This integrated approach corresponds to the concept of biorefinery and is gaining more and more attention in many parts of the world.

Similar to conventional refineries where energy and chemical petroleum products are produced, biorefineries will produce many different industrial products from biomass. These products will be both LVHV (low-value and large-volume), such as transport fuels and large-volume

Received 25 September 2019; Received in revised form 12 December 2019; Accepted 15 January 2020
Available online 30 March 2020

chemicals and other materials, and HVLV (high-value and low-volume), such as specialty chemicals, such as cosmetics. In some types of installations, you can also produce food and feed for animals [4].

Biorefinery systems are nothing more than a type of open systems, where biomass, waste and energy are part of the input streams to the system. Inside the system there are a number of processes resulting in, among others exchanging the energy of the system with the environment in the form of heat and work. As output streams from biorefinery systems comes a number of products, such as fuels, chemicals both high-value, which are obtained in small quantities and low-value, obtained in large quantities, feed and food products, polymers and other materials, as well as energy produced in cogeneration or trigeneration (heat, electricity and cold) and process waste. It should be remembered that this waste is a waste only for a specific biorefinery process. For another biorefinery process, this waste may be a substrate [4]. The schema of biorefinery concept is presented in Fig. 1.

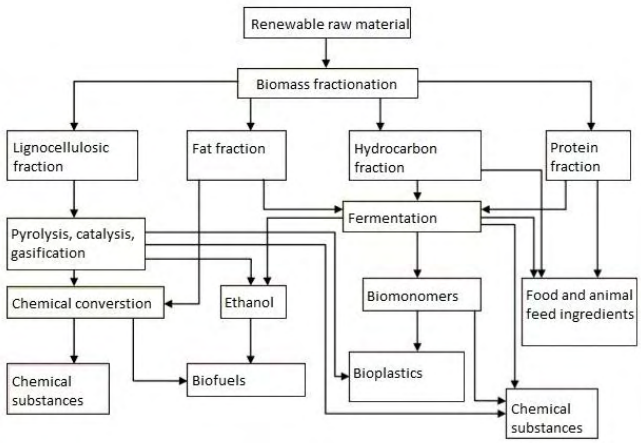

Fig. 1. Biorefinery concept schema [4]

By definition, biorefinery is a complex technological system that combines the processes of biomass conversion and further processing of products of this conversion into fuels and final chemicals, or for further processes. The biorefinery (Fig. 3) is therefore the equivalent of crude oil processing plants (Fig. 2), where the feedstock is crude oil or natural gas and other fossil energy resources. These resources are processed through petrochemical processes for various types of products, mainly fuels as well as electricity and heat as well as chemicals and various materials.

In the case of biorefineries, the substrate is organic materials such as wood, energy crops, grasses and organic waste, which are processed through biorefinery processes that largely coincide with refinery processes used in conventional oil refineries. The biorefinery products also include fuels and energy in cogeneration or trigeneration, chemicals and materials as well as food products and animal feed. The basic scheme of petrorefinery is presented in Fig. 2, while Fig. 3 presents the general ideological scheme of the biorefinery.

Fig. 2. Basic schema of classic refinery plant [4]

Fig. 3. The idea schema of biorefinery [4]

3. Waste fats

The processed vegetable fats and some animal fats can be collected both in gastronomy and in other industries. The processing of these fats is difficult due to the high content of free fatty acids. However, their price is very attractive, because it is only a fifth part of the price of fresh raw materials [5]. In one of the Austrian biofuel plants it is allowed to add up to 10% of used fats to the raw material, provided that the feedstock meets the quality requirements presented in Table 1.

Table 1. Quality requirements of raw material to the transesterification process in austrian biofuels plant [5]

Designation type	Unit	Permissible amount
Water content	% m/m	0.5
Free fatty acids content	% m/m	3.0
Iodine number	–	115
Melting temperature	°C	50
Sulphur content	% m/m	0.02
Phosphorus content	ppm	10
Polymers content	% m/m	2

Waste frying fats, expired food fats and oils stored for a long time in unfavorable conditions, i.e. with the access of air, humidity and sunlight, are characterized by different physicochemical properties in relation to fresh fats. As a result of the hydrolysis process, their acid number increases, oxygen processes change the peroxide number, and free radical reactions affect the density and viscosity of fat. Although these fats do not meet the requirements of the food industry and are treated as troublesome waste, they still contain significant amounts of unchanged triglycerides and can therefore be a very valuable raw material for the biofuel industry.

Initial purification of processed fats improves their color and odor, and also allows to reduce the density, viscosity, free fatty acid content and oxidized derivatives. Thanks to this, methanolysis reaction is easier, limiting the tendency to emulsion formation [6].

The obtained fatty acid methyl esters are characterized by better physicochemical properties, falling within the selected ranges given by the applicable fuel standard.

Diagram of an exemplary biorefinery installation producing a number of high-value products, such as various types of chemical substances, fatty acid methyl esters (FAME), hydrocarbon liquid, oleochemical products, chemicals, engine fuels and heat and electricity in cogeneration or trigeneration, using waste feed fats as a substrate are shown in Fig. 4.

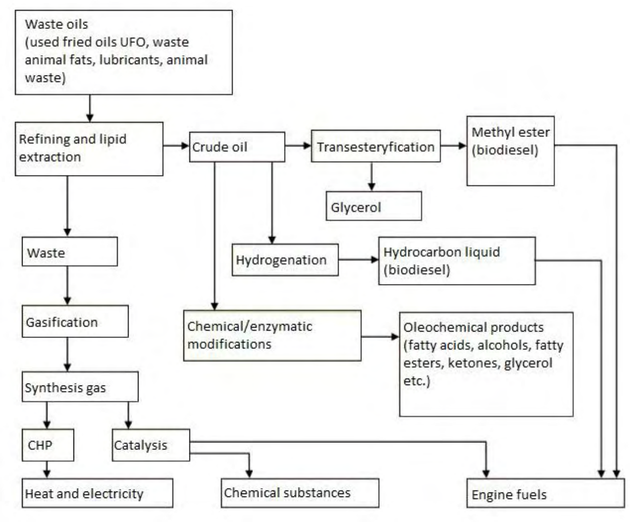

Fig. 4. Concept of biorefinery based on oily waste substances [4]

4. Biorefinery in Venice

An example of a biorefinery installation that uses waste fats from the Venetian restaurants and not only is a biorefinery from the Italian company Eni in Venice.

In 2014, the first conventional oil refinery in Europe was transformed into a biorefinery. In a difficult period for the European refining industry, the Venetian refinery found a way to re-use the catalytic hydrodesulfurization process.

Biorefinery produces biofuels with very high quality – mainly green diesel (Green Diesel), but also "green petrol" (green naphtha), LPG gas and potentially even aviation fuel – all produced from biological raw materials. In this way, it helps to meet the requirements of the EU Renewable Energy Directive and ensure that conventional fuels produced in this biorefinery will have at least 10% share of components from renewable sources (biocomponents) by 2020 [7].

In this biorefinery, about 360,000 Mg of vegetable oil is produced annually. The value is to increase to the value of 600,000 Mg when the construction works, converting a conventional refinery into a biorefininery, will come to an end. Currently, palm oil is used for the production of biofuels and biocomponents due to its wide availability. This is due to the existing low availability of second and third generation raw material. However, these alternative fuels have already been tested and biorefinery is preparing to produce them in the near future [7].

Industrial research has confirmed which raw materials that do not compete with the food supply chain, such as used vegetable oils from around the country and animal fats, are suitable for biofuel processing. For this reason, it is advisable to talk about cooperation with public waste authorities in order to increase the collection of used oils from households for use it in biorefineries. In addition, waste products from the oily biomass refining process – i.e. "advanced" fuels, such as distilled fatty acids and glycerin – should be re-used.

The process is based on innovative Ecofining technology, developed by Eni and tested in its laboratories. It produces very high-grade, sustainable biofuels without any of the disadvantages which affect other fuels currently on the market (fatty acid methyl esters – FAME). Consequently, it offers reduced particulate emissions and improved engine efficiency in line with current legislation and EU directives. The raw materials of biological origin used in the process can be divided into first generation feedstock (vegetable oils in competition with the food supply chain), second generation feedstock (waste animal fats, used cooking oils and agricultural waste) and third generation feedstock (oils from algae or waste). Ecofining technology can also be applied to second and third-generation feedstock, so anticipating any future changes in the regulations.

The Green Diesel fuel production process is based on innovative technology by Eni and tested in laboratories. Very high quality, balanced biofuels (advanced biofuels) are produced here, in which there are no disadvantages that currently exist on the market of biofuels, such as FAME. Consequently, these fuels provide reduced particulate emissions and improve engine performance, all in accordance with applicable EU regulations and directives.

5. Green Diesel – biofuel and biocomponent

The end product, known as hydrotreated vegetable oil (HVO) or green diesel, is a very high-quality diesel with excellent cetane levels (cetane number over 70, similar to top quality diesel obtained from GtL processes). It has a high heating value and is free from aromatic compounds and heteroatoms (sulphur, nitrogen or oxygen). The product is also immiscible with water and entirely compatible with diesel produced from petroleum (to which it can be added in a proportion of even up to 30% without any issues). Thus the obtained fuel respects the strictest regulations and offers the best performance for both engines and the environment [8].

The high calorific value of green diesel allows reduced consumption of plant feedstock (initially palm oil, certified to European standards) compared with traditional processes. In addition, in the near future, second and third-generation feedstock will also be able to be used, such as animal fats, used cooking oil, agricultural waste, oil from algae and other waste.

The main product of the HVO process is the, so called, Green Diesel. It has to be noted that the HVO plant is a type of biorefinery and thus allows for production of a wide range of products from biofuels to biochemicals. Except for Green Diesel, the HVO installation can be used to produce Green Jet Fuel while Green Naptha and Green LPG, together with propane, are the by-products of the production process [7].

The raw materials used in this process may have the same or lower quality in relation to the requirements in the production of classic biodiesel, whereas the product obtained in the HVO fuel production process has better properties. The main advantages of the fuel obtained in the HVO process are: high cetane number, high energy density and lack of oxygen in the molecule of the obtained fuel.

The key advantage of Green Diesel fuel is its CFPP level (cold filter plugging point), which can drop to –20°C or even –50°C (Table 2) regardless of the raw material used. This in turn makes the HVO suitable for use in cold winters, even in Scandinavian countries, as well as jet fuel [9].

Table 2. Comparison of properties of diesel oil, FAME fatty acid methyl esters and HVO diesel (Green Diesel) [9]

Parameter	Diesel oil	FAME	HVO diesel
Bio Raw material [%]	0	100	100
Oxygen content [%]	0	11	0
Specific weight	0.84	0.88	0.78
Sulphur content [ppm]	< 10	< 1	< 1
Calorific value [MJ/kg]	43	38	44
Cold filter clogging temperature CFPP [°C]	–15	–14	do –50
Cloud point [°C]	–5	–5 – +15	do –20
Distillation range [°C]	200–350	340–355	200–320
The contribution of polycyclic compounds [%]	11	0	0
Emissions of nitrogen oxides NO_x	Standard	+10%	–10%
Cetane number	51	50–65	70–90
Oxidation stability	Standard	Poor	Excellent

Research and comparative analysis of other fuels sold in Italy confirmed the excellent properties of the Green Diesel additive. Due to the fact that 15% of solid fuel is renewable, this fuel significantly reduces emissions, reducing the number of unburned hydrocarbons and carbon monoxide by up to 40%. In addition, a more durable production cycle helps reduce CO_2 emissions by an average of 5% [8]. Cold starting is easier and engine noise is reduced due to the high cetane ratio, compared to the standard minimum of 51 (Table 2 and Table 3).

Table 3. Comparison of properties of classic biodiesel and Green Diesel fuel (HVO) [10]

Biodiesel	Green Diesel HVO
Poor chemical stability	Excellent chemical stability and excellent compatibility with diesel
Variable quality depending on the raw material used	Constant quality regardless of the raw material used
High probability of bacterial contamination and resulting filter installation	Waterproof and able to avoid bacterial contamination
Low calorific value	High calorific value and high cetane number
Causes the dilution of the lubricating oil	It does not dilute the oil, its distillation properties are similar to diesel oil
Limiting the additive in diesel to 7% (the „blend wall”)	It can be mixed with diesel oil in an unlimited way. It can also act as 100% biofuel.

6. Green Diesel development predictions in Europe and in the World

In connection with the forecasted increase in the demand for biodiesel in the RED II by 35% by 2030, the expansion of the range of raw materials used for the production of renewable fuels used in self-ignition engines and the necessity of systematically increasing the share of advanced biofuels, it is expected that the demand for Green Diesel (HVO) will grow steadily.

It is estimated (Fig. 5) that by 2025, HVO fuel production will increase twice on the European scale and will be trippled on a global scale in relation to the base year 2018, when HVO fuel production accounted for 17% of total biodiesel production (data do not concern installations producing HVO as a result of the co-hydrogenation process).

Fig. 5. Production capacity of HVO diesel in Europe [11]

HVO fuel is already known, manufactured and used in some European countries. These countries chose the Green Diesel fuel because of its favorable properties such as low freezing temperature, and also because of the possibility of exceeding the so-called "blend wall", meaning the threshold for the maximum amount of biodiesel that can be mixed with diesel. The concept of "blend wall" stands for the quality specifications of fuels issued by engine manufacturers.

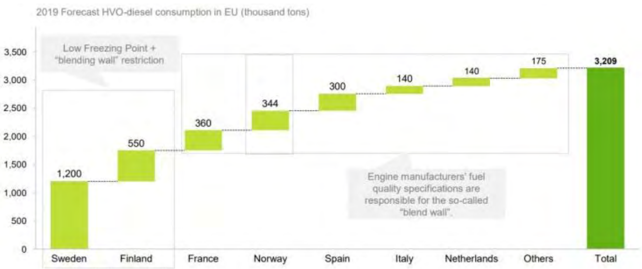

Fig. 6. Forecast of HVO fuel consumption in European countries [11]

It is forecasted that in 2019, the consumption of HVO fuel in European countries will reach a total of 3,209,000 Mg, with Sweden, Finland, France, Norway and Spain being the largest consumers of this fuel (Fig. 6).

7. Conclusions

The Green Diesel fuel produced in the biorefinery in Venice can be blended with diesel oil, making up 15% of the mixture, and in this form it can be used in existing self-ignition engines. This is possible due to a number of good engine properties of this biofuel. This mixture maintains the efficiency of the engine at the level of efficiency of the engine powered by conventional diesel fuel, while it is also responsible for a 4% reduction in fuel consumption compared to diesel with 5% FAME addition. The research shows that the use of 15% Green Diesel blend with diesel fuel reduces CO_2 emissions by 5%, reduces hydrocarbon emissions and CO by 40% and also reduces noise emissions due to high cetane number.

Green Diesel is the first significant step towards more and more advanced solutions that meet or even exceed the strict Italian and European biofuel regulations. Italian legislation requires that as much as 10% of fuels sold in Italy should be produced from renewable raw materials, of which about 1.6% are to constitute the so-called advanced biofuels. Green Diesel fuel can be blended with conventional diesel in large proportions to power vehicles equipped with self-ignition engines. Due to the fact that it is obtained from the hydrogenation of vegetable oils, it does not contain oxygen and is a pure hydrocarbon, unlike traditional biodiesel. It should also be noted that the European Commission has established mandatory criteria for sustainable development for biocomponents that cover soil, water and air protection, ensuring socio-economic sustainability, while preventing competition from the food supply chain.

Green Diesel meets all these requirements, and thanks to the flexibility of its production process it can be obtained from waste animal fats or household waste oil, as well as from the so-called "advanced" sources such as suitable pretreated lignocellulose waste. Work is continuing on the implementation of future European directives in the field of the increasing use of advanced biofuels, which will definitely reduce the emissions of greenhouse gases and harmful compounds into the environment.

Nomenclature

CFPP	cold filter plugging point
CI	compression ignition
EU	European Union
FAME	fatty acid methyl esthers
GtL	gas to liquid
HVLV	high value low volume
HVO	hydrotreated vegetable oil
LVHV	low value high volume
LPG	liquid petroleum gas
RED II	Renewable Energy Directive II
RES	renewable energy sources
RME	rapeseed methyl esthers
WtW	well to wheel

Bibliography

[1] Dyrektywa Parlamentu Europejskiego i Rady 2009/28/WE z dnia 23 kwietnia 2009 r. w sprawie promowania stosowania energii ze źródeł odnawialnych zmieniająca i w następstwie uchylająca dyrektywy 2001/77/WE oraz 2003/30/WE (Tekst mający znaczenie dla EOG).

[2] BIERNAT, K., MALINOWSKI, A., GNAT, M. The possibility of future biofuels production using waste carbon dioxide and solar energy. Chapter 5 in: *Biofuels, Economy, Environment and Sustainability* Edited by Zhen Fang, IntechOpen ISBN 978-953-51-0950-1, February 2013.

[3] BIERNAT, K. The possibility of creating biorefinery in Polish bioeconomy, stakeholder event on the bio-based industries public-private partnership. Warsaw, 22 November 2013.

[4] BIERNAT, K., GRZELAK, P.L. Biorefinery systems as an Element of Sustainable development. *Biofuels – Status and Perspective.* InTech, 2015. https://doi.org/10.5772/60448

[5] KLECAN, R. Paliwa do silników Diesla. *Archiwum Gospodarki Odpadami i Ochrony Środowiska*. 2006, **3**, 55-68.

[6] SKRZYŃSKA, E., KMIEĆ, A., STANKIEWICZ, R. Oczyszczane oleje posmażalnicze jako surowiec do EMKT. *Czasopismo Techniczne Technical Transactions*. 2011, **10**(108).

[7] Eni Refinery in Venice, 7.12.2016: https://www.eni.com/docs/en_IT/enicom/operations/stories-people/green-refinery/ENI-Raffineria-Eni-Venezia-07.12.16.pdf

[8] BALDINI, L., FACCINI, S. Eni contribution to Energy Transition. New fuels for transportation and sustainable mobility, Facoltà di Ingegneria Civile e Industriale, Università La Sapienza, Roma, 19 Aprile 2018.

[9] Green Refinery: reinventing petroleum refineries, 23.05.2014: https://www.eni.com/docs/en_IT/enicom/publications-archive/company/operations-strategies/refining-marketing/eni_Green-Refinery_esecutivo.pdf

[10] MORANDI, P. Biodiesel vs Green Diesel, Cavalli Vapore, 18.12.2017: https://www.cavallivapore.it/2017/eni-diesel-piu-potenza-del-motore-e-piu-vita-alla-vostra-auto-grazie-alla-nuova-tecnologia-ecofining/

[11] HILLAIRET, F. European renewable diesel and emerging feedstocks. *The 8th Annual Jacobsen Conference – Forecasting Agriculture and biofuels interplay*. Denver, May 2019.

Paulina Luiza Grzelak, M.A. – Motor Transport Institute, Warsaw.

e-mail: *paulina.grzelak@its.waw.pl*

Andrzej Żółtowski, DEng. – Motor Transport Institute.

e-mail: *andrzej.zoltowski@its.waw.pl*

Article citation info:
MERKISZ, J., BAJERLEIN, M., ZIELINSKI, B. The impact of parameter modifications in the Diesel engine power system on the emissions of harmful compounds. *Combustion Engines*. 2020, **180**(1), 36-40. https://doi.org/10.19206/CE-2020-106

Jerzy MERKISZ
Maciej BAJERLEIN
Bartłomiej ZIELIŃSKI

CE-2020-106

The impact of parameter modifications in the Diesel engine power system on the emissions of harmful compounds

The article presents the results of emission tests and vehicle operation indicators fueled with diesel oil. The tests were carried out for a passenger vehicle equipped with a diesel engine meeting Euro 3 emissions standard, moving in urban traffic. The measurements were carried out using modern PEMS (Portable Emission Measurement System) enabling the emission of gaseous components from exhaust systems of the tested object. On the basis of the conducted tests, the load characteristics were determined using the torque values obtained along with the engine speeds. The measurement route included two cycles: urban driving and fast acceleration. The aim of the study was to assess the impact of modifications to the control maps on CO, CO_2, PM and NO_x exhaust gas emissions under real operating conditions.

Key words: *IC engine, chip-tuning, CI, PEMS*

1. Introduction

The operation of the drive units in the currently manufactured vehicles corresponds to ECU electronic controlers. (ECU – Engine Control Unit). In comparison to the mechanical solutions, these controlers take into account, among others, the degree of wear of power system components. Thanks to this, it is possible to apply some necessary compensations that allow a proper engine operation. Besides controling other parameters affecting the operation of the drive unit, the electronic control introduces the possibility of changing the control algorithm. This procedure is known as chip-tuning. The user's desired effect is to increase the power and torque generated by the engine without the need for mechanical changes. The side effect of the change in the control algorithm is a change in the engine's operating conditions that cause a critical increase in the emissions of harmful compounds [1, 2].

2. Parameter modifications in the engine power system

2.1. Test unit

The unit under test was an Audi A4 passenger car manufactured in 2001. It is equipped with a self-ignition engine with AWX pump injectors. The engine displacement is 1896 cm3. The maximum torque declared by the manufacturer is 285 Nm and occurs within the speed range 1750-2500 rpm, while the maximum generated power is 96kW at 4000 rpm.

2.2. Measuring apparatus

Figure 2 presents a mobile Axion R/S + device, manufactured by Global MRV, which was used to carry out the measurements. It is intended for research in the real traffic conditions and classified in the PEMS (Portable Emissions Measurement Systems) group. The device allows testing both CI and SI engines. To measure the mass flowing through the air motor, an external Semtech EFM flowmeter was used as shown in Fig. 3.The analyzer enables synchronization with the GPS positioning system as well as communication with the vehicle OBD. Based on the obtained road emissions results, it is possible to determine the fuel consumption using the carbon balance method.

Fig. 1. The car used for tests

Fig. 2 View of the Axion R/S + mobile device

Fig. 3. Semtech EFM flowmeter

Received 25 September 2019; Received in revised form 12 December 2019; Accepted 15 January 2020
Available online 30 March 2020

2.3. The test route in Poznań

The measurements of exhaust emissions were carried out during rapid acceleration of the car from 0 km/h to 90 km/h along the test route in the urban traffic conditions shown in Fig. 4. The vehicle traveled the same route three times. Once for every set of control maps. The vehicle was heated to a coolant temperature of 90°C at the start of the measurements. The measurements were made on the same section of the route at a constant external temperature.

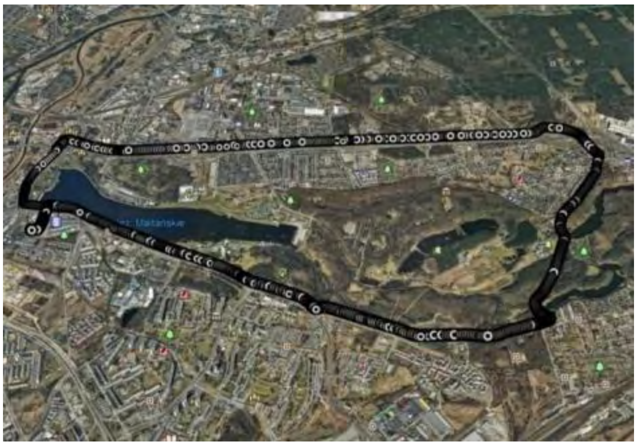

Fig. 4. Test route in Poznań

2.4. Parameter modifications in the engine power system

Parameter modifications were carried out within the speed ranges in which the drive unit reaches the highest power and the highest torque. Within the range of maximum torque, the fuel dose increased by 23%, while at the speed at which the engine reaches the highest power, the fuel dose increased by 15%. Whereas the two modified sets of control maps have the same injection maps to define the amount of injected fuel, they have different recharge pressure. The changes are shown in Fig. 5 for modification 1 and Fig. 6 for modification 2 [5].

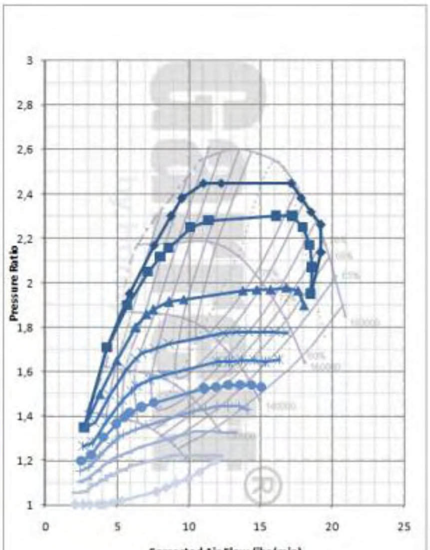

Fig. 5. The course of the boost pressure – modification 1

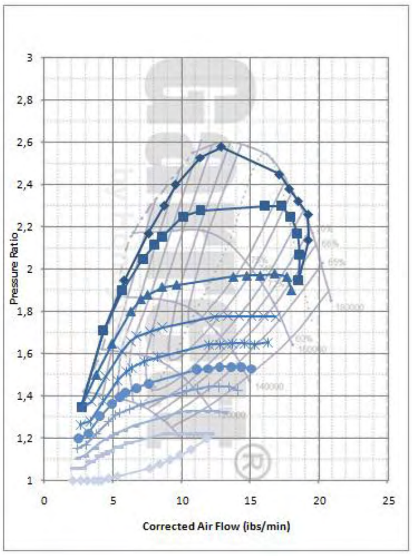

Fig. 6. The course of the boost pressure – modification 2

3. Research results with analysis

3.1. Power and torque measurements

Measurements of power and torque were made with the Dynomet portable road test bench, characterized by a measurement error of 2%. The measuring device was mounted next to the wheel of the vehicle as shown in Fig. 7. Before performing the measurements, the dynamometer was configured with the following parameters:

- ambient temperature,
- atmospheric pressure,
- the dynamic radius of the wheel,
- mass of the vehicle with passengers.

The measurement results are in Table 1.

Fig. 7. Assembly of the road test bench

Table 1. Results of power and torque measurement

Set of maps	Ne [KM]	n [rpm] Ne max	Mo [Nm]	n [rpm] Mo max
The original	142.1	4040	294	2250
Mod. 1	157.7	3772	338.5	2385
Mod. 2	154.9	3812	337.4	2271

3.2. Measurement of emissions in the city traffic

Figure 8 shows the course of change of the fuel dose injected for one cycle of work as a function of engine speed. The maximum fuel dose stored in the original torque limiter map determines the maximum amount of fuel that can be injected into the combustion chamber. The area above the straight line consists of points that refer to engine work with modified maps. The closed field encompasses an area of change in the boost pressure and shows the engine work in which the boost pressure was modified. The chart shows the dependence of the fuel dose on the rotational speed, since the value of the boost pressure generated by the turbocharger depends on the engine speed and the fuel dose. During the measurements, the engine worked mainly within the same range of rotational speed and amount of fuel dose. This means that the engine worked mainly in unchanged areas of the engine map, and that the changes in the burned fuel result mainly from changes in the time interval of the car run. The points visible in the fields of the modified engine work determine the results obtained during the exhaust emission tests at the moment of acceleration. This issue will be described in detail in the next paragraph.

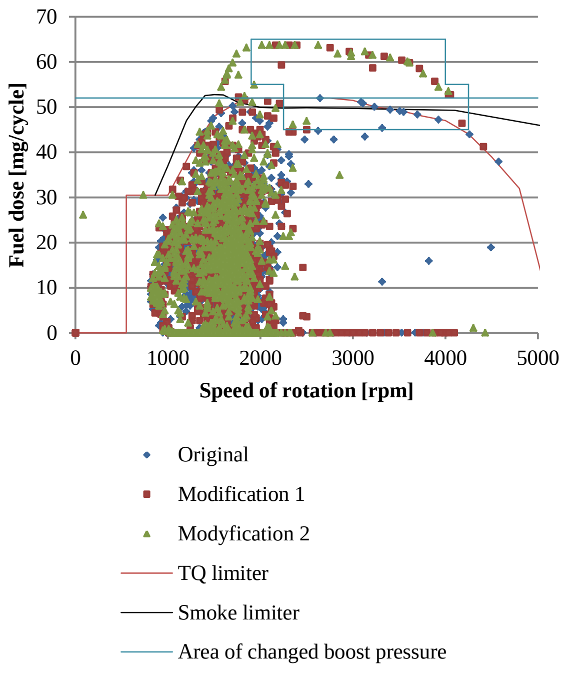

Fig. 8. Engine work points during car run

3.3. Emissions measurement during acceleration.

Figure 9 shows the course of rotational speed during acceleration from 0 km/h to 90 km/h while making emissions measurements. The figure shows how the driver changed gears while taking measurements.

During the second measurement, the change from the first to the second gear was made faster than in the case of the first and the last measurements. This means that during the second measurement the motor was more loaded until it reached the rotational speed of 2,600 rpm. The first gear has a higher gear ratio than the other ones, hence the load on the drive unit is higher and the acceleration takes more time.

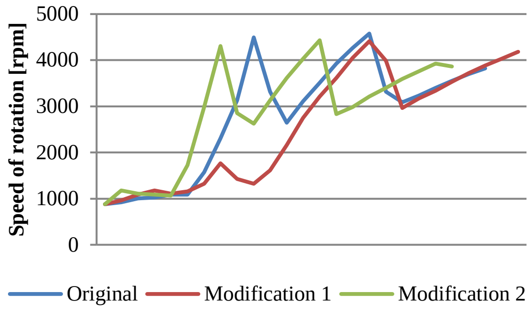

Fig. 9. Changing the rotational speed during acceleration

The emissions of the 1.9 TDI engine with the AWX factory mark during acceleration from 0 km/h to 90 km/h is shown in Figure 10. The emissions of nitrogen oxides from an engine operating on the first set of modified maps increased by 2.7%, while operating on the second set of modified maps the nitrogen oxide emissions decreased by 2.5%. In both modified sets of maps, the excess air ratio was significantly reduced, which means that blends formed in the combustion chamber were richer. On the basis of the course shown in Figure 11, it can be concluded that together with the decrease of the excess air coefficient, the concentration of nitrogen oxides in the exhaust gas increases. The mass number of the particulate matter PM emitted by the engine also increased in the case of the modified engine control maps. In the case of the first modification, with a lower boost pressure, the increase is by 88%, while in the case of the second modification, with a larger amount of air supplied by the turbocharger, the increase is by 16%.

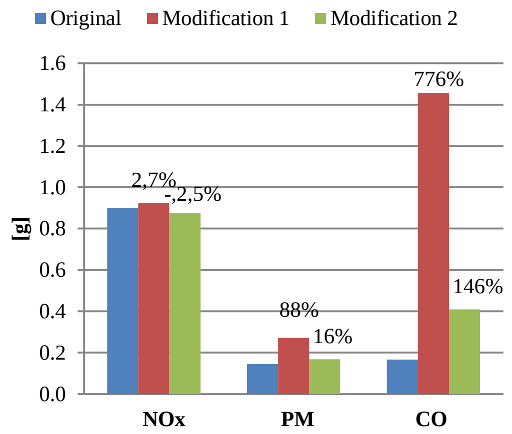

Fig. 10. Emissions of toxic compounds during acceleration

The biggest changes were observed during measurements of carbon oxides emissions. In the case of the first set of maps, the increase in emissions increased by 776%, which is significant in comparison to the original software. When measuring the emissions from the engine working on the second modification, this increase also occurred, but definitely to a lesser extent than compared to the first set, which was 146%.

During the acceleration of the car with the first set of modified maps, the driver changed the first gear to the second one faster than in the case of the original maps and the second modification. For this reason, in order to increase the accuracy of the test, the emissions of toxic components were measured from the rotation speed above 2600 rpm on the second transmission ratio to the end of the measurements. Measurement results show no change in the particulate matter emissions, contrary to emissions of nitrogen oxides and carbon monoxide which changed. The emissions of nitrogen oxides within this range of rotation speed increased for each set of modified control maps. It is consistent with the course shown in Fig. 11. The measurement results of the carbon dioxide emissions (Fig. 12) indicate that the highest emissions appear during engine operation on the first set of modified maps.

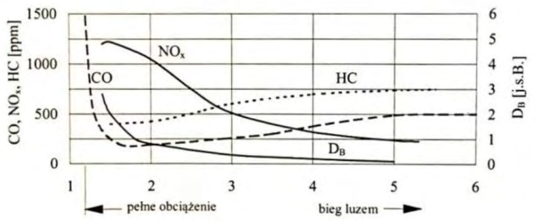

Fig. 11. Dependence of CO, HC, NOx, De concentration on the λ excess air ratio for the SI engine[3,4].

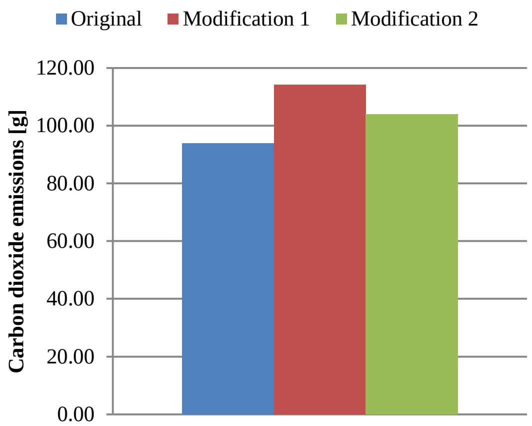

Fig. 12. Carbon dioxide emissions during the test in similar engine operating conditions

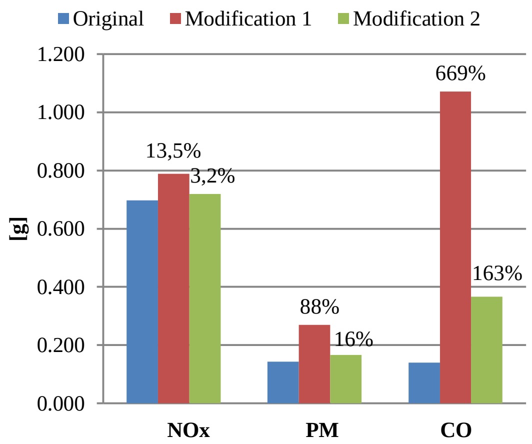

Fig. 13. Emissions of toxic compounds during acceleration in similar engine operating conditions

4. Summary

The tested car was equipped with one of the most popular SI engine, which was a 1.9 TDI VW engine. Due to its durability, it is often subjected to power boosting. Its durability is also the reason why there are so many depleted cars still in use whose worn piston-cylinder units significantly increase the emissions of harmful compounds as the outcome of burning engine oil. The wear of these parts, combined with the increased boost pressure and the increased fuel dose, leads to an increase in the indicated pressure, and thus a higher performance power. The increase of the indicated pressure facilitates the increase of the so-called "blows" in the crankcase. The desecration of the crankcase is most often directed to the intake manifold. Together with the gases that permeate from the combustion chamber into the crankcase, small quantities of engine oil permeate into the crankcase ventilation system. The increase of the indicated pressure facilitates blowing. As a result, the amount of engine oil fed to the combustion chamber along with the gases entering the crankcase is higher, which is also the reason why the emissions of harmful compounds increase, too. During the tests, emissions were measured along the route that reflects the traffic in the urban cycle and the acceleration when the engine was operating at the highest load. The measurement results in the urban cycle indicate that the car worked mainly in the unchanged areas of the control maps. By contrast, with modified maps controlling the boost pressure and the amount of injected fuel, the measurement results of emissions during rapid acceleration clearly show that such modifications increase the emissions of toxic compounds. While boosting the engine power by applying chip-tuning at a very low AFR coefficient, the carbon monoxide emissions of the tested car during the acceleration was greater than the emissions from 7 cars controlled by the original set of maps. Applying a higher charge with the same amount of injected fuel increased the emissions of CO, which was higher than CO emissions from 2 cars controlled by the original set of maps. The particulate matter emissions increased by 88% and 16% respectively for the first and the second set of modified maps. These values are very high, however it has to be pointed out that in the homologation process the test car met the Euro 3 emission standard, so it is not equipped with a PM filter. The emissions of nitrogen oxides increased in the case of each modification, but higher values occurred for the first one, where the amount of supplied air was much smaller. The increase is respectively 13.5% and 3.2% for the first and the second set of modified maps. Although power and torque reached their highest values while the engine operated on the first set of modified maps, its emissions were significantly greater than the emissions from the engine operated with the original set of control maps. The engine operated with the second set of modified control maps generated approximate values of power and torque, but the emissions from the engine running on these algorithms was much smaller than from the engine running on the first set. Treatments such as chip-tuning may, despite providing similar values of power and torque, harm the environment to a different extent. While defining more and more restrictive standards for the homologation of new cars, it has to be pointed out that attractive purchase price of the older cars, their low maintenance cost and servicing, encourages their owners to apply power-boosting measures. Therefore, the concentration of toxic compounds in the exhaust gases should be carried out both before and after the applied modifications.

Nomenclature

CI compression ignition
CNG compressed natural gas
DI direct injection
LPG liquified petrolum gas
SI spark ignition

Bibliography

[1] BOSCH. Control of compression ignition engines. *WKiŁ*. Warszawa 2009.

[2] RYMANIAK, Ł. Comparison of the combustion engine operating parameters and the ecological indicators of an urban bus in dynamic type approval tests and in actual operating conditions. *MATEC Web of Conferences*. EDP Sciences, 2017. p. 00009.

[3] PIELECHA, J. et al. Badania emisji zanieczyszczeń silników spalinowych. *Wydawnictwo Politechniki Poznańskiej*. Poznań 2017.

[4] RYMANIAK, Ł. PIELECHA, J. BRZEZIŃSKI, Ł. Determining the NO_x emission from an auxiliary marine engine based on its operating conditions. *E3S Web of Conferences*. EDP Sciences, 2018. p. 00155.

[5] BELL, C. BOOST, M. Designing, Testing and Installing Turbocharger. *Bentley Publishers*. Cambridge 1997.

Prof. Jerzy Merkisz, DSc., DEng. – Faculty of Civil and Transport Engineering, Poznan University of Technology.
e-mail: *jerzy.merkisz @put.poznan.pl*

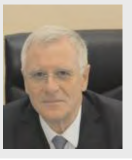

Maciej Bajerlein, DSc., DEng. – Faculty of Civil and Transport Engineering, Poznan University of Technology.
e-mail: *maciej.bajerlein@put.poznan.pl*

Bartłomiej Zieliński, Eng. – Faculty of Civil and Transport Engineering, Poznan University of Technology.
e-mail: *bartlomiej.j.zielinski@student.put.poznan.pl*

Article citation info:
ORCZYK, M., TOMASZEWSKI, F. Diagnostic and reliability model of an internal combustion engine. *Combustion Engines*. 2020, **180**(1), 41-46. https://doi.org/10.19206/CE-2020-107

Małgorzata ORCZYK
Franciszek TOMASZEWSKI

CE-2020-107

Diagnostic and reliability model of an internal combustion engine

The article presents a diagnostic and reliability model of an internal combustion engine that allows to assess the reliability status of the engine's systems for a two-state model of operation and maintenance: functional – failed. The proposed diagnostic model is a qualitative-quantitative probabilistic model combining the reliability states of the engine systems with the values of the vibroacoustic diagnostic signal parameters. The conducted diagnostic and reliability experiments and simulation tests showed that based on the developed diagnostic and reliability model, it is possible to determine the reliability states of the engine.

Key words: *diagnostics, internal combustion engine, diagnostic and reliability model*

1. Introduction

The basic task of technical diagnostics is to assess the technical condition or correctness of the tasks performed by a technical object without its disassembly. The technical condition of the object is most often defined by a set of parameters defining the features of its elements, e.g. their geometric features, their mutual position, unbalance, quality of cooperation, etc. In complex mechanical objects, it is not always possible to fully assess the status of individual elements [4].

In operational practice, especially in the operation system of technical facilities, including internal combustion engines, the exact value of the state (wear) of individual elements of the object is often not required, as it is sufficient to receive qualitative classification of the state of the object or its systems. The qualitative assessment comes down to determining the reliability state of the object, systems and assemblies in the form of a binary evaluation: functional or failed.

A study of mutual relations between diagnostic parameters and the damage process described by means of reliability indicators was carried out based on correlation and regression studies for a locomotive engine [11]. The conducted correlation research allowed to choose parameters of the vibration signal, which best represent the process of engine damage [7, 10].

The aim of the work is to present the concept of a diagnostic and reliability model that allows to assess the technical (reliability) state of the internal combustion engine systems, adopting a two-state model of operation and maintenance: functional – failed. To determine the parameters of the diagnostic and reliability model, diagnostic and reliability tests of internal combustion engines were carried out based on a passive-reliability diagnostic experiment [2, 3, 8].

2. The general diagnostic model of the object

The general model of the object can be presented, for example, in the form of a diagram, the so-called black box shown in Fig. 1 [5, 6].

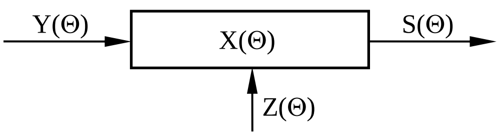

Fig. 1. Diagram of the object general model

This model can be described by the equation in the form:

$$S(\Theta) = \Phi[(Y(\Theta), X(\Theta)] + Z(\Theta) \quad (1)$$

where: $Y(\Theta)$ – a set of operational parameters, also called input parameters, which can include, for example, the load status of the object, the amount of energy consumed, etc., $Z(\Theta)$ – a set of environmental parameters, which include, among others, various kinds of interference in the surroundings of the object, the condition of the environment (temperature, humidity of air), etc., $X(\Theta)$ – a set of features characterising the state of modules (sub-assemblies) of the object, their state of regulation, etc., $S(\Theta)$ – a set of output parameters generated during the operation of the object: related to its function (torque, rotational speed, etc.) and accompanying parameters (vibrations, noise, thermal processes, etc.), Θ – measure of aging of the object.

Set of operational (input) parameters Y(Θ)

A set of operational (input, control) parameters of the object $Y(\Theta)$ is a collection of elements:

$$Y(\Theta) = \{y_1(\Theta), y_2(\Theta),.....,y_n(\Theta)\} \quad (2)$$

where: $y_i(\Theta)$, $i = 1,2,..,n$ – parameters characterising the object's operating status (state of regulation). These parameters can be: load, power supply status, rotational speed, operating conditions, state of regulation, etc.

It was assumed that during subsequent measurements (realisations), i.e. for subsequent time periods Θ_n, elements of $y_1(\Theta)$, $y_2(\Theta)$,..,$y_n(\Theta)$ of the set $Y(\Theta)$ are constant. The constant value of operational parameters for subsequent diagnostic measurements is a condition of repeatability of results for the same values of state parameters. Constant values of parameters from the set $Y(\Theta)$ were obtained by providing a determined energy state described by: constant speed and constant control settings. Assuming that:

$$y_1(\Theta_n) = \text{const},\ y_2(\Theta_n) = \text{const},........,\ y_n(\Theta_n) = \text{const}$$

for subsequent diagnostic measurements Θ_n; $n = 1, 2,....,j$, the set $Y(\Theta)$ is a set of constant input parameters independent from Θ_n, which can be written as:

$$Y(\Theta_n) = \text{const}$$

Received 25 September 2019; Received in revised form 12 December 2019; Accepted 15 January 2020
Available online 30 March 2020

Set of environmental parameters Z(Θ)

Set of environmental parameters (interferences) Z(Θ) that can affect the working conditions of the object is a collection of elements:

$$Z(\Theta) = \{z_1(\Theta), z_2(\Theta),......., z_n(\Theta)\} \quad (3)$$

where: $z_i(\Theta)$, i = 1,2,..,n – parameters influencing the object's functions and recorded output parameters (diagnostic signals) generated during the operation of the object. These parameters are related to the conditions of how the object is mounted, conditions of surroundings, instability of the test conditions, interferences in the measuring equipment, influence of other cooperating objects, etc.

The adopted criterion regarding the environmental parameters (interferences) is to minimise the influence of interferences on the measured parameters of diagnostic signals, i.e.:

$$Z(\Theta) = \min$$

or providing a comparable level of interference for subsequent diagnostic measurements (realisations) Θ_n, n = 1,2, ..., j, i.e.:

$$Z(\Theta) = \text{const}$$

Set of technical condition parameters – features of the object X(Θ)

The set of technical condition parameters (features) of object assemblies X(Θ) contains the following features:

$$X(\Theta) = \{x_1(\Theta), x_2(\Theta),.....,x_k(\Theta)\} \quad (4)$$

where: $x_i(\Theta)$, i = 1, 2, .., k – features describing the reliability status of the k of object's assemblies. For the constructed diagnostic and reliability model, in which the binary reliability model was assumed, each x_i can take values of 0 or 1 (functional, failed).

Set of output (diagnostic) parameters S(Θ)

The set of output parameters S(Θ) is a set of measured diagnostic parameters containing the following elements:

$$S(\Theta) = \{s_1(\Theta), s_2(\Theta),.....,s_n(\Theta)\} \quad (5)$$

where: $s_{ij}(\Theta)$ – the value of the i-th measured diagnostic parameter for the j-th measurement (time Θ_n).

The output parameters are obtained as a result of measurements of the diagnostic signal parameters made in the time interval Θ_n. These measurements can be made, for example, from the beginning of the service life Θ_1 to Θ_k, which is the end of operating time, in n moments in time. We assume that the i-th output parameter (i = 1, 2, ..., n) contains the values from the linearly ordered set of U_i called the range of variability of the i-th output parameter.

If in the process of perceiving the value of the object's features (indirectly by means of diagnosing) the following were assumed:

$$Y(\Theta_n) = \text{const}$$

and

$$Z(\Theta_n) = \text{const}$$

than general diagnostic model has the form:

$$S(\Theta) = f[X(\Theta)], \quad (6)$$

which means that if we assume constant conditions of the object's operation and constant values of the environmental parameters (interferences), then the object's output parameters will only be a function of the technical condition parameters (features) of the object.

3. Diagnostic and reliability model

The diagnostic and reliability model is a model combining the reliability states of object systems with the values of diagnostic signal parameters, therefore for its elaboration the following were determined:

- space of reliability states of the object,
- equations of binary (reliability) states of the object,
- model equations.

Construction of state space

The state X of the object is described by the set of status parameters of individual object systems:

$$X=\{x_1, x_2, x_3, ..., x_k\} \quad (7)$$

During the implementation of tasks, the object changes its properties, which is manifested in the changes in the values of the features that describe it. In practice, changes in the values of features are generally perceived in discrete form (due to periodic measurements of diagnostic parameters).

Construction of model equations

Diagnostic parameters assume values in space:

$$U = \underset{i=1}{\overset{n}{\times}} U_i \quad (8)$$

where: U_i (i = 1, ..., n) – is the range of variability of the i-th diagnostic parameter.

Values of diagnostic parameters s = [$s_1 s_2$... s_n] ∈ U are dependent on the physical state of the object x = [x_1, x_2, ..., x_k] ∈ W. The ideal situation would be if the system of recorded diagnostic parameters depended in a deterministic and unambiguous manner on the selected system of states of the object. Then this relationship can be expressed functionally in the following form:

$$\begin{aligned} s_1 &= f_1 (x_1, x_2,...,x_k) \\ s_2 &= f_2 (x_1, x_2,...,x_k) \\ s_n &= f_n (x_1, x_2,...,x_k), \end{aligned} \quad (9)$$

or shorter with vector notation:

$$s = f(x) \quad (10)$$

In order to identify functional relationships between the signal parameter vector and the object's state vector, taking into account the specificity of the experimental issues, probabilistic and statistical methods must be used. The use of the probabilistic model is required due to the existence of interferences caused mainly by the practical limitation of both the finite number of parameters of the diagnostic signal and the finite length of the object's state vector.

Construction of binary states

In practice, as already mentioned, the exact value of the status of individual elements of the object (e.g. the value of clearance) is not always important, as the qualitative classification of the state of the object, its systems or assemblies is sufficient. The binary classification of the states of the object, its systems or assemblies takes place by means of established permissible limit states.

Let ‘0’ indicate the state ‘functional’, while ‘1’ indicates the state ‘failed’. The task is to determine the relationship between reliability states of systems or assemblies of an object $x_i \in \{0,1\}$, i = 1, 2, ..., k with output parameters (signals) including a random error:

$$s = f(x_1, x_2, ..., x_k, \varepsilon) \tag{11}$$

As a probabilistic model, a system of qualitative regression equations with additive random errors was chosen:

$$\begin{aligned} s_1 &= \beta_{10} + \beta_{11}x_1 + \beta_{12}x_2 + \ldots + \beta_{1k}x_k + \varepsilon_1 \\ s_2 &= \beta_{20} + \beta_{21}x_1 + \beta_{22}x_2 + \ldots + \beta_{2k}x_k + \varepsilon_2 \\ s_n &= \beta_{n0} + \beta_{n1}x_1 + \beta_{n2}x_2 + \ldots + \beta_{nk}x_k + \varepsilon_n \end{aligned} \tag{12}$$

It should be noted that in the given system of equations the dependent variables $s_1, s_2, ..., s_n$ are of quantitative type, and the independent variables $x_1, x_2, ..., x_n$ are of qualitative type (binary).

Based on experimental data, the parameters of the probabilistic regression model can be estimated, as a result of which a system of regression equations is obtained:

$$\begin{aligned} \hat{s}_1 &= \hat{\beta}_{10} + \hat{\beta}_{11}x_1 + \hat{\beta}_{12}x_2 + \cdots + \hat{\beta}_{1k}x_k \\ \hat{s}_2 &= \hat{\beta}_{20} + \hat{\beta}_{21}x_1 + \hat{\beta}_{22}x_2 + \cdots + \hat{\beta}_{2k}x_k \\ \hat{s}_n &= \hat{\beta}_{n0} + \hat{\beta}_{n1}x_1 + \hat{\beta}_{n2}x_2 + \cdots + \hat{\beta}_{nk}x_k \end{aligned} \tag{13}$$

The above set of equations can be written as the following matrix:

$$\hat{s}^T = \hat{\beta} x^T \tag{14}$$

where: $\hat{s}^T$ – transposed matrix of diagnostic signals, $\hat{\beta}$ – regression coefficient matrix, x^T– transposed matrix of the engine states.

The system of regression equations determined on the basis of experimental data was used to determine the states of the object, its systems or assemblies coming from the population for which this system of equations was determined.

With the vector of signals s of the tested object and the matrix $\hat{\beta}$ of the estimated parameters of the model, the reliability states of individual object systems were estimated from the transformed dependence (14) in the form of:

$$x^T = \hat{\beta}^{-1} x^T \tag{15}$$

4. Construction of the diagnostic model at the object’s system level

Assuming the decomposition of systems into assemblies, one can determine the vector of states of the assemblies that make up individual systems. An analogous assumption was made as for systems where the states of the assemblies are binary and the system of n diagnostic signals remains constant. It was also assumed that the parameters of the diagnostic signals $s = [s_1, s_2, ..., s_n]$ are determined by the state of the assemblies that make up the individual object systems.

Let x_{ij} denote the state of the j-th assembly of the i-th system (i = 1, 2,....,k), which takes the values 0 or 1; in this case the description of states can be summarised in the form of Table 1.

Table 1. Description of states at the level of engine systems and assemblies

states of systems	X_1			X_2			..	X_z		
states of assemblies	X_{11}	..	X_{1m1}	X_{21}	..	X_{2m1}	..	X_{z1}	..	X_{zmk}

The approach described earlier at the systems level was used to build this model. It is assumed that the change in the state of any of the assemblies of the i-th system affects the change of at least one of the output signals. The goal is to estimate object states at the assembly level based on the diagnostic signal vector. After adopting the same assumption for assemblies, as before for systems, the task is to determine the relationship between reliability states $x_j \in \{0,1\}$ (j = 1, 2, ..., m_i) of the assemblies of the i-th system and signals $s = [s_1, s_2, ..., s_n]$.

As a probabilistic model for the i-th system of the object, a system of regression equations with additive random errors and binary states of assemblies was adopted:

$$\begin{aligned} s_1 &= \beta_{i10} + \beta_{i11}x_{i1} + \beta_{i12}x_{i2} + \ldots + \beta_{i1m_i}x_{im_i} + \varepsilon_{i1} \\ s_2 &= \beta_{i20} + \beta_{i21}x_{i1} + \beta_{i22}x_{i2} + \ldots + \beta_{i2m_i}x_{im_i} + \varepsilon_{i2} \\ s_n &= \beta_{in0} + \beta_{in1}x_{i1} + \beta_{in2}x_{i2} + \ldots + \beta_{inm_i}x_{im_i} + \varepsilon_{in} \end{aligned} \tag{16}$$

In the given system of equations, the diagnostic signals $s_1, s_2, ..., s_n$ are of the quantitative type, while the states x_{ij}, j = 1, 2,..., m_i take binary values.

The introduced model parameters for the i-th system:

$$\beta_i = \begin{bmatrix} \beta_{i10} & \beta_{i11} & \cdots & \beta_{i1m_i} \\ \beta_{i20} & \beta_{i21} & \cdots & \beta_{i2m_i} \\ \cdots & \cdots & \cdots & \cdots \\ \beta_{in0} & \beta_{in1} & \cdots & \beta_{inm_i} \end{bmatrix} \tag{17}$$

and interference of diagnostic signals that are unknown:

$$\varepsilon_i = [e_{i1}, e_{i2}, \ldots, e_{in}] \tag{18}$$

It is obvious that the actual parameter values β_i and interference values cannot be calculated. It is assumed, however, that the interferences have a normal distribution with an expected value of 0 and unknown, but equal, variances. With this assumption it is possible to estimate the parameters of the probabilistic regression model, based on experimental data, as a result of which a system of regression equations for the i-th system of the object can be obtained

$$\hat{s}_1 = \hat{\beta}_{i10} + \hat{\beta}_{i11} x_{i1} + \hat{\beta}_{i12} x_{i2} + \dots + \hat{\beta}_{i1m_i} x_{im_i}$$
$$\hat{s}_2 = \hat{\beta}_{i20} + \hat{\beta}_{i21} x_{i1} + \hat{\beta}_{i22} x_{i2} + \dots + \hat{\beta}_{i2m_i} x_{im_i} \quad (19)$$
$$\hat{s}_n = \hat{\beta}_{in0} + \hat{\beta}_{in1} x_{i1} + \hat{\beta}_{in2} x_{i2} + \dots + \hat{\beta}_{inm_i} x_{im_i}$$

which can be written as the following matrix:

$$\hat{s}^T = \hat{\beta}_i x_i^T \quad (20)$$

where: $\hat{s}^T$ – transposed matrix of diagnostic signals, $\hat{\beta}$ – matrix of regression coefficient for the i-th system of the object, x^T – transposed matrix of states of the assemblies of the i-th system.

Having the given signal vector s of the examined object and the matrix $\hat{\beta}_i$ of the estimated parameters of the model, it is possible to estimate the states of individual assemblies of the i-th system, using the formula:

$$x_i^T = \hat{\beta}_i^{-1} s^T \quad (21)$$

Knowledge of the coefficients of the system, however, does not allow to estimate the discrepancy between the estimated and actual states of the assemblies, the more so because the estimated states do not take binary values, but are real numbers. To determine the intensity of the relationship between the actual parameters of the diagnostic signal s and estimated values $\hat{s}$ the coefficient of determination $R^2 = R^2(s, \hat{s})$ was used.

The determination coefficient, as a normalised measure of linear relationship between the diagnostic signal and the states of the assemblies that make up the subsequent systems of the object, is the basis for the selection of equations. Equations with determination coefficients that are as close as possible to 1 should be chosen. The low value of the determination coefficient indicates a weak relation between the actual parameters of the diagnostic signal s and the estimated values $\hat{s}$ [1].

The diagnostic states of the object s are a vector of random variables with the expected value:

$$E(s^T) = \beta_i x_i^T \quad (22)$$

Coefficients $\hat{\beta}$ of the model:

$$\hat{s}^T = \hat{\beta}_i x_i^T, \quad (23)$$

that estimates the states of the assemblies of the i-th object's system as functions of a random sample, are random variables – estimators of the actual values of the object's parameters. These estimators, obtained on the basis of the minimum of the sum of squares, are unbiased.

5. Model identification

The identification of the diagnostic and reliability model at the object assembly level was based on the results of the diagnostic observation of an internal combustion engine of a rail vehicle under operating conditions. The scope of the research was carried out according to the principles of the passive-reliability experiment [7].

The columns of the matrix of observation results contain observed diagnostic parameters; the rows contain the realisations of parameters, which were normalised to the first measurement (the first realisation of a given parameter) separately for each signal parameter, according to the following formula:

$$s_{i,j}^n = \frac{s_{i,j}}{s_{i,1}} \quad (24)$$

where: $s_{i,j}^n$ – normalised value of the i-th signal parameter for the j-th measurement (realisation), $s_{i,j}$ – actual value of the i-th parameter for the j-th measurement (realisation), $s_{i,1}$ – actual value of the i-th parameter for the first measurement (realisation).

As a result of normalisation, dimensionless parameter values are obtained, thus it is not necessary to consider various ranges of their values and various units. The normalised parameter values are an indicator of the parameter's changes for subsequent realisations and a measure of the sensitivity of the individual parameters to changes in the state of the engine.

On the basis of reliability data (acquired during the experiment), a binary matrix of reliability (qualitative) states of individual engine systems was created, assuming '0' as the 'functional' state and '1' as the 'failed' state of the engine, for the same values of locomotive mileage as in case of the measurement of the signal vector.

For such prepared data, calculations were made based on a developed digital simulator. Linear regression calculations were performed separately for each parameter of the vibration signal treated as a (dependent) variable. The reliability states (0 or 1) of individual engine systems were used as independent variables. As a result of the calculations, values of regression coefficients were obtained, and then according to the relationship (12), systems of regression equations.

An example of the equation with a constant value for Ask (effective value of vibration acceleration) is the equation (27) and without this constant – the equation (28).

$$\text{Ask} = 1.175 - 0.19\cdot\text{KOR} - 0.38\cdot\text{PAL} + 1.1435\cdot\text{SMA} - 0.505\cdot\text{WYM} - 0.248\cdot\text{GLO} + 0.4037\cdot\text{ROZ} - 0.027\text{CHL} + 0.4656\cdot\text{POZ} \quad (25)$$

$$\text{Ask} = -0.134\cdot\text{KOR} - 0.338\cdot\text{PAL} + 2.1531\cdot\text{SMA} - 0.409\cdot\text{WYM} - 0.145\cdot\text{GLO} + 0.9606\cdot\text{ROZ} - 0.639\cdot\text{CHL} + 0.2518\cdot\text{POZ} \quad (26)$$

where: KOR – crank system, PAL – fuel system, SMA – lubrication system, WYM – scavenging system, GLO – engine heads, ROZ – timing system, CHL – cooling system, POZ – other engine systems.

The presented equations (25) and (26) allow, based on the measured effective value of vibration accelerations, to determine the reliability status of the internal combustion engine systems.

6. Model verification

Regression coefficients β, calculated on the basis of experimental data, created a matrix of regression coefficients, from which a square matrix was selected, for which the signal parameters obtained the highest values of the determination coefficient R^2 [9].

For the example shown, these were the following parameters of the vibration signal:

Aav – average value of vibration acceleration,
Ask – effective value of vibration acceleration,

Xav – average value of vibration displacement,
Xsk – effective value of vibration displacement,
Xsz – peak value of vibration displacement,
Kx – shape coefficient of vibration displacement,
fx – rice frequency of vibration displacement,
Hv – harmonic factor of vibration velocity.

The matrix obtained from the regression coefficients with the biggest R^2 is a square matrix with 8 columns and rows. In the presented example, the assessment of the engine's condition at the level of its main systems was adopted.

A system of non-constant regression equations was adopted for further analysis. Such a set of equations, assuming that all the engine systems are functional, does not contain any terms and the equation equals zero, which means that the whole engine is in functional state. However, when an engine system or systems fail, then the equation has terms corresponding to these failed systems.

Matrix β of regression coefficients with the largest R^2 was inverted and multiplied by columns corresponding to subsequent measurements (realisations) of the transposed matrix of standardised signal symptoms. After multiplying the inverted matrix of the regression coefficients by normalised values of the signal parameters, the theoretical states of individual engine systems were obtained. These were then normalised to the maximum obtained value.

Figure 2 presents exemplary results of calculated theoretical states and actual states of engine systems observed in operation.

The actual statuses observed in operation are shown in the figures in the form of bars taking the value '0' ('functional' state) and the value '1' ('failed' state). The calculated states of the engine systems are shown in the form of points connected by a line. If the calculated value of the system state equals to $x_i > 0$, then the system is in the 'failed' state; if, however, the calculated value of the system state equals to $x_i \leq 0$, the system is in the 'functional' state. The presented results of calculations were satisfactory while assessed with values of diagnostic signal parameters known from operation.

Based on the results of the calculations of the state of the engine systems obtained in the presented example, the probability of correctness of the diagnosis was calculated according to the formula (27). It can be considered as an indicator of the model's compliance with the real object.

$$P_d = \frac{n_e}{n_s} \qquad (27)$$

where: P_d – probability of correctness of the diagnosis, n_e – number of engine system states for which the state determined from the calculation is consistent with the state registered in operation, n_s – total number of engine system states.

For the presented example, the probability of a correctness of the diagnosis amounts to $P_d = 0.75$.

7. Conclusions

The article presents a developed diagnostic and reliability model of a complex mechanical object, for which validation of results and verifications was carried out on the example of the internal combustion engine systems of a rail vehicle. This model has been developed assuming that on the basis of the vector of the vibration signal parameters it is possible to assess the technical condition of a complex object by adopting a two-state model of operation and maintenance.

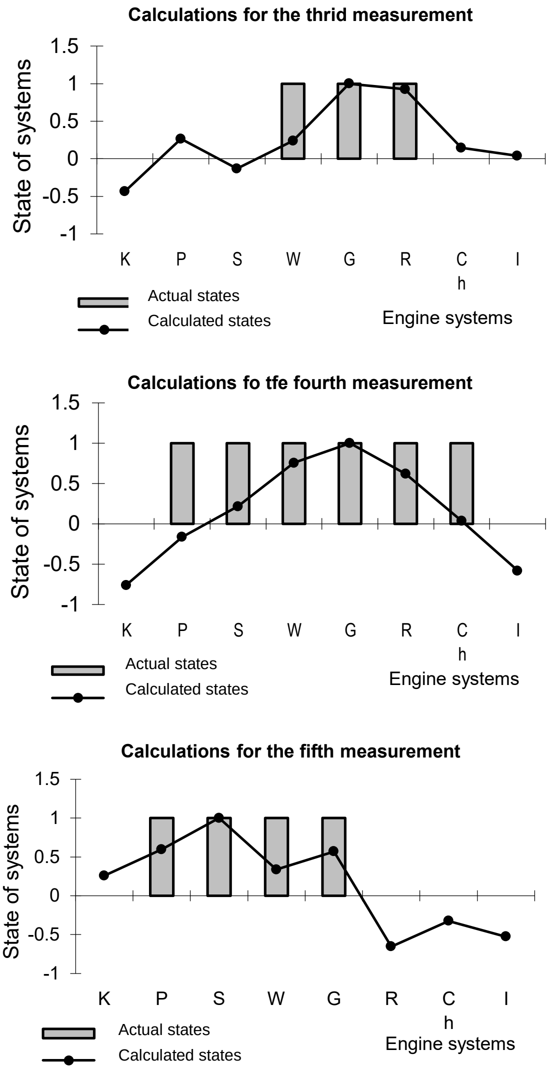

Fig. 2. The results of calculations of the engine systems states for the third measurement in operation of engine

The verification of the developed diagnostic and reliability model of a complex mechanical object allows to specify the following conclusions:

– for a complex mechanical object, it is possible to determine a diagnostic model binding the parameters of the vibration signal – quantitative assessment – with the parameters of the state of its systems – quality assessment,
– on the basis of the presented and verified diagnostic and reliability model, with knowledge of the signal parameters, it is possible to determine the (binary) reliability states of the internal combustion engine and its systems,

it is possible to use the developed diagnostic and reliability model for other complex mechanical objects.

Acknowledgements

Presented research and the paper are partly funded by Statutory Activities fund of the Institute of Combustion Engines and Transport, PUT (PL) 5/52/DSPB/1277.

Bibliography

[1] AMPUŁA, D. Regresja jako metoda procesu predykcji. *Problemy Techniki Uzbrojenia*. 2014, **130**, 67-78.

[2] BOBROWSKI, D. Probabilistyka w zastosowaniach technicznych. *WNT*. Warszawa 1980.

[3] CEMPEL, C. Podstawy wibroakustycznej diagnostyki maszyn. *WNT*. Warszawa 1982.

[4] GAVRILIUK, E.A., MANTSEROV, S.A. Fuzzy reliability model of systems for decision support in technical diagnostics. *Proceedings of the II International Scientific and Practical Conference "Fuzzy Technologies in the Industry"* (FTI 2018), Ulyanovsk, 2018.

[5] MURPHY, M.D., PAASCH, R. Reliability centered prediction technique for diagnostic modeling and improvement. *Research in Engineering Design*. 1997, **9**(1), 35-45.

[6] NIZIŃSKI, S., RYCHLIK, A. Model diagnostyczny złożonego obiektu technicznego. *Biuletyn WAT*. 2011, **LX**, 1, 195-209.

[7] ORCZYK, M., TOMASZEWSKI, F. Method of reduction of diagnostic parameters during observation on the example of a combustion engine. *MATEC Web of Conferences*, 2017, **118**, 00034. https://doi.org/10.1051/matecconf/201711800034

[8] PIELECHA, I., SKOWRON, M., WISŁOCKI, K. Mathematical models formulation for the delay of SIDI injectors opening based on optical tests. *Combustion Engines*. 2016, **167**(4), 8-21. https://doi.org/10.19206/CE-2016-402

[9] RABIEJ, M. Statystyka z programem Statistica. *Wydawnictwo Helion*. Gliwice 2012.

[10] SZYMAŃSKI, G.M., MISZTAL, W. Analysis of measurement points sensitivity of vibration signals on the stand of jet engine. *Combustion Engines*. 2017, **171**(4), 279-282. https://doi.org/10.19206/CE-2017-448

[11] TOMASZEWSKI, F. Diagnostyczno-niezawodnościowe modele regresyjne silnika spalinowego lokomotywy. *DIAGNOSTYKA 2000, II Międzynarodowy Kongres Diagnostyki Technicznej*. 239-240, Warszawa, 2000.

Małgorzata Orczyk, DSc., DEng. – Faculty of Civil and Transport Engineering, Poznan University of Technology.

e-mail: *malgorzata.orczyk@put.poznan.pl*

Prof. Franciszek Tomaszewski, DSc., DEng. – Faculty of Civil and Transport Engineering, Poznan University of Technology.

e-mail: *franciszek.tomaszewski@put.poznan.pl*

Article citation info:
LONGWIC, R., WOŹNIAK, G., SANDER, P. Compression-ignition engine fuelled with diesel and hydrogen engine acceleration process. *Combustion Engines*. 2020, **180**(1), 47-51. https://doi.org/10.19206/CE-2020-108

Rafał LONGWIC
Gracjana WOŹNIAK
Przemysław SANDER

CE-2020-108

Compression-ignition engine fuelled with diesel and hydrogen engine acceleration process

The paper presents the results of research consisting in acceleration of a diesel engine powered by diesel and hydrogen. The test stand included a diesel engine 1.3 Multijet, hydrogen cylinders and measuring equipment. Empirical tests included engine testing at idle and at specified speeds on a chassis dynamometer, vehicle acceleration in selected gears from specified initial values of engine revolutions was also tested.. Selected parameters of the diesel fuel combustion and injection process were calculated and analyzed. The paper is a preliminary attempt to determine the possibility of co-power supply to diesel and hydrogen engines.

Key words: *hydrogen, compression-ignition engine, acceleration process, diesel fuel*

1. Introduction

Combating the greenhouse effect is the most important challenge facing humanity over the next decade. In the field of combustion engines, this is done by tightening the emission standards, increasing the combustion efficiency to maintain fuel economy and searching for new low-emission fuels. One of the possibilities of improving the parameters and pro-ecological properties of engines is the use of hydrogen as a fuel. In many publications the results of the research were presented, showing the benefits and possibilities related to the use of hydrogen as a fuel, among others, in the form of reduction of toxic exhaust gas components emission. [1–4].

Hydrogen (H) is an alternative to traditional fuels and can be used to power automobiles in two ways:

– as a fuel in a traditional engine, which is the source of thermal energy,
– in fuel cells to generate energy to drive an electric motor [5, 6].

Hydrogen can be used as a stand-alone fuel or as an 'additive' to other fuels. It is characterized by favourable properties in relation to hydrocarbon fuels such as: no carbon, high combustion rate, wide flammability range. Hydrogen is currently considered to be the most environmentally friendly energy carrier and it is predicted that hydrogen will be the fuel of the future [2, 5]. It is assumed that in 2050, 20-25% of passenger transport will be serviced by vehicles powered by this gas [7, 8]. A separate issue is how to obtain hydrogen and the ecology of this process.

2. Research site and research methodology

2.1. Research site

The tests were carried out on a stand consisting of a diesel engine 1.3 Multijet built in a Fiat Qubo vehicle meeting the Euro 5 standard, to which hydrogen was supplied from the cylinder to the inlet channel by means of wires. The technical data of the engine is presented in Table 1 into non-return valves. The pressure of hydrogen dosed was regulated by a valve and read on a manometer, and the flow rate was measured by means of a digital mass flow meter Vogtlin, located in the pipe directly supplying the gas to the system. Additionally, the test stand was extended by an external fuel supply system, which allows the vehicle engine to be supplied with other alternative fuels without the need to change the fuel in the main fuel tank every time. [9].

The INDIMICRO 602 system by AVL was used to indicate the engine in dynamic conditions. It included a computer with AVL software, AVL measuring module and AVL transmitter. The basic functions of this system include [9]:

– recording the pressure course inside the cylinder – using the AVL GH13P piezoeletric sensor installed in the glow plug nest of the first cylinder,
– recording of the crankshaft position signal,
– analysis of injection parameters – using an analogue signal of injector control after conversion into a digital signal.

The tests were carried out on Dynorace chassis dynamometer designed for two axle drive vehicles type DF4FS-HLS, consisting of a control system and a load generating system. The vehicle is shown on the chassis dynamometer in Fig. 1. The elements of the test stand are shown in Fig. 2.

Table. 1 Technical data of the test engine (1,3 Multijet) [9]

Maximum power [KM]	75
Maximum power [kW]	55
Total capacity [cm^{3}]	1248
The number of cylinders	4
Diameter of a cylinder [mm]	69.6
Piston stroke [mm]	82
Rotations on neutral gear [rot/1’]	850 ± 20
Maximum moment [Nm]	190
Maximum moment [kgm]	19.4
Rotational speed at maximum moment [rot/1’]	1500

Fig. 1. Research car, Fiat Qubo with engine 1.3. MultiJet

Received 25 September 2019; Received in revised form 12 December 2019; Accepted 15 January 2020
Available online 30 March 2020

Fig. 2. Research site: 1. The view inside the vehicle with research apparatus: computer with AVL software, measuring module AVL and AVL converter, 2. Hydrogen cylinder, 3. The view of the engine compartment with the hydrogen supply location

2.2. Research methodology

Tests were carried out to determine the effect of hydrogen addition (fed to the inlet channel) on the operating parameters of a ZS motor. The measurements were carried out during the acceleration of the vehicle for two variants of operation, i.e. for diesel oil and for diesel oil with the addition of hydrogen fed to the engine intake system. The pressure in the combustion chamber, engine speed and fuel injection parameters were recorded. The hydrogen flow was set at 20 ln/min. Engine tests included engine idle and at specific rotational speeds of 2000 rpm, 2500 rpm, 3000 rpm, 3500 rpm, 4000 rpm in vehicle driving conditions on a chassis dynamometer. The vehicle was then loaded with rolling resistance forces. An additional variant of the tests was acceleration of the vehicle on a chassis dynamometer in gear II and IV from the initial engine speeds of about 840 rpm and 2000 rpm respectively.

The research cycle included the following steps:

1. temperature stabilisation of the motors
2. engine speed stabilisation as indicated in the table.
3. hydrogen flow stabilisation

3. Analysis of test results obtained

Table 2 shows the engine operating parameters diesel fuelled with diesel and hydrogen fuelled diesel at selected speeds. The values of acceleration lever position, fuel temperature, bus pressure, amount of injected fuel, charge pressure and air flow are presented.

The addition of hydrogen slightly reduces the amount of injected diesel fuel at most engine speeds. The difference is within the range from 0.31 to 0.75 mm^3/cycle. Detailed data are presented in Fig. 3.

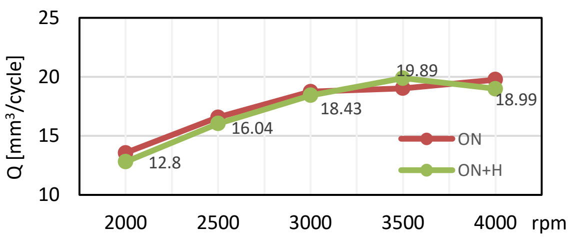

Fig. 3. Amount of injected fuel depending on the rotational speed at the supply of diesel and diesel with the addition of hydrogen

Table 2. Compression-ignition engine operating parameters

Engine operating parameters DF					
n_s [rpm]	2000	2500	3000	3500	4000
Position sensor for accelerator lever [%]	29	21	31	32	36
Fuel temperature sensor [^{o}C]	48	48	48	48	48
Bus pressure sensor [bar]	614	704	834	946	1022
Injected quantity ON [mm^3/cycle]	13.55	16.57	18.74	19.03	19.76
Charge pressure sensor [mbar]	1241	1400	1542	2000	1664
Air flow meter [mg]	313	451	549	584	477
Motor operating parameters DF+ H at 20 ln/min flow rate					
Position sensor for accelerator lever [%]	2000	2500	3000	3500	4000
Fuel temperature sensor [^{o}C]	21	30	37	42	39
Bus pressure sensor [bar]	39	39	40	40	40
Injected quantity ON [mm^3 /cycle]	576	734	896	962	1014
Position sensor for accelerator lever [%]	12.84	16.04	18.43	20.3	18.99
Charge pressure sensor [mbar]	1279	1307	1639	1740	1643
Air flow meter [mg]	317	379	424	563	451

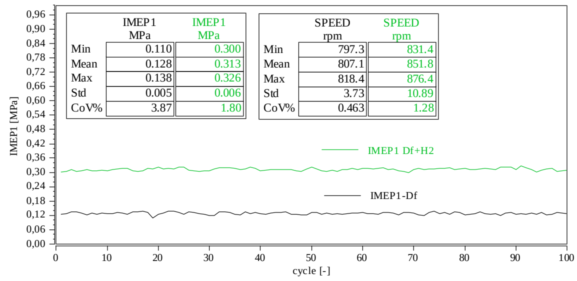

Fig. 4. Mean indicated pressure for 100 subsequent working cycles of the engine powered by diesel oil (black colour) and diesel oil and HHO (green colour) at idling speed; additionally, the tables show minimum, maximum, average values and standard deviation for mean indicator pressure (IMEP1) and engine speed

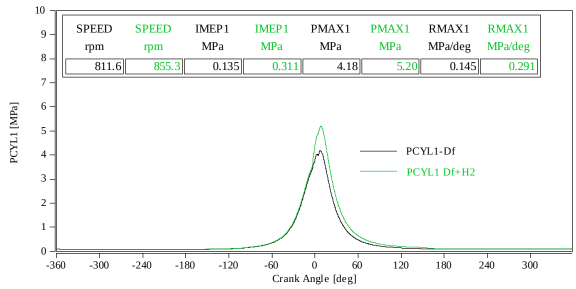

Fig. 5. Pressure inside the combustion chamber for idle operation, with diesel (black colour), diesel and H (green colour), additionally the table shows the average index pressure (IMEP1), maximum combustion pressure (PMAX1), maximum pressure rise speed (RMAX1) and engine speed (SPEED)

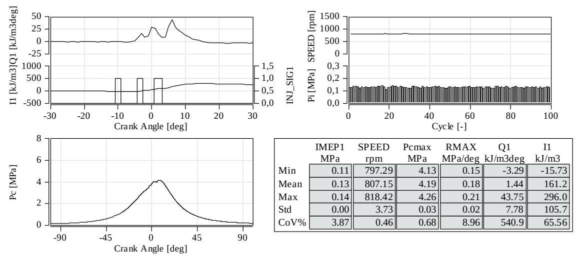

Fig. 6. Engine idle running with diesel supply; The courses of developing heat (Q1) and amount of developed heat (I1), mean indexed pressu-re (IMEP1) are presented

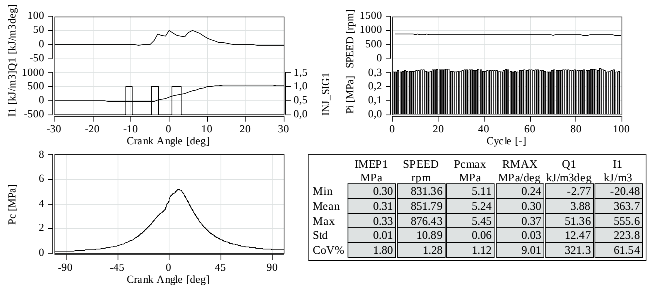

Fig. 7. Engine idle running, diesel fuelled, with the addition of hydrogen. The courses of developing heat (Q1) and amount of developed heat (I1), mean indexed pressure (IMEP1) are presented

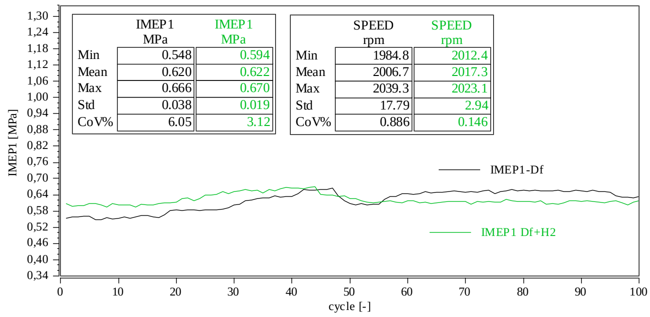

Fig. 8. Mean indicated pressure for 100 subsequent working cycles of the engine powered by diesel oil (black colour) and diesel oil and HHO (green colour), a vehicle driving with engine rotational speed of about 2000 rpm – gear 4; additionally, the tables show minimum, maximum, average and standard deviation for average indicator pressure (IMEP1) and engine speed

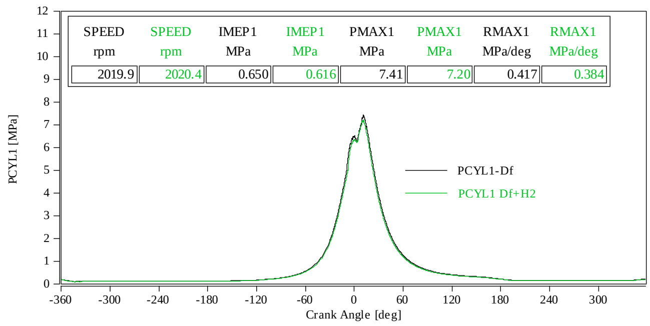

Fig. 9. Pressure inside the combustion chamber at engine speed about 2000 rpm – gear 4, at diesel fuel supply (black colour) and diesel oil and H (green colour), additionally the table shows average indexed pressure (IMEP1), maximum combustion pressure (PMAX1), maximum pressure rise speed (RMAX1) and engine speed (SPEED)

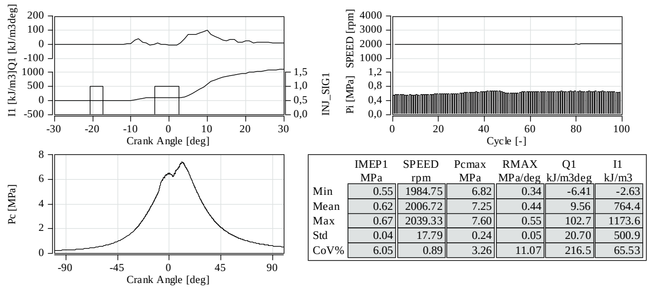

Fig. 10. A vehicle driving with engine rotational speed of about 2000 rpm in the fourth gear, with diesel fuel supply; The courses of developing heat (Q1) and amount of developed heat (I1), mean indicator pressure (IMEP1) are presented

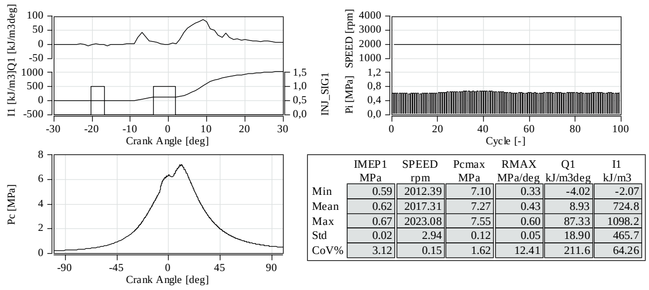

Fig. 11. A vehicle driving with engine rotational speed of about 2000 rpm in the fourth gear, with diesel fuel with the addition of hydrogen; The courses of developing heat (Q1) and amount of developed heat (I1), mean indicator pressure (IMEP1) are presented

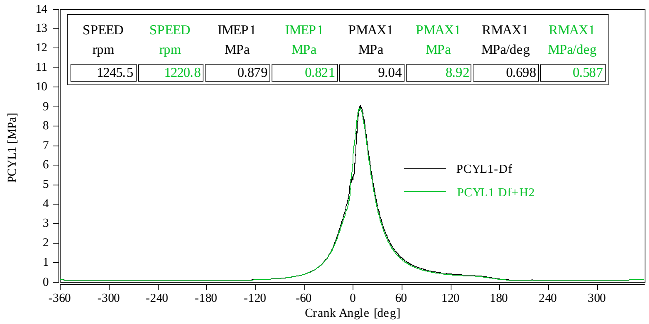

Fig. 12. Internal combustion chamber pressure during vehicle acceleration for second gear at engine speed 1245 rpm, for diesel (black colour) and diesel and H (green colour), in addition the table shows the mean index pressure (IMEP1), maximum combustion pressure (PMAX1), maximum pressure rise speed (RMAX1) and engine speed (SPEED)

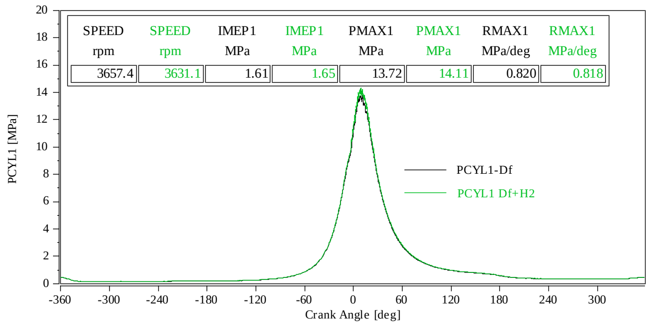

Fig. 13. Internal combustion chamber pressure during vehicle acceleration for second gear at engine speed 3657 rpm, for diesel (black colour) and diesel and H (green colour), in addition the table shows the average indicator pressure (IMEP1), maximum combustion pressure (PMAX1), maximum pressure rise speed (RMAX1) and engine speed (SPEED)

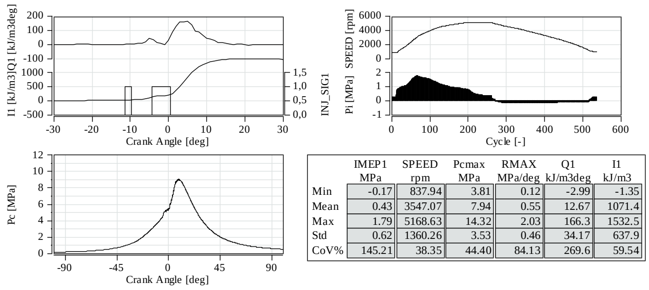

Fig. 14. The vehicle acceleration in the second gear with the throttle open at maximum, with diesel supply; The courses of developing heat (Q1) and amount of developed heat (I1), mean indexed pressure (IMEP1) are presented are presented

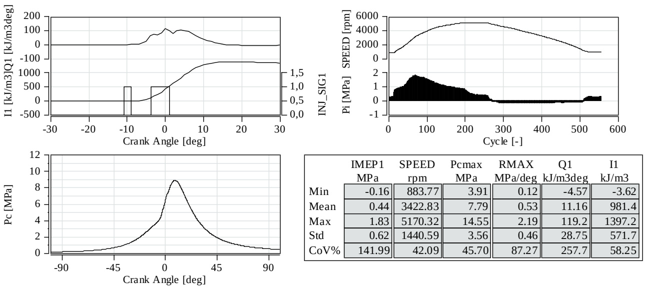

	IMEP1 MPa	SPEED rpm	Pcmax MPa	RMAX MPa/deg	Q1 kJ/m3deg	I1 kJ/m3
Min	-0.16	883.77	3.91	0.12	-4.57	-3.62
Mean	0.44	3422.83	7.79	0.53	11.16	981.4
Max	1.83	5170.32	14.55	2.19	119.2	1397.2
Std	0.62	1440.59	3.56	0.46	28.75	571.7
CoV%	141.99	42.09	45.70	87.27	257.7	58.25

Fig. 15. The vehicle acceleration in the second gear with the throttle open at maximum, with diesel fuel with the addition of hydrogen; The courses of developing heat (Q1) and amount of developed heat (I1), mean indexed pressure (IMEP1) are presented

Figures 4 to 7 show the engine operating parameters at idling speed supplied with diesel (black colour), diesel and hydrogen (green colour). The tables show minimum, maximum, maximum, average and standard values for mean indexed pressure (IMEP1), maximum combustion pressure (PMAX1), maximum pressure rise speed (RMAX1) and engine speed (SPE-ED). In the range of average values of measured parameters it was found that the average value of average indexed pressure (from 100 consecutive cycles of engine operation) increased by about 144% when the engine was supplied with diesel and hydrogen at the same time. The maximum value of the average indexed pressure increased by 136% with simultaneous increase of the average engine speed. The addition of hydrogen also increases the maximal speed of pressure rise, the maximum value of the heat transfer rate and the amount of heat transfer coefficient. These parameters increase by 76%, 17% and 87% respectively in relation to the diesel supply. Figure 3.3 shows the course of pressure inside the combustion chamber at a speed of approx. 800 rpm. The maximum value of pressure inside the combustion chamber increased by approx. 24% in the case of ON+H engine power supply relative to ON power supply alone.

Figures 8 to 11 show the engine operating parameters for a vehicle travelling in fourth gear at engine speed of about 2000 rpm, supplied with diesel (black colour) and diesel and hydrogen (green colour). The value of the average pressure indexed in the case of diesel oil supply with the addition of hydrogen slightly decreased. The pressure inside the combustion chamber decreased by 2.8%. The addition of hydrogen to the combustion process also affects the reduction of the maximum heat discharge values and the amount of heat discharge, respectively by 17.5% and 6.9%.

Figures 12 to 13 show the engine operating parameters for a vehicle being driven in the second gear with the fuel delivery control unit open at the maximum speed of 1245 rpm and 3657 rpm, respectively, for diesel (black colour) and diesel oil and hydrogen (green colour) – the vehicle was loaded with rolling resistance and inertia resistance forces. It was noted that the maximum pressure inside the combustion chamber at a speed of 1245 rpm decreased by about 1.3%, and for 3657 rpm it increased by about 2.8% in the case of ON+H engine power supply relative to ON power supply alone. Additionally, it can be stated that the maximum values of the heat discharge course and the amount of heat discharge decreased by 28% and 8%, respectively, in relation to the diesel supply – Fig. 14 and 15.

4. Conclusion

On the basis of the conducted research, the influence of the addition of hydrogen administered to the inlet system on the operation of a compression-ignition engine was evaluated. When the engine is simultaneously supplied with diesel oil and hydrogen added to the intake manifold, the average indexed pressure increased at idling speed by about 144% in relation to the supply with diesel oil only. The amount of heat produced, the maximum combustion pressure and the maximum rate of pressure rise also increased.

On the basis of the presented initial measurements it was stated that for the engine operating at idling speed, the addition of H affects the increase of engine parameters. For engine operating conditions other than idling, a decrease in heat output, heat output, pressure inside the combustion chamber and average indexed pressure was observed. In the course of the research, hydrogen expenditure was selected so that in all engine operating conditions it did not have an extremely negative impact on engine operation – so that there was no explosion of gas deposited in the intake manifold. The original maps of diesel fuel injection time control have not been modified. At present, it seems that hydrogen supplied to the intake manifold may influence the improvement of engine energy parameters, but in order for this influence to be safe and observable outside the idle gear, it is necessary to modify both the dose of hydrogen and the dose of diesel oil each time to the engine operating conditions. It should also be considered whether it would be possible to replace hydrogen with Brown HHO gas obtained from the on-board gas generator.

Nomenclature

ON	diesel	DF	diesel fuel
H	hydrogen	ZS	compression ignition
SPEED	engine speed	Q1	developing heat
IMEP	mean indexed pressure	RMAX1	maximum rate of increase of combustion pressure
PMAX1	maximum combustion pressure	I1	amount of developed heat

Bibliography

[1] KRUCZYŃSKI, S., ŚLĘZAK, M., GIS, W. et al. Evaluation of the impact of combustion hydrogen addition operating properties of self – ignition engine. *Eksploatacja i Niezawodnosc – Maintenance and Reliability*. 2016, **18**(3), 343-347. https://doi.org/10.17531/ein.2016.3.4

[2] LEJDA, K. Wodór w aplikacjach do środków napędu w transporcie drogowym. Oficyna Wydawnicza Politechniki Rzeszowskiej, Rzeszów 2013.

[3] MERKISZ, J., IDZIOR, M., BAJERLEIN, M. et al. The impact of hydrogen in diesel fuel on the parameters of CI engine's performance. *Mechanika Czasopismo Techniczne*. 2012, 261-274.

[4] SURYGAŁA, J. Wodór jako paliwo. *Wydawnictwa Naukowo-Techniczne*. Warszawa 2008.

[5] GIS, W. Implementation of vehicles equipped with fuel cells and hydrogen refueling infrastructure in Europe. *Combustion Engines*. 2015, **162**(3), 782-787.

[6] WOŹNIAK, G., LONGWIC, R. Initial assessment of the course of combustion process in a diesel engine powered by diesel oil and Brown's gas. *IOP Conference Series Materials Science and Engineering*. 421, 042085. https://doi.org/10.1088/1757-899X/421/4/042085

[7] Raport Energetyka zrównoważona. www.feri.org.pl. Wodór. 2018.

[8] Automotive Industry Raport. www.pzpm.otg.pl.2018/2019

[9] LONGWIC, R., SANDER, P. The characteristics of the combustion process occurring under real operating conditions of traction. *IOP Conference Series Materials Science and Engineering*. **148**(1). https://doi.org/10.1088/1757-899X/148/1/012071

Rafał Longwic, DSc., DEng. – Faculty of Mechanical Engineering, Lublin University of Technology.
e-mail: *r.longwic@pollub.pl*

Sander Przemysław, MEng.– Faculty of Mechanical Engineering, Lublin University of Technology.
e-mail: *p.sander@pollub.pl*

Gracjana Woźniak, MEng. – Faculty of Mechanical Engineering, Lublin University of Technology.
e-mail: *g.wozniak@pollub.pl*

Article citation info:
STOECK, T. Simplification of the procedure for testing common rail fuel injectors. *Combustion Engines*. 2020, **180**(1), 52-56. https://doi.org/10.19206/CE-2020-109

Tomasz STOECK

CE-2020-109

Simplification of the procedure for testing common rail fuel injectors

The paper presents a simplified methodology for generating the characteristic curve of fuel doses for common rail injectors, which consists in limiting the number of measurements on the test bench and calculating missing data using predefined (array) functions of the Microsoft Excel spreadsheet. This allows checking the method of fuel delivery in a wide spectrum of predefined pressures and atomiser opening times, while reducing the arduousness and time-consumption of the active experiment phase. The proposed solution is particularly useful in problematic situations when standard manufacturer's tests, referred only to selected work points, make it impossible to clearly assess the technical condition of the injector.

Key words: *common rail injector, fuel doses characteristic curve, simplification of test procedures*

1. Introduction

All tests of fuel injection apparatus requiring the dismantling of its actuators from the engine belong to invasive methods [13]. The most reliable and precise way to diagnose fuel injectors are test-bench tests, which are performed on dedicated test benches [11]. They are universal bench devices equipped with single or multiple measuring chain systems. They can be compact in design or modular, enabling the installation of equipment compatible with the capabilities and the profile of operations of a given car workshop or service company. The benches have all the necessary adapters and connectors, both for fixing the fuel injector and connecting the hydraulic and electric lines. This allows not only for diagnostic tests, but also for thermochemical flushing, i.e. the process of internal cleaning under high pressure and at elevated detergent temperature [12].

Standard tests of the common rail fuel injector are performed in automatic cycles or, much less often, with manual settings. Usually they include several operating points for different pressures of the supplied fuel and atomiser opening (actuation) times, according to the manufacturer's recommendations [8]. Unfortunately, many years of workshop and laboratory practice indicates that such measurements may prove to be insufficient, primarily due to improper fuel dosing in other areas of engine operation. Detection of these irregularities is possible, but after preparing the full characteristics of the fuel doses. Despite the undoubted benefits, this function is rarely used, only in justified cases, which results from the arduousness and time-consumption of the test phase. As a result, the process of checking a set from one engine becomes problematic and economically unjustified. Therefore, an own methodology was proposed, the idea of which is based on limiting the number of measurements to the necessary minimum and calculating the remaining data in the environment of a popular spreadsheet.

2. Methods

2.1. Test object and test beds

The test was carried out on the example of a Bosch CRI1 electromagnetic fuel injector (Fig. 1), which was dismantled from a Fiat 1.3 JTD 16V MultiJet diesel engine with an operating mileage of 158 thousand km.

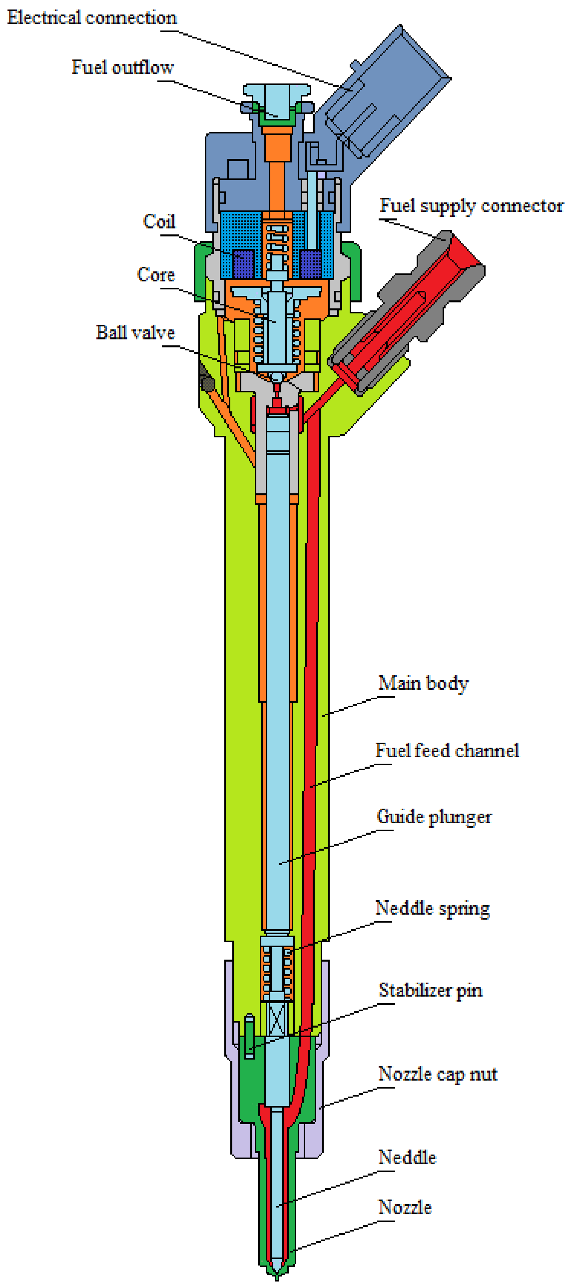

Fig. 1. CRI1 Bosch fuel injector design

Received 30 January 2020; Received in revised form 20 February 2020; Accepted 20 February 2020
Available online 30 March 2020

Fuel injectors of this type are commonly used in the combustion engines of passenger cars, working at maximum fuel injection pressures of up to 140 MPa [16]. Because the manufacturer has made available the technology for their diagnostics, while offering a set of original spare parts, they can be regenerated to almost full extent [14].

Fig. 2. Test bench STPiW-3 [17]

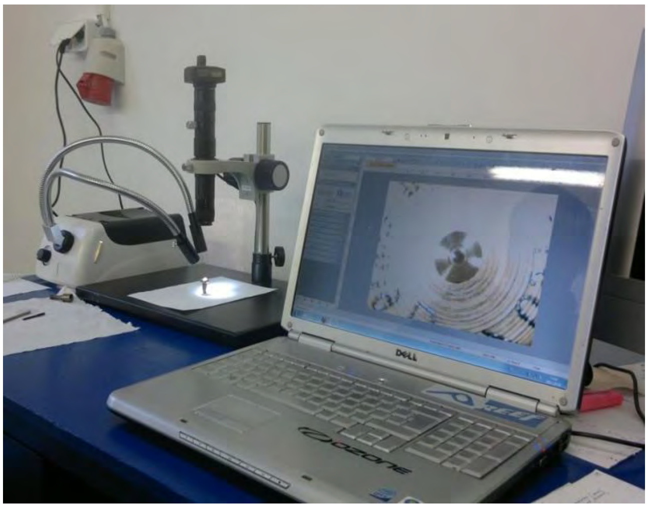

Fig. 3. Microscope Meiji FL150/70 [19]

The following systems and instrumentation were used in the repair process:
– STPiW-3 test bench (Fig. 2),
– 3-phase Bosch gear (CRR 120 pneumatic generator and CRR 220 electric generator, CRR 420 digital sensor, LAB/SM135 power supply, CRR 320 torque wrench),
– Meiji FL150/70 microscope (Fig. 3),
– MIC-40700 multimeter,
– ultrasonic baths (Carbon Tech Ultrasonic Bath S15/C2, Elmasonic S10H),
– vices and gear required for the disassembly and assembly phase.

In order to prepare a full characteristics of the fuel doses in a simplified way, measurements on the test bench were carried out at the predefined actuation times (main nodes) t [µs]: 200, 300, 600, 1200. The obtained test results were entered into a Microsoft Excel spreadsheet, after which the missing data were estimated in indirect points.

2.2. Predefined (array) functions

For the calculation of fuel injector fuel doses d that were not included in the experiment phase, predefined functions: LINEST and TREND, were used. The first of them allows you to fit a straight line to a set of points, but it can be successfully used to determine the coefficients in the multiple regression equation in the form of a polynomial. For this purpose, a column of t-values raised to the appropriate power is prepared for each word, or array operations are used, but the order of the exponents should be reversed by creating the following formula:

$$= \mathrm{SUM}(\mathrm{LINEST}(\mathrm{known\_d`s};\ \mathrm{known\_t`s}\hat{}\{1\backslash 2\} * \mathrm{t}\hat{}\{2\backslash 1\backslash 0\})) \qquad (1)$$

On the other hand, the TREND function is used directly for data interpolation (e.g. polynomial, rational), hence the following expression is used to calculate its value at any selected point of the discrete interval:

$$= \mathrm{SUM}(\mathrm{TREND}(\mathrm{known\_d`s};\ \mathrm{known\_t`s}\hat{}\{1\backslash 2\});\ \mathrm{t}\hat{}\{1\backslash 2\})) \qquad (2)$$

In the next step, the addresses of the cells in which the results of the measurements were entered are substituted, i.e. the ranges of data known_t`s and known_d`s, as well as the value of the sought indirect argument t.

Formulas (1) and (2) can be used interchangeably because they offer the same quality of approximation [5]. In addition, when dividing a discrete area into two parts, low degree polynomials are used to create the so-called spline [6]. In this way, the risk of interference and oscillation (local extremes) that could occur with a single interpolation function [4] is eliminated.

3. Analysis results and discussion

3.1. Preliminary tests

Before starting the tests on the STPiW-3 test bench, the fuel injector was dismantled into its components, which were subjected to baths in ultrasonic baths and thoroughly dried.

During the microscopic examination, traces of initial frictional wear of the surface of plunger and barrel assemblies were found, which due to increased resistance limited the dynamics of the operation of the needle with the atomiser (Fig. 4). This negatively affects the fuel delivery process and uneven engine operation, in particular at idle or when setting low loads [7]. This type of defect is found very often and is detected even at low operational mileage [1]. In addition, valve seat deformation (Fig. 5) was observed, which leads to an overestimation of the volume of fuel going to the overflow. The occurrence of this malfunction results from various reasons, including the wrong ball travel [22]. However, this parameter was checked after the plunger and barrel assembly, guide piston and control valve assembly were replaced. Both in the mechanical AH (Ger. *Ankerhub*) and electric AHe (Ger. *Ankerhub elektrisch*) tests, the result was 0.051 mm, which is within the manufacturer's acceptable range (0.0030–0.060 mm) [18]. Then the fuel injector was mounted on the STPiW-3 bench, where it successfully passed the approval procedures, including leakage and electrical tests.

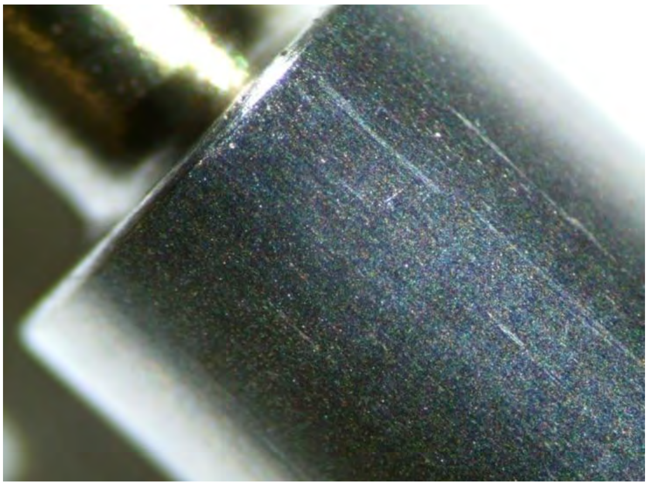

Fig. 4. Friction wear traces on the needle

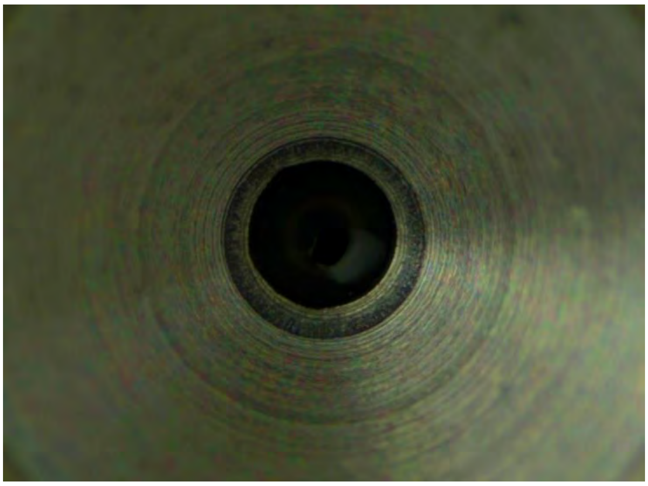

Fig. 5. Valve seat deformation

3.2. Main tests

Table 1 presents the results of measurements carried out on the test bench. The data obtained in the calculation process is also specified, the course of which is discussed on the example of selected fuel doses at fuel injection pressure p_{inj} = 140 MPa.

The introduction of cell addresses in formulas (1) and (2) allowed to estimate the value of interpolation polynomial for the first indirect argument t = 250 µs:

$$7.6 = \mathrm{SUM(LINEST(5.8{:}\,36.6;\,200{:}\,600\hat{}\{1\backslash 2\}} * \mathrm{250\hat{}\{2\backslash 1\backslash 0\})} \quad (3)$$

or

$$7.6 = \mathrm{SUM(TREND(5.8{:}\,36.6;\,200{:}\,600\hat{}\{1\backslash 2\});\ 250\hat{}\{1\backslash 2\})} \quad (4)$$

The fuel doses for the remaining atomiser opening times were calculated in a similar way. However, in the case of the second discrete interval, the formula was simplified due to the smaller number of measuring points. In this aspect, the predefined functions are much more flexible than the classic interpolation methods that are being implemented in a spreadsheet environment [9]. Hence for t = 1000 µs we obtained:

$$52.4 = \mathrm{SUM(LINEST(36.6{:}\,60.3;\,600{:}\,1200\hat{}\{1\}} * \mathrm{1000\hat{}\{1\backslash 0\})} \quad (5)$$

or

$$52.4 = \mathrm{SUM(TREND(36.6{:}\,60.3;\,600{:}\,1200\hat{}\{1\});\ 1000\hat{}\{1\})} \quad (6)$$

For obvious reasons, conducting two-way calculations is not required, but it does not pose any major difficulties and allows you to control the results obtained at every stage of this process. The correctness of the formulas can also be checked in another way, namely by substituting any selected root node. In this case, the value of the interpolating function must be equal to the measurement result at this point [3]. For example, for t = 1200 µs, we obtained:

$$\mathbf{60.3} = \mathrm{SUM(LINEST(36.6{:}\,}\mathbf{60.3}\mathrm{;\,600{:}\,1200\hat{}\{1\}} * \mathrm{1200\hat{}\{1\backslash 0\})} \quad (7)$$

or

$$\mathbf{60.3} = \mathrm{SUM(TREND(36.6{:}\,}\mathbf{60.3}\mathrm{;\,600{:}\,1200\hat{}\{1\});\ 1200\hat{}\{1\})} \quad (8)$$

Figure 6 shows the characteristic curve of fuel doses for the tested injector d = f(t), which were generated based on all results. By contrast, the measured points are marked in colour, and the calculated points are left without any fill.

The shape and course of individual curves should be assessed positively because they do not overlap or intersect the entire working area in question [20]. This indicates that there are no irregularities in the fuel delivery process [2]. In addition, the implementation of pre-defined functions simplified the active experiment phase and enabled the estimation of correct fuel doses values at any atomiser opening time. For example, according to Bosch diagnostic coordinates, the pilot dose VE (Ger. *Voreinspritzung*) and idling LL (Ger. *Leerlauf*) should be within 0.3–4.1 mm^3/inj at t = 260 µs, p_{inj} = 80 MPa and 0.3–3.9 mm^3/inj at t = 420 µs, p_{inj} = 30 MPa [15]. In both cases these requirements were met because the values d_{VE} = 3.9 mm^3/inj and d_{LL} = 2.3 mm^3/inj were obtained.

It is worth emphasising that the detection of irregularities in this area would require the dismantling of the fuel injector again and fuel delivery correction. In addition to adjusting the ball travel, the air gap between the control unit disc and the coil body, the needle travel, and the valve spring force should be checked. The steps included in respective stages regulation match the standard Bosch procedures.

4. Conclusions

Despite the variety of diagnostic methods, more and more often directed at conducting measurements under the conditions of real operation on the engine, the basis of modern research laboratories are test benches. They enable a comprehensive assessment of common rail fuel injectors,

Table 1. Results of test-bench test and calculations for CRI1 Bosch injector

Lp.	Injection pressure, p_{inj} [MPa] / Actuation time, t [μs]	Fuel dose d [mm³/inj.]						
		140	120	100	80	60	40	30
1	200	5,8	5,2	4,5	3,1	1,7	0,2	0,1
2*	250	7,6	6,2	5,1	3,8	2,4	0,8	0,4
3	300	9,9	7,8	6,4	4,9	3,5	1,5	0,8
4*	400	16,4	13,1	11,0	8,7	6,6	3,5	2,0
5	600	36,6	32,0	28,3	22,2	16,8	9,7	5,7
6*	800	44,5	40,2	36,1	29,7	24,1	16,2	11,9
7*	1000	52,4	48,5	44,9	37,2	31,3	22,6	18,2
8	1200	60,3	56,7	53,2	44,7	38,6	29,1	24,4

* analytically estimated data

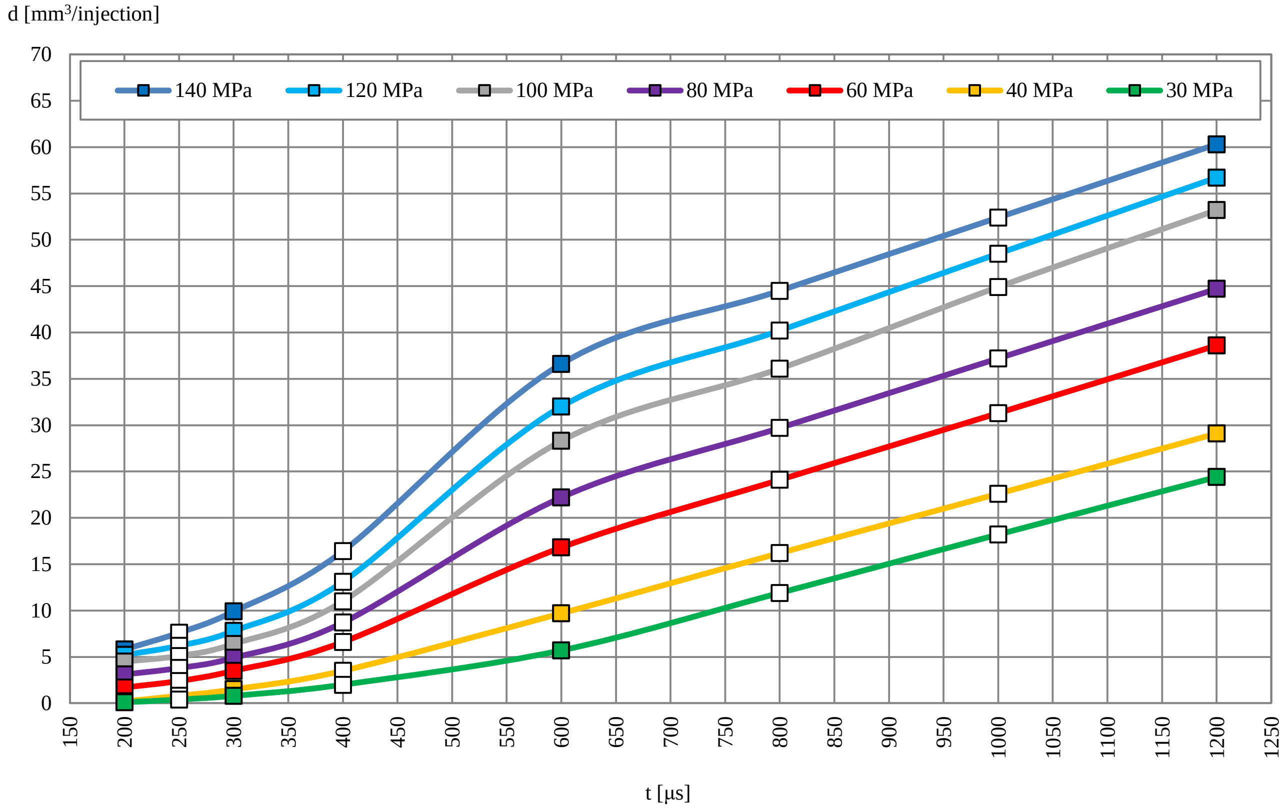

Fig. 6. Fuel doses characteristic curve for the injector tested

indicating at the same time areas of their incorrect operation [10]. Therefore, improving test procedures seems to be the most reasonable, taking into account technical criteria (accuracy, repeatability, durability), as well as economic ones (cost, efficiency, labour consumption). The proposed methodology can be useful to meet them, as it has been used in laboratory and workshop practice.

One of the most important advantages of a spreadsheet is the ability to automatically recalculate all formulas after changing the input variables [21]. In this way, a quick preview of their effect on the final results is obtained, which, with a wide set of implemented predefined functions, gives a very useful tool for processing and presenting data. In the analysed case, two of them were used, simplifying the active experiment phase by eliminating 28 measuring points. In addition, calculations in the digital environment did not require the presentation of the final form (formulas) of interpolation polynomials, but only an estimate of their values for each indirect argument.

Nomenclature

AH mechanical measurement of ball travel (Ger. *Ankerhub*)
AHe electrical measurement of ball travel (Ger. *Ankerhub elektrisch*)
d fuel dose
CRI1 first generation common rail injector made by Bosch
JTD multiJet Turbo Diesel
LINEST predefined linear regression function

LL idling dose (Ger. *Leerlauf*)
p_{inj} injection pressure
t actuation (atomiser opening) time
TREND predefined interpolating function
VE pilot dose (Ger. *Voreinspritzung*)

Bibliography

[1] ABRAMEK, K.F., STOECK, T., OSIPOWICZ T. Statistical Evaluation of the corrosive wear of fuel injector elements used in common rail systems. *Strojniški vestnik – Journal of Mechanical Engineering*. 2015, **61**(2), 91-98. https://doi.org/10.5545/sv-jme.2014.1687

[2] BUSZ, W., WALASZYK, A. Optimize the testing process common rail fuel injectors. *Combustion Engines*. 2015, **162**(3), 978-981.

[3] CHENEY, W., KINCAID, D., Numerical Mathematics and Computing (7th Ed.). *Books/Cole Publishing Company*. 2012, Pacific Grove.

[4] GAUTSCHI, W. Interpolation before and after Lagrange. *Rendiconti del Seminario Matematico Università e Politecnico di Torino*. 2012, **70**(4), 347-368.

[5] GONET, M. Excel w obliczeniach naukowych i technicznych. *Wydawnictwo Helion*. 2010, Gliwice.

[6] HOFFMAN, J.D., Numerical methods for engineers and scientists. *Marcel Dekker, Inc*. 2001, New York-Basel.

[7] JUŚCIŃSKI, S., PIEKARSKI, W., CHOMIK, Z. Analysis of injection systems types used in agricultural machines. *Agricultural Engineering*. 2017, **21**(4), 37-46. https://doi.org/10.1515/agriceng-2017-0034

[8] KARPIUK, W., BOR, W., SMOLEC, R. Possibilities of analysis of condition and repair of common-rail system injectors. *Journal of KONES Powertrain and Transport*. 2018, **23**(4), 209-216. https://doi.org/10.5604/12314005.1217208

[9] KARRIS, S.T. Numerical analysis using MATLAB® and Excel® (3th Ed.). *Orchard Publications*. 2007, *Berkeley*.

[10] KLUCZYK, M., GRZĄDZIELA, A. Marine diesel engine common rail injectors monitoring with vibration parameters. *Diagnostyka*. 2019, **19**(3), 37-44. https://doi.org/10.29354/diag/109793

[11] KLUCZYK, M., GRZĄDZIELA, A. Vibration diagnostics of common rail injectors. *Journal of Marine Engineering & Technology*. 2017, **16**(4), 177-184. https://doi.org/10.1080/20464177.2017.1387088

[12] KNEBA, Z., STRASZAK, P., JAKÓBCZYK, K. The effectiveness of fault detection in common rail injectors examination methods. *Combustion Engines*. 2017, **170**(3), 49-56. https://doi.org/10.19206/CE-2017-308

[13] OLSZOWSKI, S., CHOJNACKI, T., OLSZOWSKI, T. Nieprawidłowa praca wtryskiwaczy common rail pomimo pozytywnego wyniku badania. *Autobusy – Technika, Eksploatacja, Systemy Transportowe*. 2017, **6**, 1003-1007.

[14] OSIPOWICZ, T., ABRAMEK, K.F. Diagnosing methods common rail fuel injectors. *Combustion Engines*. 2017, **168**(1), 56-61. https://doi.org/10.19206/CE-2017-109

[15] OSIPOWICZ, T., KOWALEK, S. Evaluation of Modern Diesel Engine Fuel Injectors. *TEKA – Commission of Motorization and Energetics in Agriculture*. 2014, **14**(3), 83-87.

[16] REIF, K. (Ed.). Automotive Mechatronics. Bosch Professional Automotive Information. *Springer Fach-medien*. 2015. https://doi.org/10.1007/978-3-658-03975-2

[17] STOECK, T. Application of the experimental design technique in fuel dose adjustment of common rail injector. *Combustion Engines*. 2019, **179**(4), 210-215. https://doi.org/10.19206/CE-2019-435

[18] STOECK, T., OSIPOWICZ, T. Analiza uszkodzeń wtryskiwaczy Common Rail firmy Bosch stosowanych w silnikach wysokoprężnych pojazdów użytkowych. *Logistyka*. 2013, **6**, 723-727.

[19] STOECK, T., OSIPOWICZ, T. Przyczyny tworzenia się osadów we wtryskiwaczach Common Rail. *Autobusy – Technika, Eksploatacja, Systemy Transportowe*. 2016, **8**, 139-141.

[20] VASILIU, D., VASILIU, G.C., RĂDULESCU, A. et al. Predicting the dynamic performance of the fuel injectors by numerical simulation. *Scientific Bulletin. Series C: Electrical engineering and Computer Science*. 2018, **78**(4), 173-188. University Politehnica of Bucharest.

[21] WALKENBACH, J. Excel 2013 Formulas. *John Wiley & Sons, Inc.* 2013, Hoboken, New Jersey.

[22] YORDANOV, N., HADJIEW, K., STANKOW, E. Experimental simulation of common rail electromagnetic injectors wearing. *Machines, Technologies, Materials*. 2018, **12**(4), 208-211.

Tomasz Stoeck, DEng. – Faculty of Mechanical Engineering and Mechatronics, The West Pomeranian University of Technology in Szczecin.
e-mail: *tstoeck@wp.pl*

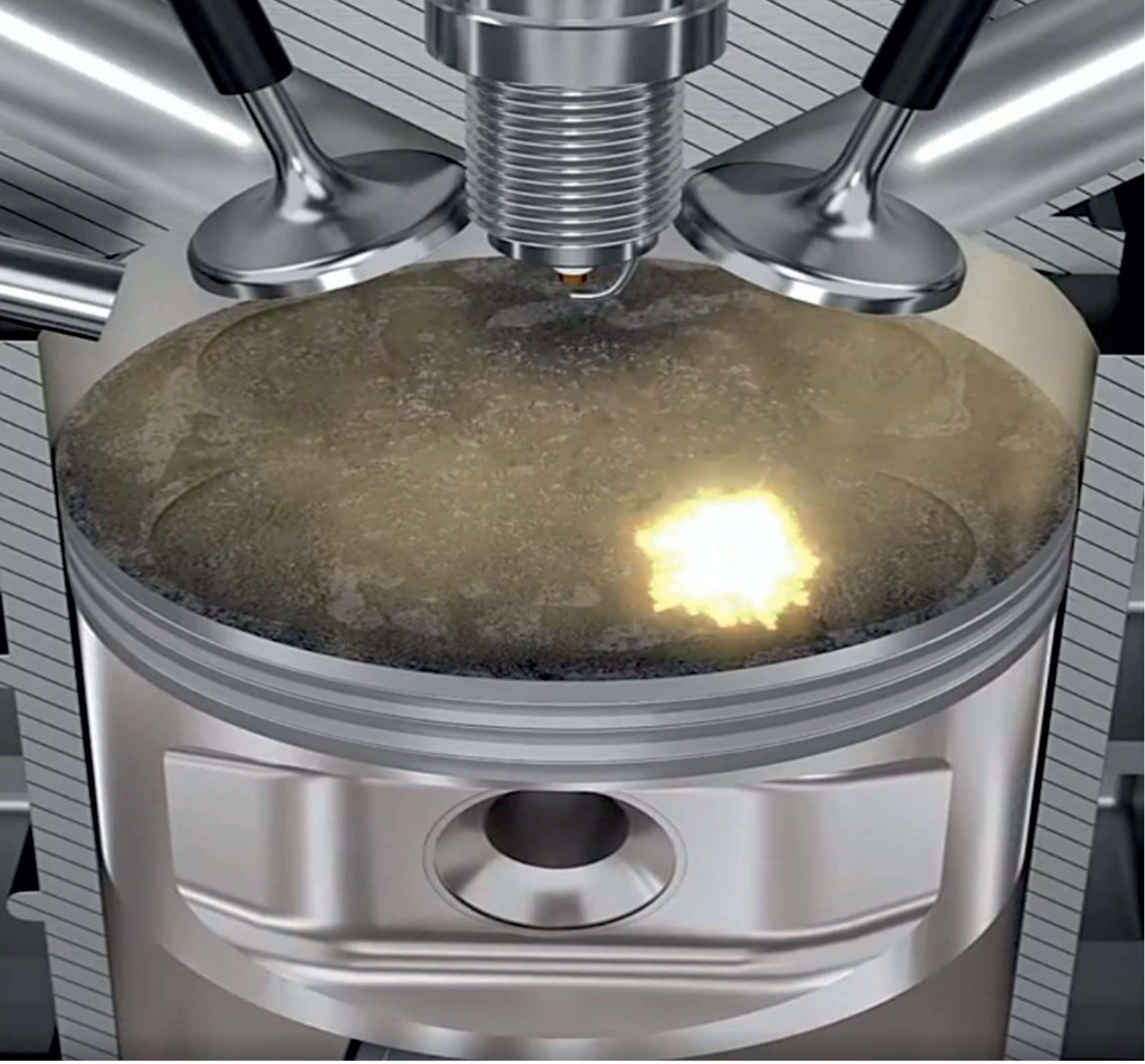

Publisher:

Polish Scientific Society of Combustion Engines

ISSN: 2300-9896
eISSN: 2658-1442

Combustion Engines

Polskie Towarzystwo Naukowe Silników Spalinowych

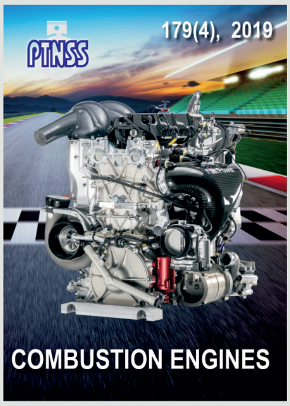

www.combustion-engines.eu